The Role of Frataxin in Doxorubicin Mediated Cardiac Hypertrophy

by

Shravanthi Mouli

A dissertation submitted to the Graduate Faculty of
Auburn University
in partial fulfillment of the
requirements for the Degree of
Doctor of Philosophy

Auburn, Alabama
August 6, 2016

Keywords: Doxorubicin, Frataxin, PPARδ, Iron overload, Oxidative stress, Cardiac Hypertrophy

Approved by

Rajesh H Amin, Chair, Associate Professor of Drug, Discovery and Development
Vishnu Suppiramaniam, Professor of Drug, Discovery and Development
Robert D. Arnold, Associate Professor of Drug, Discovery and Development
Muralikrishnan Dhanasekaran, Associate Professor of Drug, Discovery and Development
Jianzhong Shen, Associate Professor of Drug, Discovery and Development
Nancy Merner, Assistant Professor of Drug, Discovery and Development
Juming Zhong, Associate Professor of Anatomy, Physiology and Pharmacology

Abstract

Doxorubicin (DOX) is a highly effective anti-neoplastic agent, used to treat a wide range of cancer. However, the clinical application of DOX is limited due to its dose dependent cardiotoxic complications which eventually lead to heart failure. The present study investigates the role of frataxin (FXN), a mitochondrial iron-sulfur biogenesis protein, and its role in development of DOX mediated mitochondrial dysfunction and ensuing cardiac hypertrophy. In order to accomplish this, we treated our athymic mice with DOX (5mg/kg, 1 dose per week with 5 treatments, followed by 2 weeks recovery) and observed left ventricular hypertrophy. Further following DOX administration, we also observed significant reduction in FXN expression in vivo and in H9C2 cardiomyoblast cell lines which resulted in increased mitochondrial iron accumulation and ROS formation. To better understand the cardioprotective role of FXN against DOX, we constructed frataxin over expressing cardiomyoblasts (FXN-OE) which displayed cardioprotection against DOX mediated mitochondrial iron accumulation, reactive oxygen species (ROS) and reduced mitochondrial bioenergetics.

Our next objective was to better understand the mechanism by which DOX reduces FXN expression. We observed an increase in ubiquitination of FXN by DOX which may possibly lead to its degradation. Our results collectively suggest a possible post translational alteration including elevated ubiquitination and hyperacetylation of FXN with DOX.

Lastly we have determined a potential pharmacological mechanism to improve FXN expression and thus offer cardioprotection against DOX mediated cardiac damage. We have for the first time demonstrated that pharmacological activation of peroxisome proliferator activated receptor δ (PPARδ) by a high affinity PPARδ agonist GW0742 was cardioprotective against DOX mediated cardiotoxicity by increasing FXN expression levels. In this manner, we observed improvement in mitochondrial energy parameters including reduced ROS production and glutathione status in response to PPARδ activation in DOX treated H9C2 cardiomyoblasts.

Lastly, PPARδ mediated increase in FXN conferred significant protection against DOX mediated cardiac hypertrophy thereby suggesting that PPARδ mediated improvement in FXN was cardioprotective against DOX mediated cardiac damage. Together our findings reveal novel insights into the development of DOX mediated cardiomyopathy novel mitochondrial targets to mitigate its cardiotoxicity.

Acknowledgments

I am forever grateful to the almighty for his blessing and guidance in every little step I have taken.

I thank my mentor Dr. Rajesh Amin who has given me this opportunity to pursue research and for having helped me throughout this journey with his motivation and support. I express my heartfelt gratitude to Drs. Vishnu Suppiramaniam and Murali Dhanasekaran for their constant guidance and for being my pillars of support throughout this journey. I extend my sincere thanks to Dr. Robert Arnold for giving me the opportunity to work on his manuscript which earned me my first publication, for providing me with mice samples to work with and for his wonderful inputs. I thank Dr. Jianzhong Shen for his wonderful teaching and inputs, Dr. Juming Zhong for making time to provide me samples for my experiments and Dr. Nancy Merner for being for being a wonderful support and a guide. I would like to thank my external reader Dr. Satyanarayana Pondugula for accepting to be my reader.

I would like to thank Dr. David Riese for his wonderful course on grant writing which has been extremely useful. I extend my sincere thanks to Jenny for all the prompt and timely help. Lastly, this would never have been possible without the love, support, encouragement and guidance of my mother Mrs. Vijayalakshmi Mouli and father Mr. Chandra Mouli. I thank my brothers Mr. Kalyan Raman and Mr. Krishna Prasad and their families for always being there for me.

I am very grateful and thankful to my life partner Dr. Shyamsundar for having guided me at every step, for standing by me through thick and thin with a lot of patience and for being my greatest pillar of strength and support. I thank my in laws for their constant encouragement, love and support.

I thank my colleagues and friends Dr. Gayani Nanayakkara, Abdullah AlAsmari, Dr. Haitham Eldoumani, Pattanin Yooket, Dr. Manoj Govindarajulu and Dr. Sindhu Manoj for helping me progress well in my research. I also thank my friends Mathew Eggert, Ben Nie and Lingxin Zhang for all their kind help.

Table of Contents

List of Tables

List of Figures

List of Abbreviations

ABCB8	ATP-Binding Cassette, Sub-Family B Member 8
ANP	Atrial Natriuretic Peptide
AT	Angiotensin
DBD	DNA Binding Domain
DFX	Desferoxamine
DFO	Deferiprone
DHR	Dihydro Rhodamine
DOX	Doxorubicin
DOXol	Doxorubicinol
DXZ	Dexrazoxane
ET	Endothelin
EPR	Electron Spin Resonance Spectroscopy
Ft	Ferritin
FXN	Frataxin
FXN OE	Frataxin Overexpressing Cardiomyocytes
FXN KD	Frataxin Knock Down Cardiomyocytes
FRDA	Friedreich's Ataxia
GLUT	Glucose Transporter
GSSG	Glutathione di Sulfide, Oxidized Form

GSH	Glutathione
HIF	Hypoxia Inducible Factor
HF	Heart Failure
I/R	Ischemia Reperfusion
IRE	Iron Response Element
IRP	Iron Regulatory Protein
ISC	Iron Sulfur Cluster
MAPK	Mitogen Activated Protein Kinase
MHC	Myosin Heavy Chain
MI	Myocardial Infarction
MMP	Matrix Metalloproteases
MPP	Mitochondrial Processing Peptidase
mTOR	Mammalian Target of Rapamycin
JNK	Janus Kinase
LVH	Left Ventricular Hypertrophy
LBD	Ligand Binding Domain
LV	Left Ventricle
MYH	Myosin Heavy Chain
PIH	Pyridoxal Isonicotinoyl Hydrazone
PPAR	Peroxisome Proliferator Activated Receptor
PPRE	Peroxisome Proliferator Response Element
ROS	Reactive Oxygen Species
RXR	Retinoid X Receptor

NADH	Nicotinamide A Dehydrogenase
NADPH	Nicotinamide Adenine Dinucleotide Phosphate
TfR	Transferrin
TNF	Tumor Necrosis Factor
UPS	Ubiquitination Proteasome System
VEGF	Vascular Endothelial Growth factor

Chapter 1. Introduction

Doxorubicin is one of the most widely used anthracycline antibiotics in the treatment of wide range of solid and hematological tumors in children and adults. According to World Health Organization, it is considered one of the 17 essential drugs in the treatment of cancer[1]. Despite its wide therapeutic potential as an anti-cancer drug, its use is limited due its cumulative and dose dependent, cardiac damage which manifests into congestive heart failure[2]. Acute cardiotoxicity occurs immediately to weeks following DOX treatment and is characterized by arrhythmias while chronic cardiotoxicity occurs months to years after the completion of the last dosing schedule and is characterized by left ventricular dysfunction which predispose to cardiomyopathy, an enlarged and thickened heart muscle which is unable to pump blood, before leading to congestive heart failure[3, 4].

The principal mechanism leading to DOX cardiotoxicity and heart failure has been attributed to increased oxidative stress, an outcome of impaired redox state of cardiomyocytes and the consequent derangements in the mitochondrial bioenergetics[5, 6]. Impairment in redox state, characterized by increased reactive oxygen species (ROS) and reduced antioxidant balance has been implicated in activating several signal transduction protein kinases, like mitogen activated protein kinases (MAPK) and transcription factors like nuclear factor-κB, leading to the development of hypertrophy[7]. Although hypertrophy is observed as an initial adaptive ‘compensatory’ response, leading to remodeling of the cardiomyocyte structure and function, prolonged hypertrophy leads to cardiac failure[8].

The underlying mechanism of DOX mediated ROS has been primarily attributed to increase in alterations in iron regulatory system controlled by several iron regulating proteins primarily within the mitochondria. Although the role of iron has not been emphasized in the failing myocardial model, the role of iron in the formation of ROS has gained significance at the clinical setting with the usage of Dexrazoxane (DXZ). DXZ is a potent iron chelator that induces degradation of topo2β and prevents the DOX mediated initiation of the DNA damage signal, H2AX-γ in H9C2 cardiomyoblasts [9, 10]. However, the use of iron chelators such as DXZ has been limited due to its interference with antitumor activity of DOX as observed by the decrease in tumor response and due to induction of myelodysplastic syndrome [11]. These findings highlight the critical need to identify key molecular targets involved in the regulation of mitochondrial energy metabolism and mitochondrial iron homeostasis targeted and altered by DOX without altering the anticancer activity. Identification of these targets will help foster development of potential adjuvant therapy to mitigate cardiac damage mediated by DOX.

Frataxin (FXN), a nuclear encoded mitochondrial protein is centrally involved in maintaining mitochondrial iron homeostasis [12]. Although, the precise function of FXN remains elusive, studies have classified FXN as a critical component of mitochondrial energy regulation [13]. In addition, FXN is involved in the biogenesis of iron-sulfur cluster (ISC) resulting in modulating the ISC containing complexes I, and III, as well as aconitase and succinate dehydrogenase [14]. Further it has also been involved in increasing the tricarboxylic acid cycle function [15, 16] which therefore highlights the significance of FXN for maintaining the mitochondrial energy flux.

Deficiency in FXN expression results in Friedreich's Ataxia (FRDA), an autosomal inherited neurodegenerative disease caused by unstable GAA trinucleotide repeat expansion

(>120 repeats) in the first intron of the FXN gene[17]. The deficit in transcription of FXN in FRDA patients is often characterized by mitochondrial damage and the ensuing energy dysregulation[13]. The central pathological outcomes of FRDA on the heart include hypertrophic cardiomyopathy, myocardial fibrosis and myocardial infarction which often progresses the heart to congestive heart failure[18, 19].

Our findings suggest that chronic exposure to DOX with a cumulative dose of 25 mg/kg induced compensatory ventricular hypertrophy. We observed significant reduction in mitochondrial FXN levels, consequent increase in iron accumulation, mitochondrial energy dysregulation and ROS production, concurrently observed in our frataxin knock down (FXN-KD) cell lines. Although our initial findings indicated an adaptive response to the damaging effects of DOX, mitochondrial energetics were impaired severely indicating the possibility of transition of myocardium towards decompensation. Our FXN overexpressed (FXN-OE) cell lines displayed no alteration in mitochondrial energy regulation in response to DOX and was observed to be protective against the toxic effects of DOX, indicating that the stabilization of FXN as a potential therapeutic strategy to combat DOX associated oxidative damage.

The protein quality and control function is tightly regulated by ubiquitination and proteasome degradation system (UPS), regulating several processes of cellular and protein turn over, such as transcription, cell cycle and apoptosis[20, 21]. Therefore any alteration in the post translational modifications will have a significant impact on the cellular processes.

Proteolysis by UPS involves (i) the attachment of Ub molecules that target the protein molecule and (ii) degradation of the targeted protein by proteasome. Our study further investigates the maladaptations involved in FXN degradation with DOX. Our preliminary studies indicate the possibility of increased ubiquitination followed by degradation of FXN

upon DOX exposure which contributed to mitochondrial dysfunction. Previous studies have reported an increase in E3 ligases with DOX treatment which contribute to increase in UPS, by linking ubiquitin to substrate protein[22, 23]. We propose that a possible increase in E3 ligase by DOX could facilitate increased FXN protein ubiquitination and may subject it to degradation.

In light of these findings, recent studies have come up with the discovery of ubiquitin competing molecules (UCM) to prevent ubiquitination of FXN by hindering the accessibility of lysine 147 (K^{147}), a residue that mediates ubiquitination and thereby preventing its degradation[24]. Findings from these studies are in coherence with our findings and may thus serve as a potential therapeutic modality in FRDA. Alternatively a possible reduction in SIRT3, mitochondrial specific deacetylase observed with DOX leads to hyperacetylation of FXN[25] which in turn may subject it to proteolysis by UPS, leading us to test SIRT3 agonists as a therapeutic modality against degradation of FXN by DOX.

Peroxisome proliferator-activated receptors (PPARs) are a group of nuclear hormone receptors which play a major role as transcriptional factors which help regulate expression of a variety of genes involved in cardiac energy metabolism[26]. PPARδ are expressed abundantly in the heart and observed to play a major role in improving mitochondrial oxidative capacity, particularly fatty acid oxidation and has also been implicated as a major requirement in the maintaining of cardiac function under pressure overload hypertrophy[27, 28]. In the current study, we have for the first time demonstrated that pharmacological activation of PPARδ by the highly selective and potent GW0742 was cardioprotective against DOX mediated cardiotoxicity by significantly improving FXN expression levels. Our findings demonstrate an improvement in mRNA and protein transcripts of FXN with the addition PPARδ agonist

GW0742 against DOX treatment. Further we have observed PPAR transcriptional Response Elements (PPRE) in the FXN promoter region, confirmed by increased binding of PPARs to the FXN promoter region as observed by using luciferase assay. This suggests that PPARδ transcriptionally controls FXN expression. Thereby we observed improvement in mitochondrial energy parameters such as balance in ROS-antioxidant status with PPARδ against DOX treatment and in FXN deficient cardiomyoblasts that were preconditioned and treated with GW0742. Lastly, we observed protection against ROS mediated induction in p38 MAPK kinases with PPARδ agonist GW0742 which in turn led to significant protection against DOX mediated cardiac hypertrophy. Together, these results suggest that PPARδ mediated improvement in FXN was cardioprotective against DOX mediated cardiac damage.

In retrospect with these findings, we therefore propose that stabilization of FXN via (i) transcriptional regulation by PPARδ and (ii) preventing UPS mediated degradation of FXN by p38 inhibitors or SIRT3 agonists may serve as a potential therapeutic strategy to prevent DOX mediated oxidative damage and subsequent heart failure.

Chapter 2. Review of Literature

2.1 Cardiac failure

Cardiovascular diseases are a major cause of morbidity and mortality in the United States Of America (U.S.A) Hypertension and Myocardial infarction (MI), in particular are major contributors to heart failure, a debilitating disease with poor prognosis[29]. Cardiac failure arises from deterioration of the myocardium due to imbalance in the demands of the body for oxygen and nutrients and the ability to meet this demand. Especially following conditions such as pressure and volume overload, the reduced ability of the heart to generate ATP that is required for the heart to maintain its cardiac output results in reduced cardiac output. Although cardiac hypertrophy maybe the immediate adaptive response of the heart, to compensate for the adverse alterations in the hemodynamics of the heart, chronic hypertrophy by itself is a major risk for morbidity and mortality especially in populations of people with hypertension (**Figure 2.1**).

However cardiac hypertrophy may also exist in young adults with no risk factors or history of cardiovascular diseases[30]. The most common cause of cardiac death in athletes is cardiac hypertrophy with maladaptive changes in left ventricular mass contributing to approximately 36% of cardiac related deaths[31]. These emphasize the important role of hypertrophy in cardiac failure.

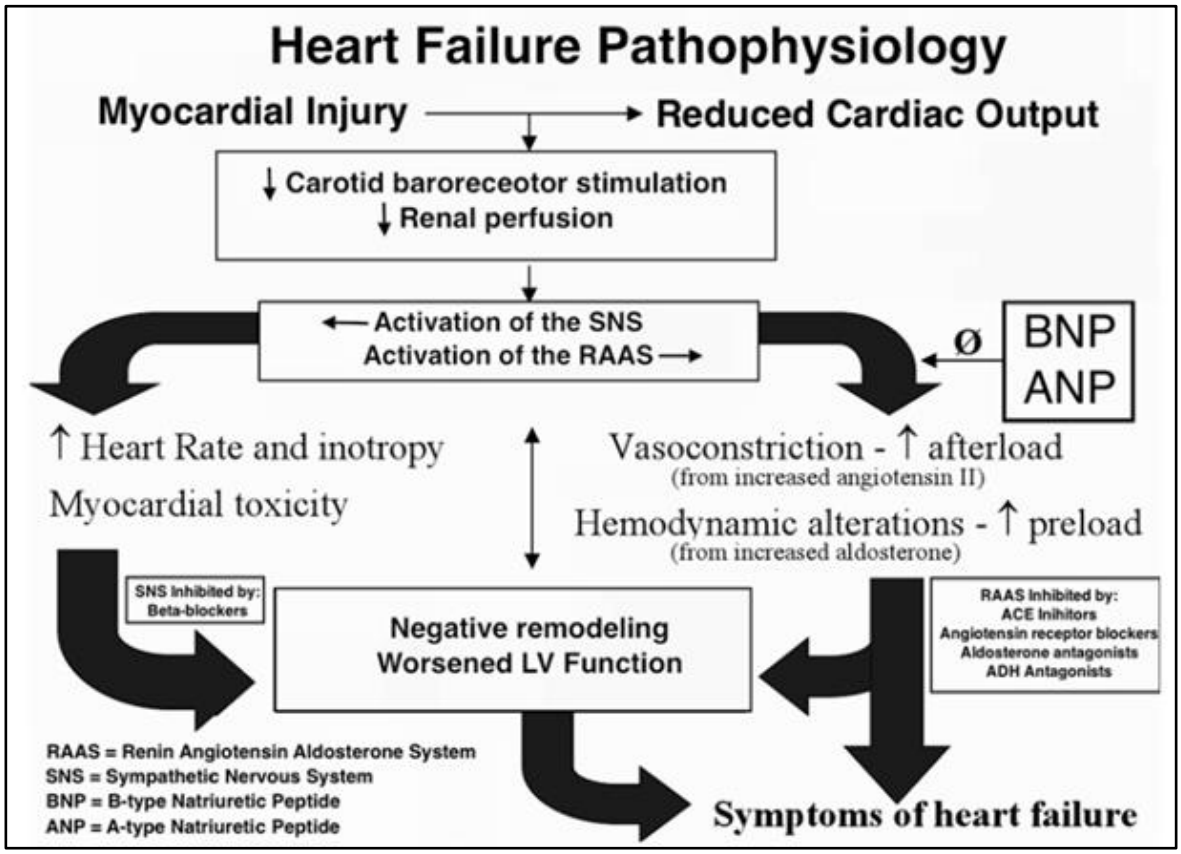

ANP - Atrial Natriuretic Peptide, BNP - Brain Natriuretic Peptide, RAAS - Renin Angiotensin Aldosterone System

SNS – Sympathetic Nervous System, ACE- Angiotensin Converting Enzyme

Congestive Heart Failure - Diastolic (June, 2016), retrieved from

http://www.healio.com/cardiology/learn-the-heart/cardiology-review/congestive-heart-failure-diastolic

Figure. 2.1 Pathophysiology of heart failure results in activation of compensatory responses. The neurohormonal response includes activation of the sympathetic nervous system and activation of renin-angiotensin-aldosterone system (RAA) and a third adaptive response include the B-type and A-type natriuretic peptide in the atrium.

2.2 Cardiomyocyte hypertrophy – An overview

Heart failure is often preceded by cellular hypertrophy (*hyper* = over and *trophy* = growth), an initial adaptive response to pressure or volume stress or mutations in the sarcomeric proteins. Hypertrophy occurs as a consequence of pressure overload and is "compensatory" in nature as it normalizes the systolic wall stress and hence facilitates ejection fraction[32]. It is characterized by an increase in cardiomyocyte size, sudden increase in protein synthesis and alterations in organization of sarcomeres[7]. Although the myocardium induces a normal compensatory response initially, prolonged hypertrophy is detrimental and eventually leads to HF[7]. The hypertrophic growth is associated with several other diseases such as diabetes, ischemic disease, hypertension and heart failure [33-35].

2.2.1 Hypertrophy – a phenotypic view

Two types of cardiac hypertrophy has been shown to exist: (i) concentric, that is caused as a result of pressure overload due to hypertension or aortic stenosis, causes an increase in afterload, leading to ventricular wall thickening and is characterized in cells by the addition of sarcomeres in parallel, with cardiomyocytes growing laterally and increase in diameter and (ii) eccentric, that is caused as a result of volume overload that leads to an increase in preload, such as in mitral valve or aortic valve regurgitation resulting in ventricular growth and chamber enlargement. This form of hypertrophy is characterized by the addition of sarcomeres in series with cardiomyocytes growing longitudinally[36] (**Figure 2.2**).

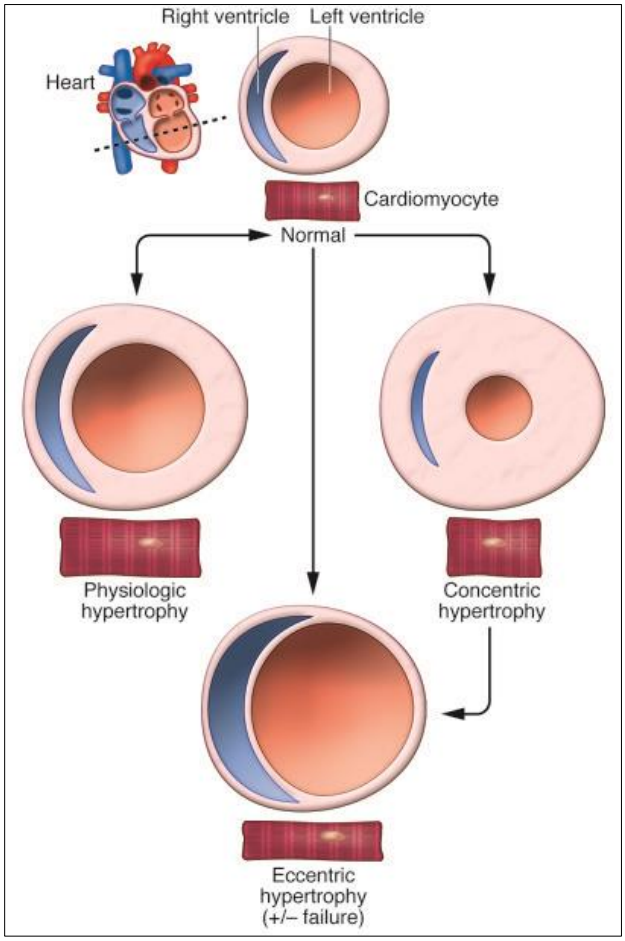

J Clin Invest. 2013;123(1):37-45. doi:10.1172/JCI62839.

Figure. 2.2 Remodeling of heart under stress response. The normal heart undergoes remodeling based on stress response. Pathological stress stimulates cardiac hypertrophy by activating neuroendocrine responses, resulting in concentric remodeling, wherein cardiomyocytes increase in width, resulting in septal wall thickening. This state can further develop into eccentric hypertrophy where individual cardiomyocytes reduce in width increases in length, leading to enlargement with loss of wall or septal thickness[37].

During heart failure, a small fraction of cardiomyocytes undergo apoptosis while the rest attempt to compensate for the metabolic demand and become enlarged.

2.2.1.1 Transition from compensatory hypertrophy to heart failure

During compensated hypertrophy, the increase in metabolic demand is met so there is no negative impact on the stroke volume or the contractile performance of the heart. However, hypertrophy progresses with time causing depression in cardiac function, wherein cardiac output of the heart is unable to meet the metabolic demands of the heart leading to decompensatory hypertrophy[8].

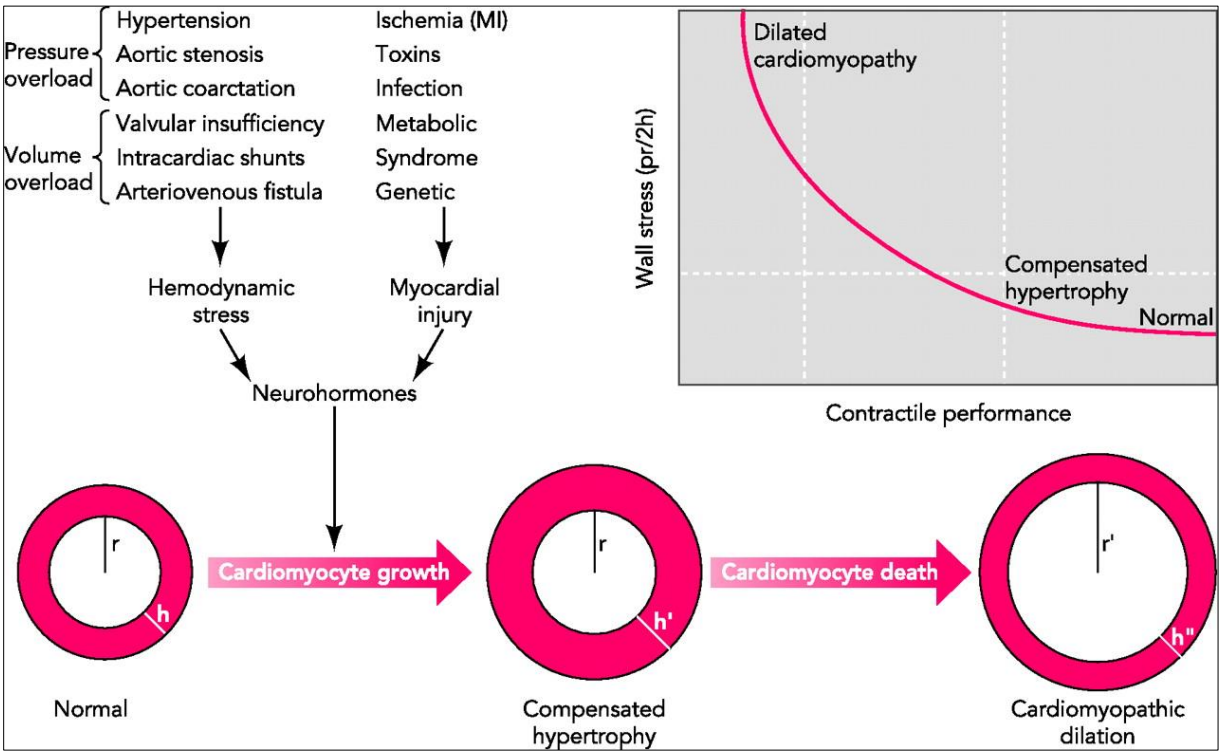

Physiology Published 8 February 2007 Vol. 22 no. 1, 56-64 DOI: 10.1152/physiol.00033.2006

Figure. 2.3 Development of decompensatory cardiac hypertrophy. Compensatory hypertrophy is characterized by increase in ventricular wall thickness observed as a result of increased growth in response to hemodynamic stress and myocardial injury[8].

2.2.2 Role of mitochondria during the transition from hypertrophy to heart failure

About ninety percent of the energy requirement in the form of ATP is provided by the mitochondria which constitutes about 30-40% of volume in cardiomyocytes. Mitochondrial plays a critical role in providing energy for cardiac contraction and relaxation. During cardiac hypertrophy, there is an increase in mitochondrial biogenesis which delays the decompensation induced by pressure overload[8]. Hypertrophy induced by aortic banding in Mammalian Target

of Rapamycin (mTOR) (that is known to regulate the transcription of mitochondrial genes) deficient mice, displayed rapid dilated cardiomyopathy[38]. Although an increase in mitochondrial density is observed initially in the beginning to match the energy demand as a hypertrophic response, a decrease in density of mitochondria is observed during decompensation[39].

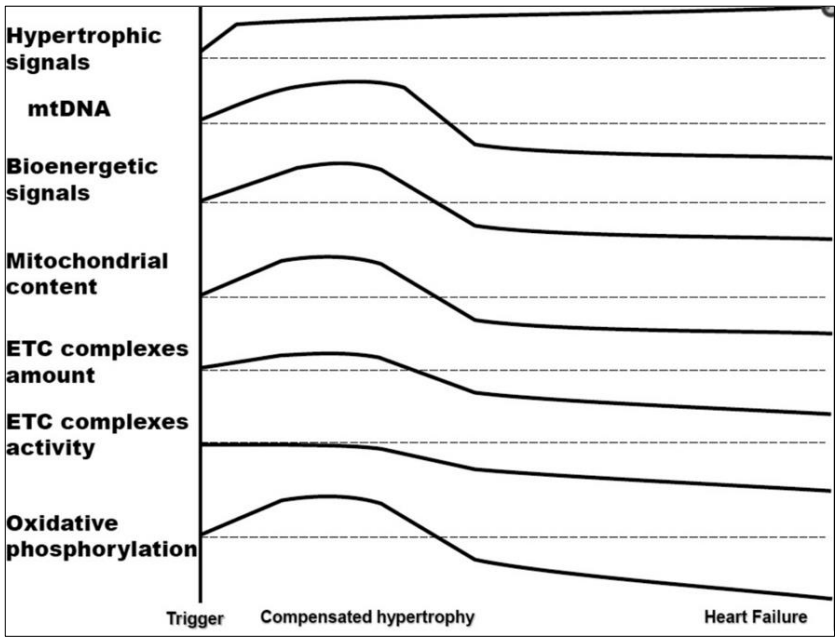

J Mol Cell Cardiol. 2013 Feb; 55: 31–41.

Figure 2.4. Biochemical features of mitochondria during transition towards heart failure. Compensatory hypertrophy is characterized by increased OXPHOS and mitochondrial bioenergetics which gradually declines during its progression towards decompensatory hypertrophy and heart failure[39].

Further, studies conducted by Garnier et al., demonstrated in a HF model induced by rat aortic banding, downregulation of transcription of all major mitochondrial genes involved in biogenesis[40]. Further evidence is provided in studies conducted by Dai et al. [41] where experimental depletion of mtDNA and AT II led to increased biogenesis of mitochondria during hypertrophy and an exponential decline was observed as it progressed towards HF.

Early studies have demonstrated a decrease in complex I and II activities in thoracic aortic banding, model of pressure overload in rabbits [42]. There have also been reports of reduction in electron transport chain complexes I, III, IV and V in mice that underwent aortic constriction[41].

2.2.3 Cardiomyocyte hypertrophy in diabetic heart

Left ventricular hypertrophy and myocardial fibrosis are the hallmarks of diabetic cardiomyopathy and display impaired cardiac contractility. Echocardiography (ECG) evidence reveals LVH as a common structural and functional change in diabetic patients, accompanied by increased afterload in patients with hypertension[43] .

Hypertrophy in diabetes has been linked to activation of vasoactive factors such as endothelin-1 and NF-κB and activating protein -1 (AP-1). Another study has attributed the diabetes induced cardiomyocytes hypertrophy to p300 mediated transcriptional regulation of MEF2[44]. Glucose mediated increase in ROS manifests as oxidative stress and has been shown to play a major role in diabetic cardiomyopathy. Although several players such as AT II, ET-1, TNF-α have been shown to stimulate the mechanism of hypertrophy in diabetic hearts, the role of ROS has gained maximum attention. ROS and oxidative stress has been discussed in several

studies to directly or indirectly to further activate several pathways downstream of hypertrophy including PKC, p38, MAPK, JNK, Akt, ERK1/2 and calcineurin[45].

2.2.4 Cellular and molecular events in hypertrophy

Hypertrophy or increase in cell size, in some cases is accompanied by an increase in protein content followed by increase in sarcomeres and the number of mitochondria. The process of cellular hypertrophy involves a cascade of events which triggers initial events, such as activation of cardiac specific transcriptional factors and altered gene expression profiles. The enlargement of cardiomyocytes is usually accompanied by decreased amplitude and velocity of contractility of muscle fibers[7].

2.2.4.1 Alterations in gene expression

Hypertrophy is known to trigger pathological response by characteristic alteration in gene expression. The initial set of genes which are activated as a result of mechanical stress (induced by physical stretching of cardiomyocytes) is the early response genes, *c-fos, c-myc,* and *c-jun,* and the fetal genes atrial natriuretic factor (ANF) and β Myosin heavy chain (MHC) and skeletal alpha actin (SKA) which are known as hypertrophic markers. The expressions of *c-fos* and *c-myc* genes are known to elevate during aortic constriction in rats [7]. The expression of *c-fos* is proportional to the mechanical stretch observed in the ventricular walls of the heart. Myosin is an important component of muscle fiber and consists of α and β isoforms. An increased ratio of β MHC has been reported in humans and in animals with hypertrophic heart[46]. Pressure and volume overload has been shown to increase the levels of β MHC and decrease the levels of α MHC. Therefore, hypertrophic heart facilitates re-induction of fetal gene program, as the

changes in gene expression pattern mimic the expressions observed during embryonic development.

2.2.4.2 Intercellular signaling in cardiomyocytes

Mechanical stress mediates signal transduction in the heart which in turn activates a myriad of pathways. In cardiomyocytes, mechanical stress in the heart has been shown to activate several pathways such as phospholipase C, D and A2, tyrosine kinase, p21ras, raf-1, and mitogen activated protein kinases (MAPK) and their downstream targets JNK kinases, protein kinase C (PKC). Activation of PLC, PLD and PLA2 in turn activates secondary messengers including inositol 1, 4, 5-tis phosphate (IP3), diacylglycerol (DAG) and arachidonic acid. The activation of IP3 produces intracellular calcium release from calcium stores, and the activation of DAG activates PKC which plays a critical role in c-fos and Egr-1[7].

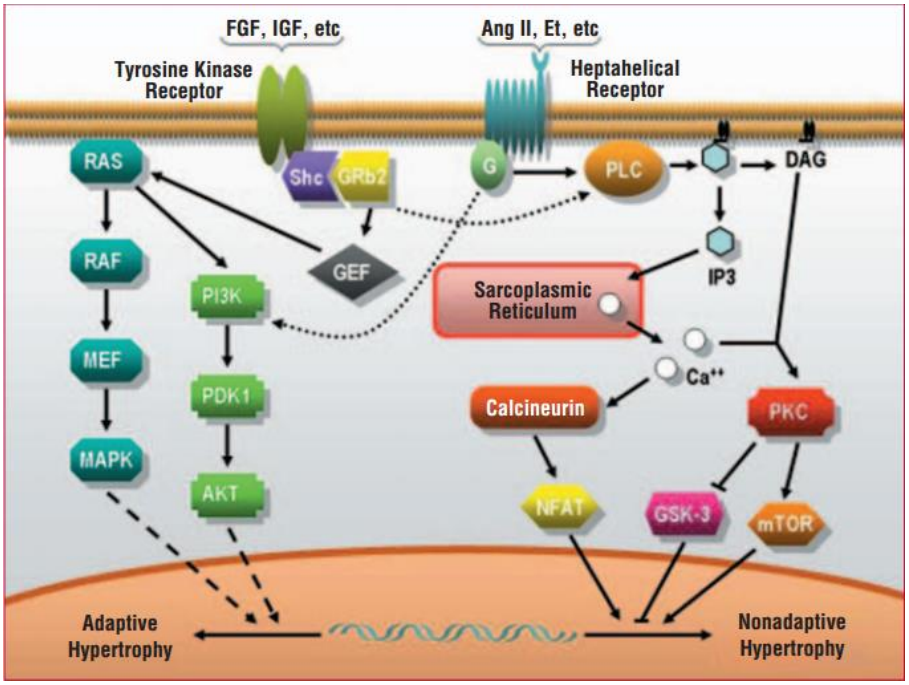

Rev Esp Cardiol. 2006;59:473-86 - Vol. 59 Num.05 DOI: 10.1016/S1885-5857(06)60796-2

Figure 2.5. Intracellular mechanisms involved in the development of cardiomyocyte hypertrophy[7]

The stimulation of adrenergic system plays a critical role in maintaining the hearts response to increased wall stress. Activation of β-AR has been shown to stimulate chronotropy, inotropy and lusitropy[47].

2.2.5 Role of ROS and oxidative stress on development of hypertrophy

Despite evidence supporting the participation of different pathways in the process of hypertrophy, several studies have attributed the cause of hypertrophy to increase in ROS production[48]. Growing body of evidence indicates the participation of redox signaling

pathways in the development of cardiac hypertrophy in response to pressure overload. Further, cultured cardiomyocytes have indicated the roles of angiotensin II (AT II), Endothelin -1 (ET-1), Tumor Necrosis Factor α (TNF- α) and alpha adrenergic agonists to induce cardiomyocyte hypertrophy in a ROS dependent manner and are said to be inhibited by ROS scavenging enzymes or antioxidants[48, 49]. Although the mechanism of ROS induced hypertrophy primarily involves the activation of MAPK and NF-κB, ROS production has also shown to lead to hypertrophy through signaling kinases and transcription factors[50]. This was confirmed in a study where overexpression of kinase-1 activates NF-κB to stimulate hypertrophy induced by ET-1, AT-II and norepinephrine. ROS has been shown to play an important role in G protein-coupled hypertrophic stimulation by AT II and alpha adrenergic stimulation[51].

Further, NADPH oxidase has been shown to play a key role in the production of ROS. In pressure overload models, increased NADPH oxidase activation is observed in concurrence to MAPK activation. There is also evidence that inhibition of NADPH oxidase prevents the ERK1 and ERK2 activation in response to ET-1 agonists and alpha adrenergic agonists indicating the major role of NADPH oxidase complex in stimulating hypertrophy. Although several mechanisms have been proposed indicative of the role of ROS in the process of hypertrophy, the exact mechanism by which free radicals are involved in this pathway is unknown.

Mitochondrial ROS plays a major role in the myocardial infarction and heart failure. Oxidative stress as a consequence of ROS plays a major role in mitochondrial DNA damage, protein damage, cellular damage and decreased membrane potential. Some studies have attributed the excessive ROS to electron leak instigated by depressed electron chain activity[52]. Although mitochondria consists of specific antioxidants such as peroxiredoxin-3 have been shown to reverse ventricular remodeling[53], the exact source of ROS is still unclear.

2.2.6 Pharmacological interventions to target hypertrophy

β-adrenergic system is a potential target of oxidative insult and is responsible for the production of free radicals. The sirtuins represent a class of histone deacetylase which may be used to scavenge the oxidative stress mediated free radicals. SIRT1 activator SRT2104 shows promising outcomes in lipid profiles but did not show positive effects in platelet, vascular and endothelial functions[54].

2.2.6.1 β adrenergic blockers

β-adrenergic blocker is administered for people with dilated cardiomyopathy and are considered first line therapy for hypertrophic cardiomyopathy. β-blockers work by decreasing the overall cardiac workload and oxygen demand. β-adrenergic stimulation leads to increase in heart rate, contraction, pressure and relaxation of smooth muscle in bronchial tubes in the lungs. When administered through veins or mouth, they block the receptors that bind to catecholamines so the heart rate and pressure is reduced so the work load of the heart is reduced, reducing the oxygen demand. In hypertrophic cardiomyopathy, where muscle is thickened and stiffened, β blockers work to relieve symptoms of chest pain and shortness of breath; e.g., Atenolol, metoprolol[55, 56].

2.2.6.2 Ca^{2+} channel blockers

The second line of therapy is the Ca^{2+} channel blocker, similar to β blockers work by inducing a negative chronotropic effect. This leads to increased diastolic relaxation time, increasing the preload. They are used in hypertension and have been used to reduce hypertrophic cardiomyopathy, e.g., nondihydropyridine (verapamil) [57]

2.2.6.3 Angiotensin Converting Enzyme (ACE) inhibitors

ACE inhibitors work by inhibiting the ACE which converts angiotensin I to angiotensin II. This reduces the pressure in the wall after ejection (i.e., afterload), vascular resistance and hypertrophy caused by angiotensin II [58, 59].

2.3 Anthracyclines

Anthracyclines are considered one of the most effective anti-cancer treatments. The first anthracyclines were isolated from *Streptomyces peucitius* and were termed Doxorubicin (DOX) and Daunorubicin (DNR)[60].

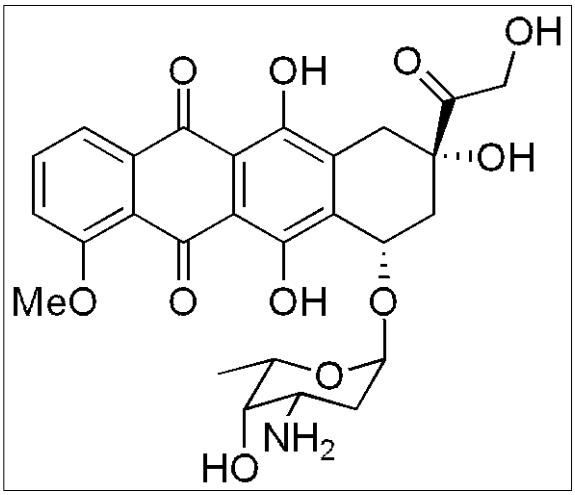

http://www.atdbio.com/content/16/Nucleic-acid-drug-interactions

Figure 2.6. Structure of Adriamycin (Doxorubicin)

Doxorubicin (commonly known as Adriamycin) is one of the most potent anti-cancer agent available today and has been utilized in a variety of solid tumors and hematological malignancies

including breast cancer, prostate, uterus, ovary, stomach, lung, liver soft tissue sarcoma, acute lymphoblastic leukemia [61, 62].

2.3.1 Chemistry and Mechanism of Antitumor activity of DOX

The structure of DOX molecule consists of a tetracyclic ring structure which is connected to a glyconic sugar containing moiety. The aglycone portion is connected to adjacent quinone-hydroquinone groups in rings C-B, a methoxy substituent in C-4 at ring D and a short side chain at C-9 with a carbonyl at C-13. Although cytotoxic in nature, they are considered the most effective antitumor drugs developed ever[60].

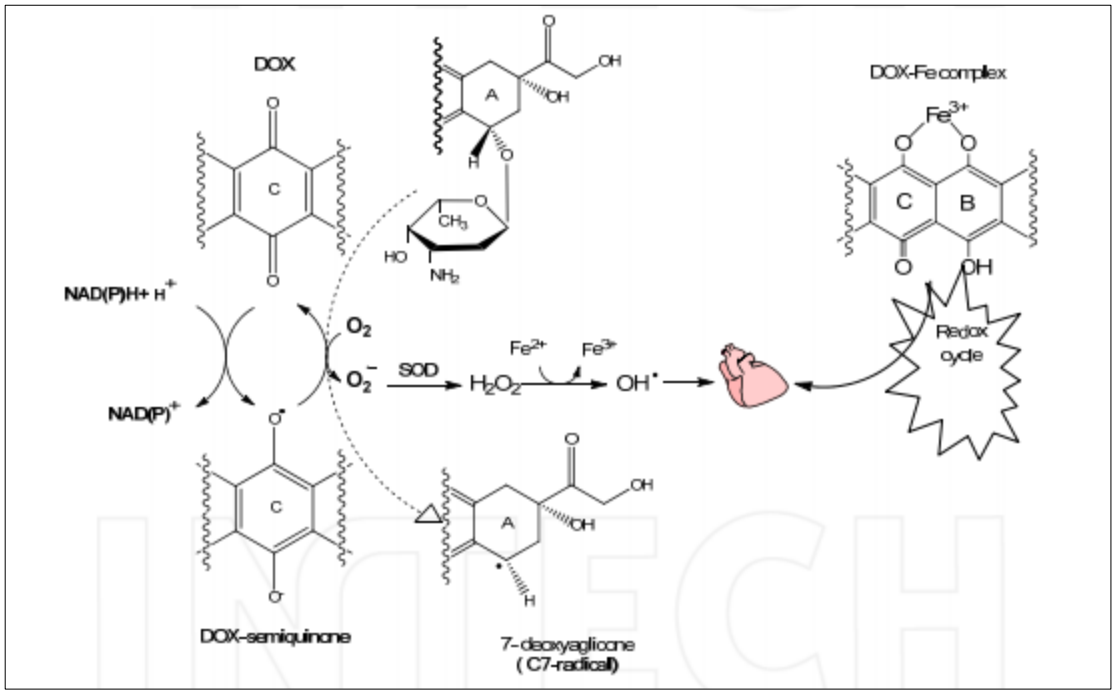

http://hdl.handle.net/10400.18/665

Figure 2.7. DOX mediated redox cycling. (A) Doxorubicin belongs to a group of anthracycline antibiotic that consists of naphthacenequinone nucleus that is linked through

a glycosidic bond to an amino sugar daunosamine. (B) The one electron addition to quinone moiety in DOX results in the formation of semiquinone that regenerates its parent quinone by reducing oxygen to ROS including superoxide anion and hydrogen peroxide[63].

Several mechanisms appear to have contributed to the antitumor mechanism of DOX. Intercalation into DNA followed by (i) inhibition of macromolecules, (ii) inhibition of topoisomerase II and initiation of apoptosis [64] (iii) free radical production leading to damage of DNA and proteins and activation of lipid peroxidation [65] (iv) direct effects on the surface membrane and (v) DNA binding and alkylation [66]. Some of the important mechanisms are discussed below.

2.3.1.1 DOX as Topoisomerase II poison

Topoisomerase II is known to lead to double stranded DNA breaks or cleavage followed by unwinding and ligation of the super coiled DNA. DOX has been demonstrated to stabilize the cleavage of the double stranded DNA by binding to the Topo II- DNA complex, preventing the unwinding and re-ligation of the DNA, thereby initiating apoptosis of cells[64].

2.3.1.2 Redox cycling (one electron reduction)

The addition of an electron to the quinone moiety of ring C of DOX has been shown to result in the formation of a semiquinone- DOX complex which may quickly regenerate back its parent quinone structure via NAD(P)H oxido-reductase (cytochrome P450, NADH dehydrogenase, Xanthine dehydrogenase, eNOS) by reducing oxygen to super oxide anion (O_2.) and ROS[67]. Redox cycling is further accompanied by release of iron from intracellular iron

sequestering proteins. Formation of DOX-Iron complex at 3:1 ratio converts the O_2^- and H_2O_2 to hydroxyl radical (OH-)[68]. Oxidative damage to tissues is therefore an important mechanism of DOX mediated anti-tumor activity.

2.3.1.3 Role of P53

The P53 tumor suppressor gene encodes p53 protein which is known to play an important role in the negative regulation of cell development and apoptosis. DOX has been shown to activate p53-DNA binding and the initiation of apoptosis. In addition, DOX mediated activation of p53 has been shown to transcriptionally activate WAF1/CIP1, which in turn encodes for p21, a 21-KDa potent inhibitor of cyclin dependent kinase that are required for the transition from G phase to S phase of the cell cycle[69].

2.3.1.4 Proteasome mediated degradation

Proteasomes are involved in cytosolic and nuclear protein complexes which participate in non-lysosomal protein degradation mechanism. Recent advances have demonstrated an important role of proteasome in transporting DOX into nucleus. DOX diffuses into cancer cells and binds the proteasome due to its higher affinity and translocates into the nucleus through the nuclear pore, a process facilitated by ATP. Following this, DOX binds to DNA due to its higher affinity for DNA than for proteasome and initiates apoptosis[70].

2.3.2 Cardiotoxicity associated with DOX treatment

Although DOX is one of the most efficacious chemotherapeutic agents, there have been early reports of cardiovascular complications which develop towards heart failure.

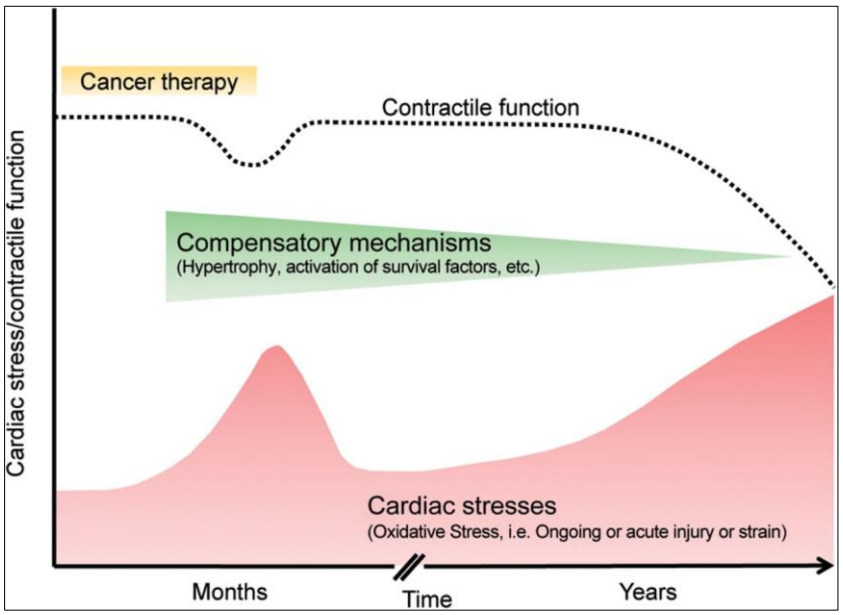

Volume 34, Issue 15, 14 April 2013 http://dx.doi.org/10.1093/eurheartj/ehs181

Figure. 2.8 Chemotherapeutic agents demonstrate myocardial oxidative stress and dose dependent dose dependent cardiac cell damage. Activation of compensatory hypertrophy delays cardiac dysfunction while exhaustion of these mechanisms leads to heart failure[71].

The cardiotoxicity of DOX is known to be cumulative, dose dependent, progressive myocardial damage, leading to clinical series of events which maybe asymptomatic reduced left ventricular ejection fraction (LVEF) (where LVEF function maybe reduced to 40% with no signs or symptoms of HF), to irreversible HF[72]. The cardiac changes associated with the treatment of DOX manifests as asymptomatic changes in cardiac rhythm, cardiac dilation and most importantly cardiomyopathy[72] (**Figure 2.8**).

2.3.2.1 Incidence of Cardiotoxicity associated with DOX dosing

The cardiovascular system is one of the most metabolically active components that is highly susceptible to toxicity associated with chemotherapy. Although several strategies have been adopted to prevent DOX mediated cardiotoxicity, heart failure remains to be an adverse consequence of DOX treatment which limits its utility. DOX cardiotoxicity can be classified as acute, chronic and late onset. Acute or sub-acute cardiotoxicity occurs immediately within 2-3 days or within weeks of intravenous infusion of drug dosing and is characterized by minor changes in the ECG such as non-specific ST-T changes and QT prolongation leading to fatal arrhythmias including sinus tachycardia and hypotension[73, 74]. Although the mechanism is not well understood, a recent report has attributed the cause of toxicity to cytoplasmic edema and fluid accumulation on the vesicles of sarcoplasmic reticulum. Rare case of left ventricular failure maybe observed as a manifestation of acute cardiotoxicity but is reversible with treatments[74].
Chronic cardiotoxicity, also known as late onset cardiotoxicity manifests months or years after last dosing of chemotherapy to develop into dilated cardiomyopathy before resulting in heart failure. Chronic DOX mediated cardiotoxicity is strictly cumulative and dose dependent. Although asymptomatic in the beginning, it may be characterized by slight echocardiographic anomalies which later develop into chronic cardiomyopathy, dilated in adulthood and restrictive in childhood[75].

2.3.2.2 Cumulative Dosing and the prevalence of cardiotoxicity

The utility of DOX is limited by dose dependent cardiotoxicity which results in permanent damage to cardiac myocytes and a progressive decline in cardiac function following a cumulative dosing[72]. Extensive studies have observed a direct relation between the incidence of heart failure and cumulative dosing of DOX (**Figure 2.9**)

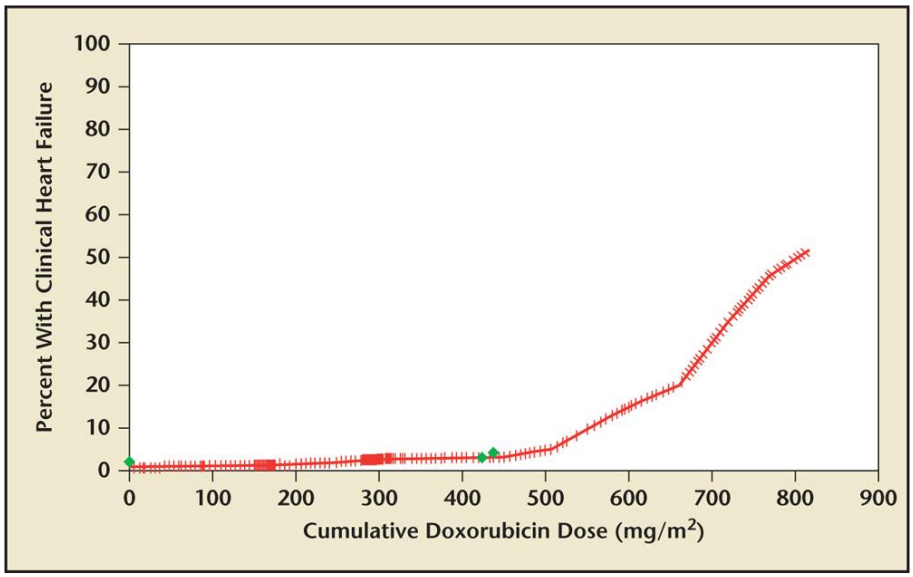

Figure. 2.9 The probability of developing heart failure increases exponentially with cumulative DOX dosing. The probability of developing heart failure is >2% at 300mg/m^2 and increases beyond this [76].

In a retrospective study of 4000 patients, about 2.2% patients developed symptoms leading to heart failure (HF) with a prominent decline in left ventricular function[77] (**Figure 2.9**). The study further reported that cumulative dosing as a major determinant of development of heart failure with an increase in incidence of heart failure at 550 mg/m$^{2.}$ Another study observed a dose dependent decrease in left ventricular ejection fraction (LVEF) at >350 mg/m^2 [72]. Another retrospective study indicated an incidence of HF at ~3% in patients who have been dosed at 400 mg/m^2 and increasing up to 7.5% at dosage 550 mg/m^2 and 18% at 700 mg/m [72]. Patients who have been diagnosed with advanced carcinoma and treated with repeated injections of DOX at a cumulative of 505 mg/m^2 - 1004 mg/m^2 over a period of several months, displayed hypotension

(70/60 mmHG), tachycardia (150 beats/min), reduction in QRS voltage, cardiac dilation and ventricular failure[78].

2.3.2.3 DOX mediates Cardiac Hypertrophy

Findings from a recent study have demonstrated that DOX mediated hypertrophy in H9C2 cells, similar to what was observed in adult cardiomyocytes during its progression towards cardiomyopathy [79]. Upon investigation of the mechanism of DOX induced hypertrophy, it was observed that DOX induced phosphorylation of protein kinase Akt at serine 473 (ser473) in H9C2 cardiomyoblasts[80]. Our preliminary data indicated that DOX treatment led to increased ROS which in turn may stimulate hypertrophic growth by activation of variety of kinases and transcription factors such as src, tyrosine kinase, GTP-binding RAS, MAPK, JNK etc. Further DOX has also been shown to activate p38 MAPK pathway which has also been associated with the development of cardiac hypertrophy.

2.3.2.4 Morphological and subcellular changes associated with DOX induced cardiotoxicity – clinical relevance to humans

Some of the early examinations in patients administered with DOX dosing have revealed two kinds of injury in cardiomyocytes: myocardial lesions characterized by reduction in density of myofibrillar bundles and loss of myocytes due to dilation in sarcoplasmic reticulum, resulting in peripheral z disks without filaments i.e., (alterations in Z disc structure) patchy and interstitial fibrosis with vacuolated cardiomyocytes can be visualized. Additional changes include nucleus-chromatin disorganization which may be observed. These alterations maybe further followed by

mitochondrial abnormalities, including increased number of lysosomes, accumulation of lipids and swollen mitochondria[78].

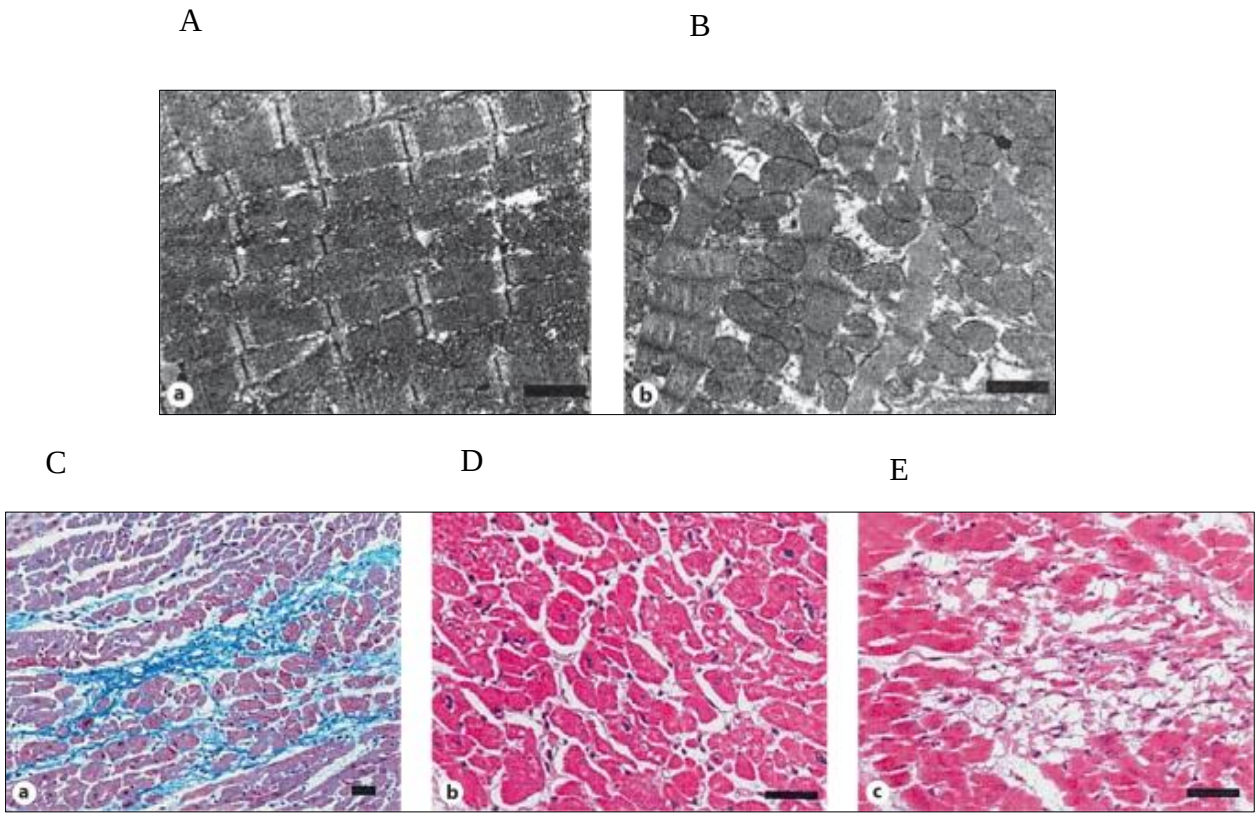

Figure 2.10 Subcellular changes associated with DOX cardiotoxicity (A) Normal myocytes without interstitial fibrosis. (B) DOX treated myocytes (also referred to as 'Adria' cells) displays patchy interstitial fibrosis and scattered vacuolated cardiomyocytes. (C) Normal myocardium with intact myocytes (D) Normal cardiomyocytes at high magnification (E) Matrix disorganization, myocyte loss and fibroblast proliferation in DOX treated cardiomyocytes[78].

Endomyocardial biopsy in DOX treated human hearts reveal an increase in sarcoplasmic reticulum and T-tubule followed by cytoplasmic vacuolization. Specific nuclear changes include,

chromatin clumping and nucleolar shrinkage, accompanied by segregation of granular components. These morphological evidences were observed with increasing doses of DOX[81]. Some of the intracellular changes can be observed in **Figure 2.10** and mitochondrial changes in **Figure 2.11.**

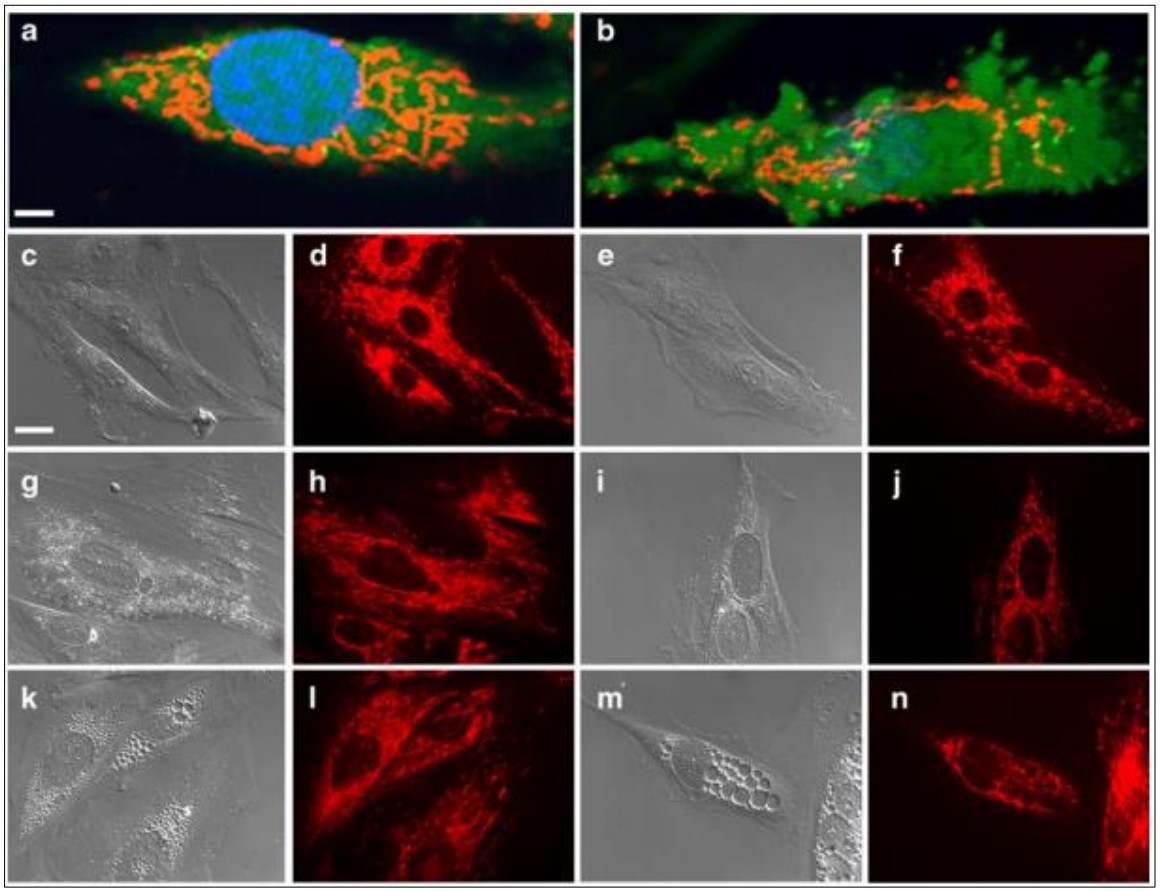

Cell Biol Toxicol. 2009 Jun;25(3):227-43. doi: 10.1007/s10565-008-9070-1. Epub 2008 Apr 3.

Figure 2.11 Mitochondrial abnormalities in H9C2 treated with DOX (a) Laser scanning confocal electron microscopy of untreated cardiomyocytes labeled with Hoechst (blue), calcein AM (green) and TMRM (red) displaying intact cell membrane and polarized mitochondria (b) Laser scanning confocal microscopy of DOX (1 μM) treated cardiomyocytes labeled with the 3 dyes displaying mitochondrial blebbing and breaking of mitochondrial network. (c, d) Differential interference contrast image (DIC) and Tetramethyl rhodamine methyl ester (TMRM) fluorescence image of cardiomyocytes of

control cells, (e, f) treated with DOX at 1 µM, (g, h) 5 µM, (i, j) 10 µM, (k, l) 20 µM, (m, n) 50 µM. The TMRM fluorescence diminishes with increasing concentrations of DOX[81].

2.3.2.4.1 Oxidative stress and generation of free radicals – The role of mitochondria

DOX induced oxidative stress can be attributed to its chemical structure consisting of tetracyclic aglycone with adjacent quinone-hydroquinone groups, which are known to generate ROS or free radicals[67]. Therefore the imbalance in the pro oxidant-antioxidant balance leads to excessive ROS which in turn can cause cellular damage.

The primary target of DOX cardiotoxicity are the mitochondria and the cardiotoxic effects of DOX in the heart has been attributed to its extensive accumulation in the mitochondria[82]. Mitochondrial enzymes NADPH (NADH dehydrogenase), cytochrome P450 reductase, xanthine oxidase (XO) transforms the quinone group of DOX to semiquinone group via one electron reduction. The semiquinone can be converted to parent quinone by reacting with molecular oxygen and generate superoxide anion, which initiates a chain reaction leading to formation of ROS[67] by Electron spin resonance spectroscopy (EPR). Thus the excessive production of ROS further contributes to the production of oxidative stress.

Endogenous antioxidant defenses play a critical role in mitigating DOX mediated damage in the heart. Cardiomyocytes are highly susceptible and vulnerable to the production of oxidative stress, especially due to their low levels of ROS scavenging enzymes such as catalase, which is expressed in low levels in cardiomyocytes. SOD acts as a free radical scavenger, which catalyzes the dismutation of superoxide anion to H_2O_2 and oxygen[82].

$$O_2^{\cdot-} + O_2^{\cdot-} + 2H^+ \rightarrow H_2O_2 + OO_2^{\cdot-}$$

However, studies have reported that DOX exacerbates cytotoxicity in cardiomyocytes which have reduced Cu^{2+}/Zn^{2+} SOD activities are thus highly vulnerable to oxidants such as xanthine oxidase, H_2O_2 etc. The H_2O_2 removal enzymes include catalase and Glutathione peroxidase (GPx)[60].

$$H_2O_2 \xrightarrow[Catalase]{} 2\,H_2O + O_2$$

$$2GSH + H_2O_2 \xrightarrow[GPx]{} GSSG + H_2O$$

Glutathione (GSH) is regarded as major cellular defense in free radical damage and plays an important role in the inactivation of reactive intermediates intracellularly. Glutathione levels are maintained with the activity of glutathione reductase (GSH), which catalyzes the reduction of oxidized glutathione (GSSG) using NADPH. DOX exposure has been shown to cause specific depletion of glutathione peroxidase in cardiomyocytes from neonatal rat heart cardiomyocytes[83].

Besides antioxidants, mitochondrial enzymes including endothelial nitric oxide synthase (eNOS) have been shown to convert DOX to unstable semiquinone which furthers the generation of ROS. Further studies have reported an increase in the transcription and activity of eNOS following DOX administration and have been reported to lead to H_2O_2 formation[84].

2.3.2.4.2 Alterations in gene expression and Inhibition of Cardiac energy homeostasis

DOX mediated cardiotoxicity has been shown to lead to reduction in contractility of the heart, which may be due to reduction in expression of cardiac muscle protein which explains myofibrillar loss observed in patients who develop cardiomyopathy upon DOX exposure. Some

of cardiac specific proteins which are a target of DOX is actin, myosin light and heavy chain, troponin I, sarcoplasmic reticulum proteins like Ca^{2+}-ATPase[85], RyR 2 and mitochondrial proteins creatinine kinase[86], ADP/ATP translocase, phospholamban and phospholipase A2[87]. Recent studies have reported GATA- 4[86], a cardiac specific transcription factor which aids in the synthesis of sarcomere and helps in regulation of cardiac specific genes MHC and troponin I thereby promoting cell survival, is a major target of DOX mediated ROS. DOX mediated reduction in GATA4 leads to myofibrillar loss, disruption of sarcomeres and reduced contractile function[86].

The heart requires constant ATP to perform cardiac relaxation and contraction. DOX is said to impair cardiac energy metabolism by inhibiting phosphocreatine-to-creatine (PCr/Cr) phosphocreatine-to-ATP (PCr)/ATP ratio[88]. Further DOX has also been reported to inhibit AMP activated Protein Kinase (AMPK) levels[89], which facilitates ATP production during nutrient deprivation, which in turn leads to decreased phosphorylation of anti-acetyl-CoA carboxylase (ACC), a downstream effector of AMPK, which further impairs fatty acid oxidation.

2.3.2.4.3 DOX regulation of HIF-1

One of the chief approaches that tumor cells utilize to resist chemotherapy is to exploit the genes involved in the homeostatic process that are activated as a normal adaptive response to help them survive better. Hypoxia Inducible Factor-1 (HIF-1) plays a critical role in the regulation of angiogenesis, homeostasis and anaerobic metabolism. HIF-1 is known to increase vascularization in the ischemic areas such as tumors and serves as transcription factor for several genes such as vascular endothelial growth factor (VEGF), p53, BNIP3, glucose transporters (GLUTs) etc. Studies have shown that DOX inhibited the transcriptional activity of HIF-1 by

blocking its binding to DNA in human prostate cancer cells and human hematoma[90]. Thus decrease in HIF-1 increases the sensitivity of ischemic tumor cells to DOX or hypoxia increases resistance of tumors to DOX. These studies suggest a combinatorial approach with chemotherapy and HIF-1 inhibition as potential target to ischemic tumor cells. Upon investigating the mechanism, studies have demonstrated that free radical species/ROS upregulate HIF-1 in tumors[91]. Further, contrasting studies have displayed DOX mediated HIF-1 accumulation and activation and accumulation during normoxia via STAT1 and iNOS signaling[92]. These studies call for therapeutic modalities that inhibit DOX mediated HIF-1 accumulation by usage of HIF-1 inhibitor or HIF-1 chelator.

2.3.2.4.4 Apoptosis

Apoptosis is a highly regulated and conserved process, crucial for normal homeostasis. The mechanism of DOX mediated apoptosis has been studied extensively in both acute and chronic cardiotoxicity[93]. Studies have demonstrated that DOX induced apoptosis is one of the major processes leading to deterioration of cardiac function (**Figure2.13**).

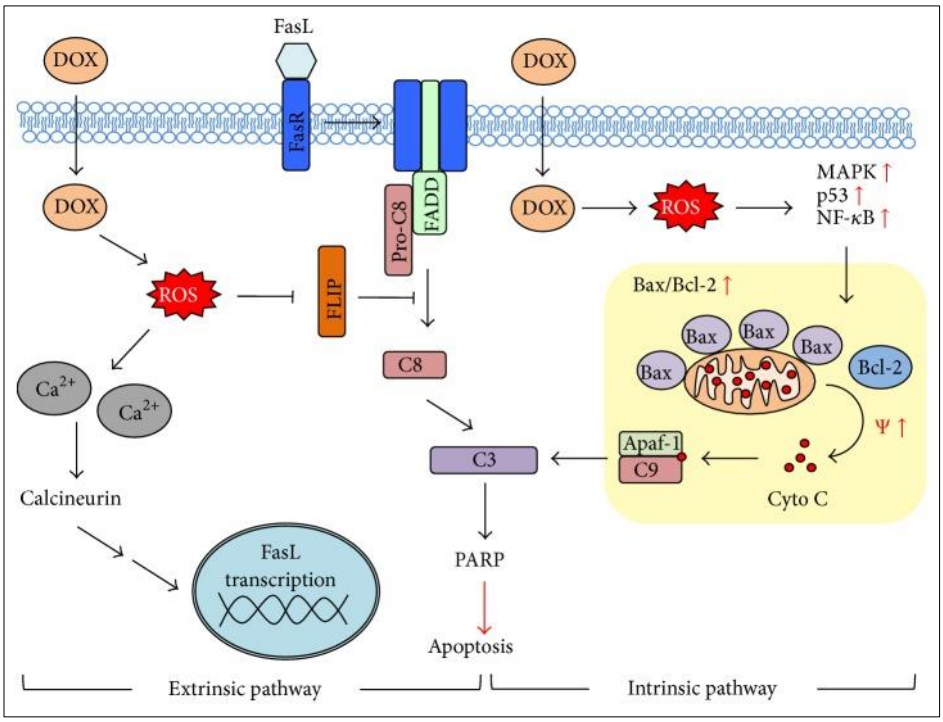

Oxid Med Cell Longev. 2015; 2015: 795602.

Figure. 2.12 DOX mediated apoptosis via ROS generation. DOX generates ROS which affects calcium homeostasis resulting in increased cytosolic calcium, which in turn activates calcineurin and increases transcription of Fas ligand (FasL). DOX mediated ROS activates p38 MAPK, JNK, and NF-κB and p53 accumulation leading to cytochrome c release, caspase 9 and 3 activation[86].

In isolated adult rat cardiomyocytes, treatment with DOX has shown to cause DNA fragmentation, nuclear chromatin condensation and cytoplasmic condensation leading to overall cell shrinkage. One of the common mediators of apoptosis observed in H9C2 rat cardiomyocyte cell line is the activation of cysteine proteases or caspases. Several studies have confirmed that

DOX induces an increase in apoptosis by facilitating cytochrome c release, a representative caspase activator, followed by upregulation of Bax which in turn promotes mitochondrial pore opening or down regulation of Bcl-$X_{L.}$ Myocyte cell death is attributed to DOX mediated ROS, which in turn activate multiple signaling pathways which promote apoptosis[94]. One of the critical determinants of apoptosis is the activation of p53, a tumor suppressor protein, which in turn leads to transcriptional activation or inhibition of genes such as mitogen activated protein Kinases (MAPK)[81, 95]. Previous studies have demonstrated that DOX induces apoptosis through activation of p38-MAPK and c-Jun N- terminal kinases [96] and further, inhibitors of p38 MAPK has been shown to prevent apoptosis (**Figure. 2.12**).

2.3.2.4.5 DOX mediates perturbations in calcium regulation

DOX has been known to disrupt calcium homeostasis[97]. One of the potential reasons has been shown to be due to change in iron homeostasis and defective ion pump caused by lipid peroxidation, which in turn activates a cascade of redox chain reaction that impairs the calcium ion channels. As discussed previously in this section, DOX has been shown to have direct effects on RyR2, SERCA2 leading to alterations in calcium homeostasis and subsequent impairment in contraction in the heart. DOX alters the function of sarcoplasmic reticulum (SR) calcium release channel by binding to the ryanodine receptor (RyR) complex[98]. DOX treatment was found to increase the binding of RyR to SR vesicle and increase its probability of mediating calcium induced open state of the channel (activated) and induces release of calcium from the SR vesicles [99].

Studies have shown that DOX increases the activity of voltage gated L- type calcium channel on the membrane[100] and another study has reported that DOX inhibited the Na^{2+}/Ca^{2+}

exchanger on sarcolemmal membrane, leading to calcium overload[101]. This increase in calcium overload may induce apoptosis through mitochondrial–caspase pathway or induce autophagy via the activation of calmodulin-dependent kinase and AMPK.

Some other studies have shown that increase in mitochondrial calcium overload and oxidative stress triggered the opening of mitochondrial permeability transition (MPT), resulting in loss of mitochondrial membrane potential, swelling reduced activity and consequent release of cytochrome c from mitochondria, indicating apoptosis[102].

Table 2.1: Mechanisms of DOX induced cardiotoxicity

Potential mechanisms involved in DOX cardiotoxicity	**Reference**
Lipid peroxidation	[103]
Inhibition of SR mediated Ca^{2+} release	[87]
Degradation of protein and nucleic acid synthesis	[104]
Phospholamban	[87]
Alterations in adrenergic and adenylate cyclase	[105]
ADP/ATP translocase, mitochondrial creatinine kinase	[106]

2.3.2.4.6 ECM modeling

The extracellular matrix (ECM) plays a major role in the adhering, aligning and orientation of cardiomyocytes, thereby facilitating a proper cellular contraction and smooth electrical transmission[107]. DOX mediated ROS has been shown to induce matrix

metalloproteases (MMP) for the degradation of ECM through activation of redox sensitive transcription factor NF-κB thereby causing impairment of cardiac function. Further studies in mouse and rats treated with DOX have demonstrated an increase in MMP-2 and MMP-9, which are involved in breakdown of ECM via p38 and MAPK and NADPH oxidase respectively. Also, DOX induced peroxynitrite (formed through induction of nitric oxide), leads to the inactivation of precursors of MMP and ECM degradation[108]. Overall mechanisms of DOX cardiotoxicity is tabulated in **Table 2.1.**

2.3.2.5 Secondary alcohol metabolites

The side chain C-13 carbonyl group of DOX is undergoes a 2 electron reduction via NADPH dependent aldo keto reductase that yields a secondary alcohol called doxorubicinol (DOXol) (**Figure. 2.13**). DOXol is said to be the primary circulating metabolite in patients and animals following treatments with DOX treatment. Pharmacokinetic studies indicate increased myocardial concentrations of DOXol and therefore indicate an increased participation in DOX cardiotoxicity[109].

The mechanism of DOXol mediated cardiotoxicity involves two mechanisms: (i) interfering in calcium handling and homeostasis and (ii) perturbations in iron homeostasis, especially by turning off the iron regulating proteins (IRP1)[110].

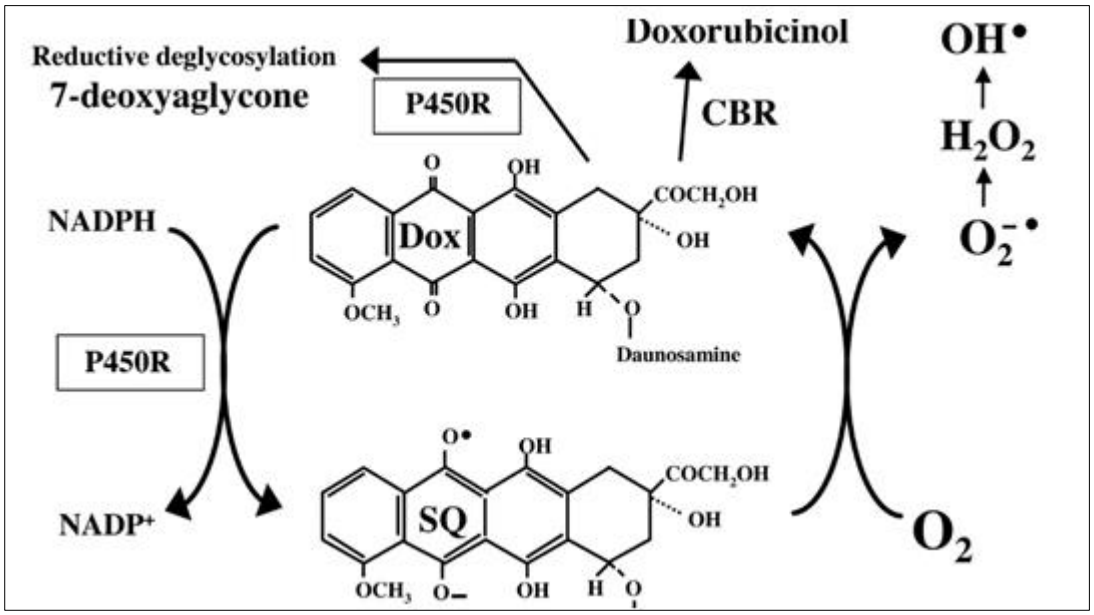

Drug Metab Dispos. 2005 Aug;33(8):1083-96.

Figure. 2.13 DOX is metabolized to DOXol by carbonyl reductase. DOXol may be involved in iron homeostasis, energy metabolism, calcium regulation, cardiac relaxation and contraction[111].

There is direct evidence to show that DOXol plays a major role in cardiotoxicity. Studies have shown that knockdown and overexpression of aldo keto reductase, which mediates the conversion of DOX to DOXol has resulted in reduced and increased cardiotoxicity respectively[112]

2.3.2.5.1 The role of iron in DOX cardiotoxicity

Free iron in most cardiomyocytes is “basal” or low in levels. In physiological conditions that ‘non-protein bound iron’ (also known as NPBI) does not exist as iron is usually sequestered

or bound to storage and transport or regulating proteins. However, several cases of free "labile" iron load or NPBI has been reported in cases high doses of chemotherapy regimen suggesting a dysfunction of iron transporter or iron regulating proteins to carry out iron homeostasis. Thus the NPBI or labile free iron is highly reactive and is capable of catalyzing the fenton chemical reaction (below), resulting in lipid peroxidation, DNA and protein damage and eventually apoptosis.

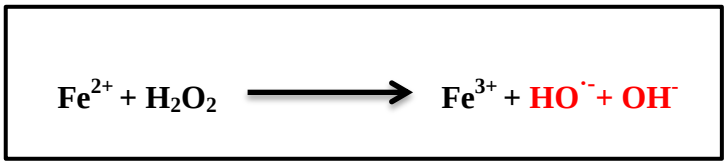

Fenton chemical reaction

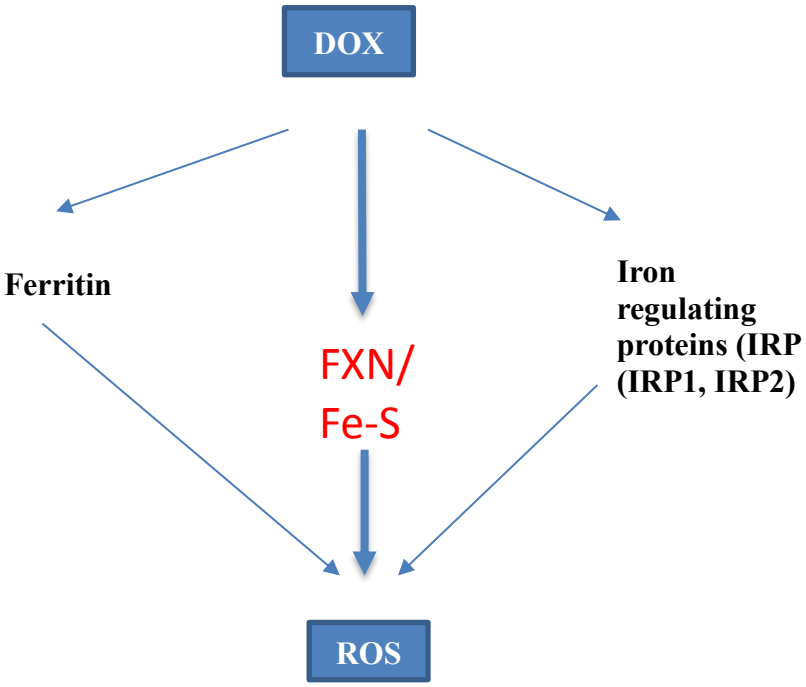

DOX alters several intra-cellular iron regulating proteins, leading to alterations in iron homeostasis which in turn contributes to ROS.

Several emerging studies have reported that the effects of DOX on iron homeostasis may not be induced by DOX-iron interactions, but may depend upon iron-sequestering intra-cellular proteins. Therefore it is imperative to understand the interaction and effect of DOX on intra cellular iron regulating proteins to determine the mechanism of DOX mediated cardiotoxicity in myocardial cells[65, 113].

2.4 DOX and Cellular iron homeostasis

Current findings indicate that DOX-iron interaction may not be the only reason for DOX mediated cardiotoxicity, but its interaction with intracellular iron controlling proteins also plays a major role in facilitating oxidative stress and cardiotoxicity. Studies by Dayie and colleagues have demonstrated that DOX binds 5' untranslated iron responsive element (IRE) of the iron controlling proteins using NMR and EMSA techniques[114]. The formation of IRE/IRP complex prevents ribosome assembly and prevents translation of iron storage proteins such as ferritin.

2.4.1 Regulation of intracellular iron

The labile iron pool controls the activity of iron regulating proteins (IRP), namely IRP1 and IRP2. The IRPs are RNA- binding proteins that bind the Iron response element (IRE), in the 3'

and 5’ untranslated region in mRNA of proteins that play a crucial role in transport, regulation and storage such as transferrin and ferritin.

The IRP-IRE binding signals when the iron is severely low. IRP1 plays a dual role by (i) regulating iron homeostasis by binding the IRE in the presence of excess iron and (ii) displaying aconitase activity in the cytosol. The IRP1 switch contains a 4Fe-4S cluster unit which controls its activity. The IRP2 is a major RNA binding protein found in vivo and undergoes proteasomal degradation in the presence of iron.

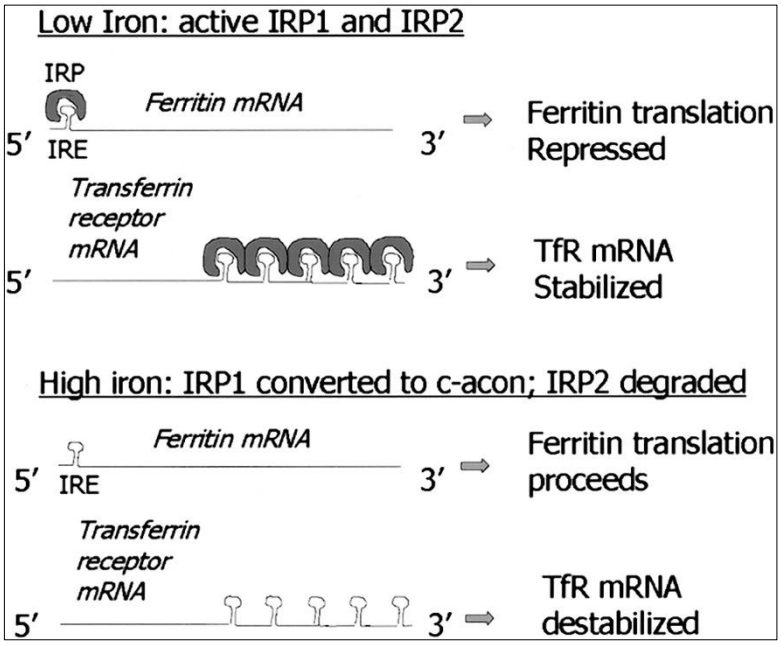

Blood 2002 99:3505-3516; doi:10.1182/blood.V99.10.3505

Figure 2.14: The IRE/IRP mediated iron regulation.

The IRP-IRE transcriptional regulatory circuit plays a major role in the regulation of iron homeostasis. It is known that transferrin and ferritin are regulated by iron at the translational level by the interaction of IRP to the specific mRNA. There have been reports of IRP1 activation

in FRDA models and in FXN knock out models as the cell senses when the cytosolic iron levels are depleted and activates IRP regulating proteins such as TfR[113].

2.4.2 DOX and IRP

Until recently, it is not completely understood how a labile pool of free iron is formed within cardiomyocyte. Previously it was established that immediately after uptake into cells, iron is incorporated into the iron sequestering ferritin, following which it is distributed into cellular components[113].

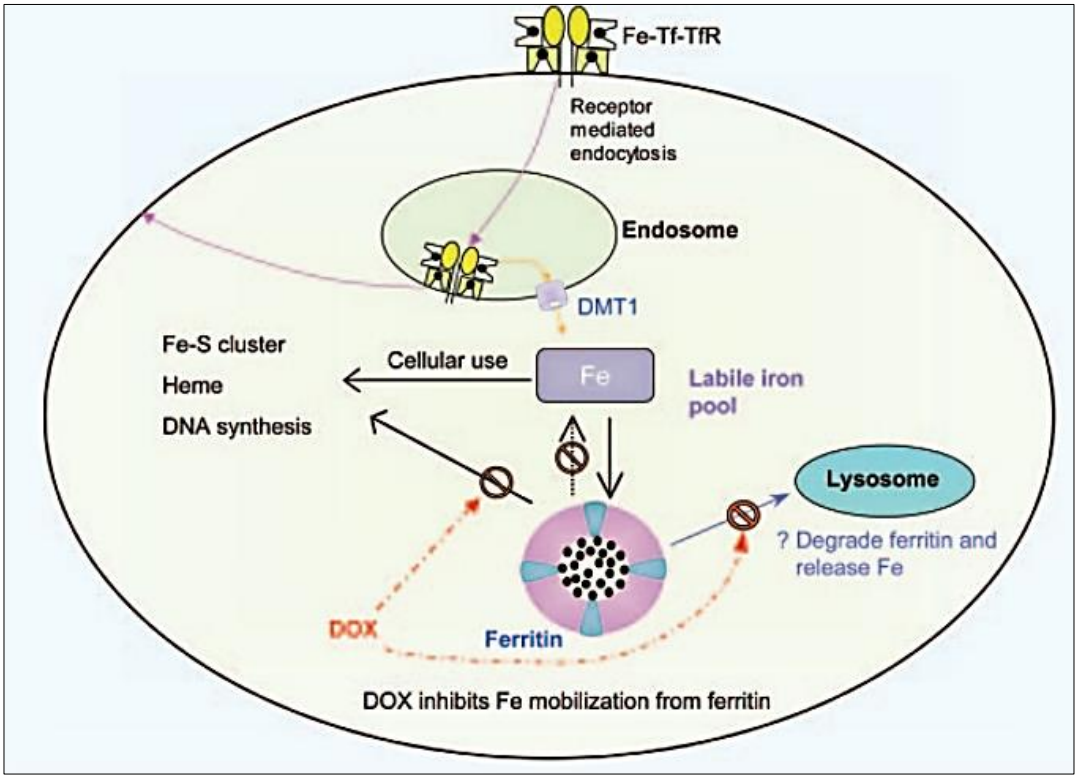

Molecular Pharmacology ***August 2005*** *vol. 68 no. 2****261-271***

Figure. 2.15: Effect of DOX on cellular iron metabolism. DOX inhibits iron release from ferritin which results in increase accumulation of iron and failure to distribute iron to the essential metabolic processes such as ISC synthesis[68].

Conflicting evidence exists that suggests different roles of DOX in the mechanism of iron mishandling from ferritin. One study demonstrated the release of toxic Fe^{2+} ferritin in the presence of $O_2^{\cdot-}$ and semiquinone (**Figure. 2.16**). Paradoxically, alternative study demonstrated that DOX lead to increased ferritin accumulation of iron, resulting in decreased iron release. Another study conducted in bovine aortic endothelial cells demonstrated an important

association between transferrin receptor mediated iron influx and DOX mediated ROS and the consequent apoptosis[115].

These reports suggest a void in understanding the mechanisms involved in alterations of iron regulation induced by DOX.

2.4.3 Mitochondrial iron homeostasis

Cells utilize mitochondrial iron for the synthesis of heme and iron sulfur clusters. Although the mechanism of intracellular iron trafficking is not completely understood, there are several factors that are widely known to be involved in transporting, regulating and storing iron within the mitochondria.

- Mitochondrial ferritin (mtFt) – Although it is known to bind iron, its role is questionable in the heart due to its distribution pattern. It is found in abundance in erythroblasts of sideroblastic anemia patients and in testes and less in the heart. Overexpression of mtFt has shown to lead to increased IRP1 RNA binding activity which led to reduced aconitase activity and ISC synthesis, increased TfR1 expression and consequent increased iron overload[116, 117].
- Transferrin – Transferrin receptor mediates iron uptake in the heart by facilitating receptor mediated endocytosis of iron bound to Tfr. Mice lacking Tfr in the heart displayed inactive ISC biogenesis due to iron deficiency and mitochondrial dysfunction which further led to poor cardiac function, impaired mitochondrial respiration and ineffective mitophagy[117, 118].

- ATP Binding Cassette protein B8 (ABCB8) – this mitochondrial inner membrane protein is an ATP dependent transporter that facilitates the export of iron to maintain iron homeostasis. An ABCB8 knock out mouse model has shown to develop cardiomyopathy and iron accumulation [119].

2.4.4 Iron Sulfur Cluster

Iron sulfur clusters are essential to perform numerous biological functions, including respiration and various enzymatic functions. Mitochondria play a major role in the synthesis of ISC. ISC consists of two or more atoms of iron bridged with sulfur anions to form a [2Fe-2S] or [4Fe-4S] clusters. Several iron sulfur proteins contain ISC which is essential for the structure, function and stability. These clusters act as prosthetic groups or cofactors in in electron transport chain, redox reaction and many other functions. While most clusters exist as [2Fe-2S] group and bound to protein backbone via the cysteine bridges, others exist as [4Fe-4S] type consisting of cubane structure bound to protein backbone via the cysteine residues.

It has been proven in several models that iron delivery of the ISC is delivered by the protein Frataxin (FXN) and sulfur by cysteine desulfurase (NFS1). Besides these, other genes such as LYR motif containing 4 protein or ISD11 have also been implicated in the formation of ISC. siRNA studies have demonstrated that complete depletion of ISC genes such as NFS1, FXN and ISCU can lead to inactivation of various metabolic enzymes such as aconitase and xanthine oxidase, cause dyshomeostasis of iron and reduce cell viability. Therefore inactivation of ISC is deleterious to human health.

2.4.5 The role of Frataxin (FXN) in mitochondria

FXN is a nuclear encoded mitochondrial protein conserved in prokaryotes and eukaryotes. FXN mRNA is predominantly expressed in tissues with high metabolic rate such as liver, heart, kidney and neurons[120, 121]. Although the exact role of this protein is unknown, FXN has been associated with several functions, including (i) maintenance of iron homeostasis, (ii) mitochondrial energy regulation and oxidative phosphorylation, (iii) biogenesis of ISC assembly, iv) heme synthesis and (v) ROS prevention and protection against oxidative insult[122] (**Figure. 2.17**). Some studies have also suggested a possible role of iron storage molecule, antioxidant and as a tumor suppressor[123]. FXN has been shown to be involved in the biogenesis of ISC by physical interaction with NFs1/Iscu1[124]. Further RNAi of FXN in HeLa cells demonstrated a reduction in the ISC containing mitochondrial aconitase and succinate dehydrogenase thereby confirming the pivotal role of FXN in the mitochondrial metabolic regulation[125].

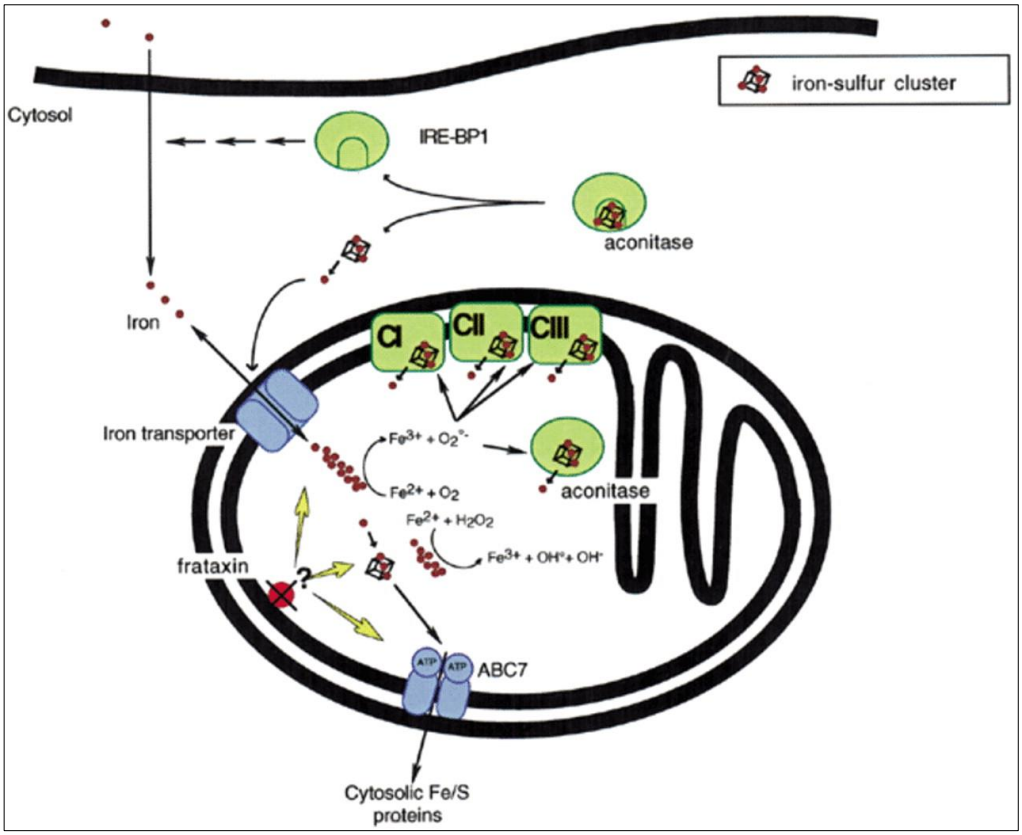

Hum Mol Genet. 2000 Apr 12;9(6):887-92.

Figure. 2.16: Frataxin regulates iron homeostasis in the mitochondria. Disruption of FXN results in inactivation of Fe-S proteins in respiratory chain complexes, aconitase and succinate dehydrogenase activities and loss of cytosolic Fe-S results in activation of Iron response element binding protein (IRE-BP)[126].

Studies conducted Bulteau et al. demonstrated a citrate dependent modulation in aconitase in response to pro-oxidants. These studies further demonstrate that FXN reduced the oxidant mediated inactivation of aconitase and converted the inactive [3Fe-4S] to active [4Fe-4S]

form[127]. Therefore FXN was known to act as an ‘iron chaperone’ that protects the ISC containing proteins from disassembly.

Severe depletion of iron homeostasis occurs when FXN is depleted or impaired where severe ‘labile’ free iron was trapped within the mitochondria, in contrast to iron scarcity[128]. This explains the inability of the mitochondria to buffer iron in the absence of FXN and the inability of mitochondria to utilize this excess iron for major biosynthetic processes such as ISC biogenesis, heme synthesis and lastly the inability to signal to the iron sensing machinery that there is excess iron.

2.4.5.1 FXN and interacting partners

Growing evidence demonstrates the critical role of FXN in the ISC biogenesis. Microarray analysis in human cells has demonstrated that FXN depletion impairs ISC and ISC related select transcripts. FXN is known to interact with mitochondrial ISC assembly components, ISCU and cysteine desulfurase Nfs1 and ISD11. Mass spectrometry analysis identified 4 proteins ISCU, NFS1, ISD11 and βMPP that demonstrated co-ip with human flag tagged FXN. Interaction with NFS1 and ISCU was also confirmed by western analysis.

FXN has also observed to interact with mitochondrial heat shock protein 70 (HSP70) or GRP75, which aids in the biogenesis of ISC and transfer of ISC to ISC requiring proteins.

2.4.5.2 FXN maturation

Studies by Koutnikova et al. have identified a mitochondrial targeting sequence in the N terminal domain of mouse and yeast FXN homologue and disruption of this gene led to mitochondrial dysfunction. The sequence alignment of FXN displays two distinct regions, an N

terminal block of 70-90 residues which is poorly conserved in eukaryotes and absent in prokaryotes and a C terminus consists of 100-120 conserved amino acids. The human FXN is synthesized as a 210 amino acid precursor, imported into the mitochondria and undergoes maturation by enzyme mitochondrial processing peptidase (MPP), through a two-step maturation process. The first maturation leads to an intermediate form (42-210 amino aicds) of ~20KDa following an additional cleavage which results in the production of mature form of 18KDa in mouse and humans.

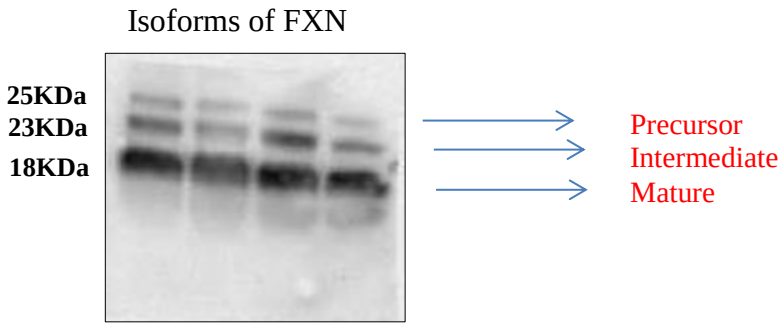

Figure. 2.17 FXN Maturation observed in H9C2 cardiomyoblasts. Precursor was observed to be 25KDa, Intermediate at 23KDa and Mature at 18KDa.

2.4.5.3 Friedreich's ataxia (FRDA)

Friedreich's Ataxia is caused by the loss of function of FXN due to impaired transcriptional activity of FXN gene[129]. Patients display a marked reduction in FXN mRNA, protein in the affected individuals ranging from 4%-29% of normal levels. Healthy asymptomatic carriers produce 50% compared to healthy people. The major neurological signs are limb and gait ataxia, tendon areflexia, dysarthria and sensory loss, degeneration of dorsal root

ganglia, peripheral nerves and spinal cord. Some patients develop skeletal deformities, ocular abnormalities, hearing loss, diabetes[130]. Cardiomyopathy is commonly observed in several FRDA patients, leading to death before the age of 50. Patients with FRDA develop severely hypertrophied myocardium with eccentric or concentric distribution, severe fibrosis and cardiomyocyte loss at the time of death[131]. Intra mitochondrial iron deposits have been observed in the muscle creatinine kinase (MCK) heart and muscle specific knock outs and in yeast artificial chromosome mouse model followed by ISC requiring enzyme impairments[132].

2.4.5.3 Transcriptional silencing in FRDA

FRDA is caused by the homozygous expansion of trinucleotide guanine-adenine-adenine (GAA) repeats within the first intron of the FXN gene, coding for FXN. GAA expansions ranging from 70-1000 result in 'sticky' DNA and epigenetic changes which impairs the transcription of FXN.

Although the exact mechanism for the Friedreich's Ataxia has not been proposed, two hypotheses have been currently prevailing[133]:

1. One is the formation of NON-B DNA structures which can occur due to a sticky DNA (formed by the association of two purine, purine, pyrimidine (R.R.Y) in a triplex in a supercoiled plasmid) or triplex structures which is known to interfere with nascent transcription process. Until date, it is not proven whether or not it is directly involved in the inhibition of FXN mRNA transcription, inhibiting the RNA polymerase II binding and thereby reducing the FXN gene transcription.
2. Second is that the GAA .TTC expansion can produce heterochromatin based gene silencing effects. The intronic GAA .TTC expansion results in condensation of gene into a chromatin

called as heterochromatin which blocks the reading of the gene into an mRNA. This results in the reduction of FXN protein production (**Figure 2.19).**

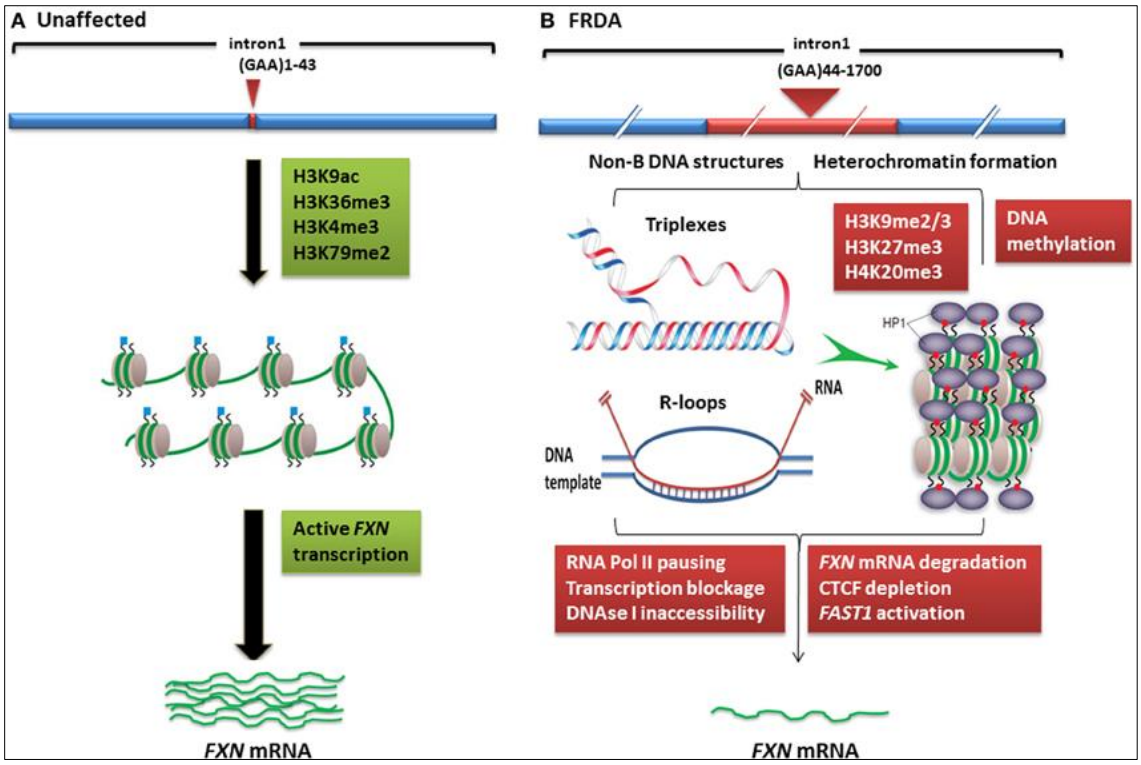

Front. Genet., 03 June 2014 | http://dx.doi.org/10.3389/fgene.2014.00165

Figure 2.18 Frataxin gene silencing in FRDA. (A) Unaffected individuals who carry upto 43 GAA repeats contain normal gene transcription initiation and elongation at FXN promoter region. (B) FRDA patients are characterized by large GAA repeats leading to FXN gene silencing by (i) adopting a non-B DNA structure which impede RNA polymerase and FXN gene transcription or (ii) increased DNA methylation with elevated levels of heterochromatin formation hp1 trigger heterochromatin formation leading to FXN gene silencing.

Studies have reported correlation between the GAA repeats and the onset and severity of symptoms[134]. The higher number of repeats is associated with earlier onset and severe cardiomyopathy.

2.4.5.4 Currently used therapeutic modulators on FRDA patients*:*

There are no effective treatments or cure for FRDA. However there have been remedies for symptoms and its associated complications which can prolong the disorder. Complications such as diabetes and heart problems may be treated with medications. The current research funded by National Institute of Neurological Disorders and Stroke (NINDS) is trying to understand the metabolic abnormalities in mitochondrial of FRDA patients[135]. The current research is aimed at understanding the cellular and molecular changes that are involved in the inactivation of the gene.

2.4.5.5 Epigenetic mechanisms – Histone Deacetylase inhibitors (HDACi)

Hyper expanded GAA repeats in case of FRDA adopt a heterochromatin structure that have high levels of di and tri methylated levels of lysine 9 of histone 3 and under (hypo) acetylated histones at H3 and H4[136]. Therefore, altering histone modification i.e., acetylation in particular, can improve FXN levels to an extent, thereby bringing the use of histone deacetylase inhibitors or (HDACi) (**Figure. 2.20).**

Histone deacetylation mechanism:

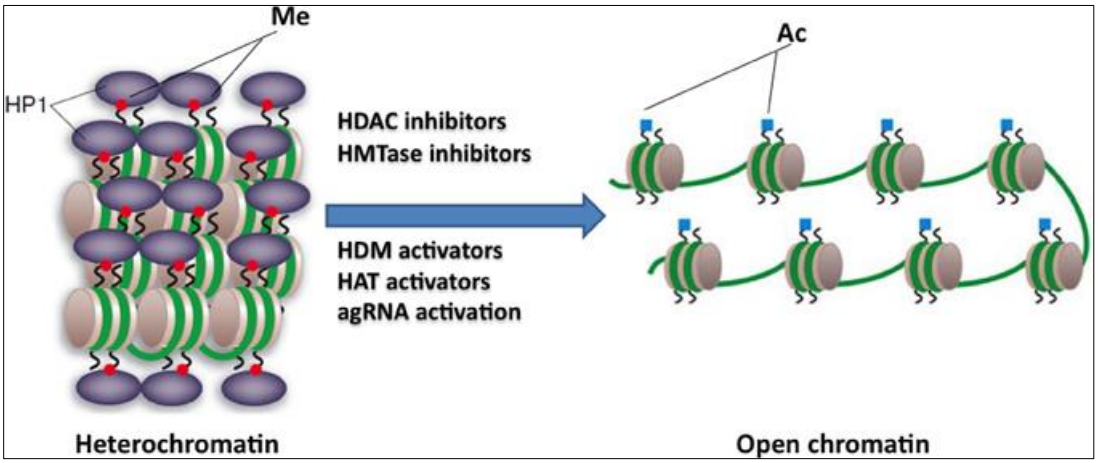

Front. Genet., 03 June 2014 | http://dx.doi.org/10.3389/fgene.2014.00165

Figure 2.19: HDAC mechanism. The use of HDAC inhibitors, histone demethylases activators (HDM) activators, histone acetyltransferases (HAT) activators and histone methyltransferases (HMTase) inhibitors reverses the heterochromatin formation and leads to a more open chromatin leading to FXN gene activation[137].

The role of HDAC causes the silencing of genes (prevents from expression), by removing the acetyl groups from the lysine residues from the histone proteins, creating a positive charge which in turn causes the DNA (negative charged) to supercoil tightly and restrict the chromatin structure. In addition to this, it is also known that they cause deacetylation of the acetylated lysine, thereby inhibiting the RNA polymerase II to inhibit transcription process.

HDACi:

As of 2014 the U.S FDA has approved two HDACi,

- Suberoylanilide hydroxyamic acid or SAHA (Vorinostat, Zolinza^{TM}) in 2006[138] and
- FK228 (Romidepsin, Istodax^{TM}) [139]

Besides this, 18 HDACs have been identified in the human genome, including Zn++ binding HDAC (Class I, II and IV) and NAD^+ protein deacetylase enzymes (HDAC Class III and SIRTs), and the most recent, Pimelic Diphenylamide, a class I HDAC inhibitor (as investigated on 2010)**[140].**

- **Compound 106 and compound 109 –** these were tested in FRDA mouse models and in KIKI mice model [141]

Advantages of the compound 106 & compound 109:

- Slow-on and slow-off kinetics leading to persistent hypoacetylation over the FDA approved SAHA.
- Displayed higher potency and specificity for HDAC3, displayed by compound 109.
- Improved (4-fold to 9-fold) increase in FXN mRNA and protein levels, lasting for more than 48 hours of dosing[141].

Known limitations and possible drawbacks of HDACi:

The common side effects observed during the administration of SAHA, were systemic and gastrointestinal effects including, nausea, diarrhea and other serious effects including: anemia, hypotension, sepsis, and pulmonary embolism. Similarly, low-dose effects including lymphopenia, leucopenia, thrombocytopenia and other adverse effects such as changes in ECG, in 71% patients were observed in patients administered with FK228[142].

Cardiotoxicity associated with HDACi

HDACi such as SAHA and Romdepsin have serious cardiotoxic side effects including prolonged QT interval (QT interval prolongation <30-60ms) in 63% patients administered with Romidepsin leading to fatal ventricular arrhythmia.

Although compound 109 and compound 106 have been tested in FRDA mouse models for potency and efficacy and have known to improve FXN mRNA levels, these drugs are currently under FDA clinical trials for gaining approval[141]. Other compounds like nitropropionic acid displayed significant improvement in FXN and HDACi BML 210 displayed improved FXN levels in homozygous knock in mouse with GAA_{230} repeats and was known to be a promising molecule for the treatment of FRDA[143]. However, these drugs display mitochondrial toxicity. Recombinant erythropoietin (rhu-EPO) although displayed increased protein levels in FXN demonstrated no change in gene levels.

Antioxidants

Since FXN depletion generates increased free radicals and oxidative stress resulting in the usage of antioxidants which may thus serve as a potential therapeutic in FRDA. CoQ and vitamin E are currently the best studied antioxidants in FRDA[144]. In a study consisting of 10 patients administered 2100 IU/day vitamin and 400 mg/day CoQ10 demonstrated improvement in cardiac bioenergetics but did not reduce cardiomyopathy[144]. Idebenone, analogue of CoQ was first tested on FRDA patients as a potential treatment. They demonstrated protective effects by reducing heart size in about 3 children with hypertrophic cardiomyopathy and reduced iron mediated toxicity and lipid peroxidation in patients[144, 145].

Iron chelation

The basic goal of iron chelator used to treat FRDA is to not increase overall iron but to be able to redistribute the cellular iron that is accumulated in the mitochondria towards the iron depleted cytosolic compartments thereby activating ISC and maintaining iron levels.

Desferoxamine (DFX) cannot be administered orally due to its poor membrane penetration[146]. Although it diminishes iron mediated toxicity it was found to reduce mitochondrial and cytosolic aconitase activities[147]. Deferiprone (DFO) was used as a potential therapeutic for FRDA but FRDA patients demonstrated agranulocytosis, which requires monitoring of blood count[148]. Together, iron chelators may be a good choice but it did not improve FXN levels and with higher doses it may even downregulate FXN levels.

2.5 Ubiquitination and proteasome degradation System (UPS)

All intracellular and extracellular proteins undergo turn over, i.e., they are hydrolyzed to their amino acids and are replaced by synthesis of new ones. The rates of protein synthesis and degradation must be balanced because a small upsurge in the synthesis or breakdown of important functional proteins compared to its normal synthesis rate will lead loss of mass in the organism. Majority of intracellular proteins are degraded by ubiquitination proteosomal pathway[149].

The UPS pathway consists of intensive actions of enzymes that link the polypeptide co-factor, ubiquitin on to the necessary proteins targeting them for degradation. The tagging process leads to the recognition of the protease complex, 26S proteasome that degrades the ubiquitinated proteins. The three enzymes that are involved in the process of ubiquitination and degradation are:

- E1 - Ub-activating enzyme
- E2 - Ub- carrier or conjugating protein prepares Ub for conjugation
- E3- Ub- protein ligase

E1 activates the glycine residue at the C terminus of the ubiquitin in an ATP dependent manner with the formation of thiol ester bond between the C-terminus and the E1. A sequential thio-ester linkage is formed between the C terminus of the ubiquitin and the cysteine groups of E2 and E3 enzymes. This thiol ester linkage culminates into an isopeptide linkage between the C terminus of the ubiquitin and the ε amino group of a lysine on the target protein or within the ubiquitin chain, resulting in the formation of chain of ubiquitin. The formation of K48 polyubiquitin chains on protein comprises the targeting signal for recognition and degradation by 26S proteasomes. After ubiquitination, the polyubiquitinated protein is recognized and degraded by the proteasome[150](**Figure 2.21**).

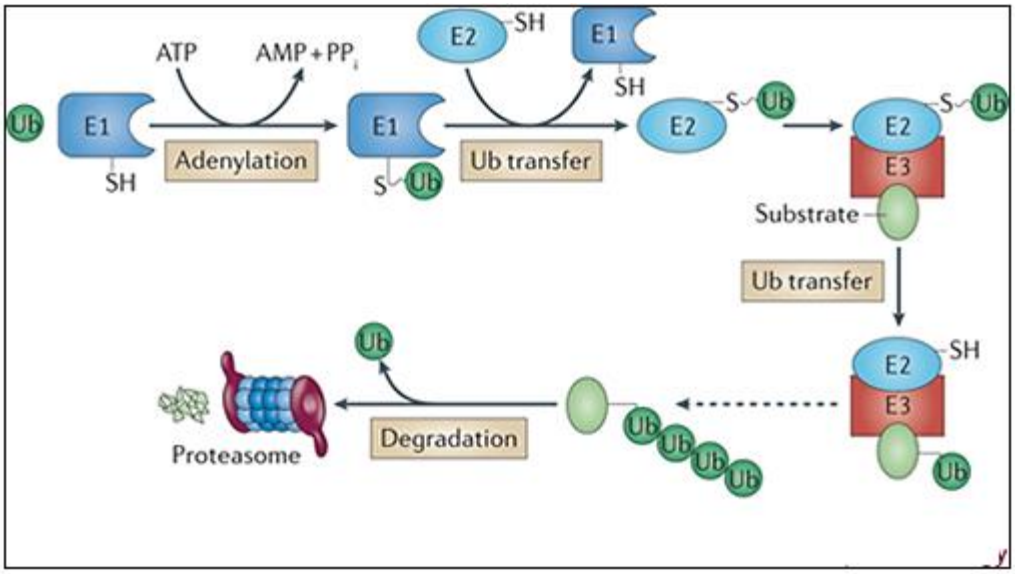

https://blogs.shu.edu/cancer/2015/09/30/ubiquitin-proteasome-system-targeting-for-cancer-nurix-and-celgene/

Figure 2.20 Ubiquitination signaling. Ubiquitinylation signals the 26 proteosome by initiating a cascade of E1 ubiquitin activating, E2 ubiquitin conjugating and E3 ubiquitin ligase enzymes.

Ubiquitination is removed by deubqiuitylating (DUB) enzymes that remove Ub from proteins yielding monomeric proteins. Ub conjugation to proteins are removed or reversed by the intracellular DUBs. Therefore the UPS plays a major role in the maintaining cellular and components of cellular quality control, regulation of transcription, cell cycle and autophagy and any acceleration or interruption of the UPS leads to deleterious consequence in the function of various cellular processes.

2.5.1 The significance of E3 ligases in the UPS

E3 determines the specificity of substrate and plays a major role in the ubiquitination mechanism. There are >1000 E3 ligases which participate in linking the Ub to proteins. They facilitate the transfer of activated Ub from E2 to the lysine on the protein and subsequently to the lysine residues within the Ub.

The majority of E3 contain a RING finger domain. They function as important scaffolds which bring together the target substrate and E2 for Ub conjugation. Some RING finger E3 include,

- Oncoprotein Mdm2, a regulator of p53 which targets it for proteasomal degradation,
- c-Cbl – catalyzes ubiquitination of cell surface receptors
- MuRF-1 (Muscle Specific RING finger proteins) and E3α – Muscle atrophy
- F-box protein atrogin 1/ MAFbx expressed highly in atrophic cardiac and skeletal muscle
- C-terminal of HSP-70- interacting protein (CHIP) helps in the removal of abnormal and misfolded proteins[151].

2.5.2 Preventing of UPS and stabilization of FXN

Most therapeutic approaches aim at inhibiting mitochondrial dysfunction by the addition of iron chelator and/or antioxidants which neither improves nor stabilizes the intra cellular FXN levels. One of the approaches to stabilize FXN expression by preventing ubiquitination mediated degradation of FXN protein which postpones the disease progression.

However recent years have observed the identification of several E3 ligases which are found on the outer membrane of the mitochondria which has opened new avenues to understand the mechanism of protein dynamics and quality control. Previous studies by Ruffini et. al, have demonstrated the accumulation of both the precursor and mature forms upon proteasome inhibition. Lysine residues on the protein are markers for ubiquitin mediated degradation by the covalent attachment of ubiquitin molecules. This event marks the process of degradation of protein in the proteasome. Studies conducted by Rufini et al. targeted the alleged ubiquitination site of FXN at K147 by utilizing ubiquitin analogues as competing molecules to target lysine residues which prevented degradation of FXN thereby elevating its expression[24].

2.5.2.1 K147 – Ubiquitination target site of FXN

Prediction and identification of lysine ubiquitination/polyubiquitinaiton sites in proteins is a challenging task is very important to understand the molecular mechanisms of ubiquitination mediated proteasomal degradation (**Figure. 2.22**). Conventional methods such as site-directed mutagenesis and high throughput screening by mass spectrometry have been employed to predict and identify the possible ubiquitination site.

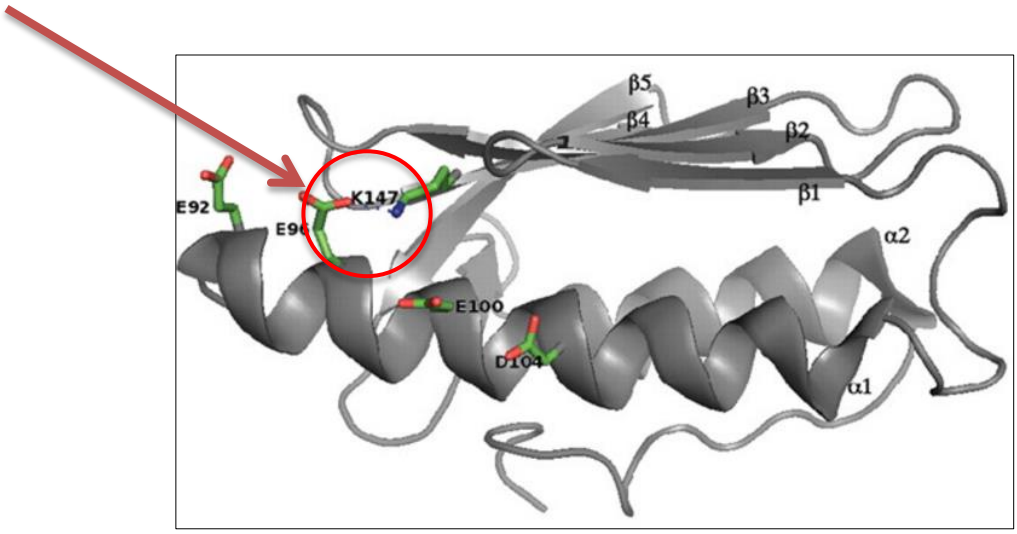

Hum Mol Genet. 2011 Apr 1;20(7):1253-61. doi: 10.1093/hmg/ddq566. Epub 2011 Jan 7

Figure. 2.21 K147 site in FXN. Ruffini et al. have demonstrated Lysine 147 residue (K147) as a potential ubiquitination and degradation site of FXN that is conserved across species [24].

FXN contains 13 lysine residues which are possible ubiquitination sites where K147 was identified as a target site for ubiquitination and was found to be the most conserved across species[24]. The FXN mutant that lacked this site was not ubiquitinated and demonstrated more stability.

2.5.3 DOX mediates proteasome degradation in cardiomyocytes

In GFPdgn transgenic mice, constructed by fusing the ubiquitination signal sequence or degradation sequence called degron to the C terminus of GFP, treatment with DOX at 25 mg/kg

demonstrated a decreased protein levels which indicated enhanced the proteolytic function. Similar results were observed *in vitro* and *in vivo* where DOX treatment demonstrated an increase in proteolytic activity in a dose dependent fashion. In order to understand the mechanism that contributed to the enhanced proteolytic function, several hypothesis were considered. Treatment with DOX increased the production of ROS which in turn led to increase in oxidized proteins[152]. These oxidized proteins may indirectly activate the UPS. In addition, DOX has been suggested to activate ubiquitination directly or the proteasome complex directly and to support this rationale, DOX treatment was found to demonstrate an increase in chymotrypsin like activity in 20S proteasome. Another study demonstrated an increase in phosphorylation of proteasome subunits and an increase in chymotrypsin like activity in 26s proteasome. These experiments led us to believe that DOX initiated a direct effect on the proteasome. However the mechanism by which DOX activates the proteasome system is not known[153].

2.5.4 DOX mediates activation of UPS

DOX has been observed to cause an increase in the proteasomal degradation by increasing key regulatory enzymes involved in the proteosomal degradation process. In this process, DOX treatment has been demonstrated to increase several ubiquitin E3 ligases which further activate proteasome degradation process[22, 151].

2.5.4.1 Stimulation of E3 ligases by DOX contributes to cardiotoxicity

Most intra cellular proteins that are polyubiquitinated needs to be degraded by the 26S proteasome system. Studies conducted by Ranek et al. demonstrated that DOX mediated an

increase in muscle specific E3 ligases such as atrogin-1 and muRF significantly contributed to the development of cardiomyocyte atrophy[22].

DOX treatment led to increase in the mRNA and protein levels of atrogin-1 via p38 MAPK which in turn led to cardiac hypertrophy. Further the significance of these findings was confirmed by overexpressing atrogin-1 that displayed cardiac hypertrophy[154] (**Figure. 2.23**).

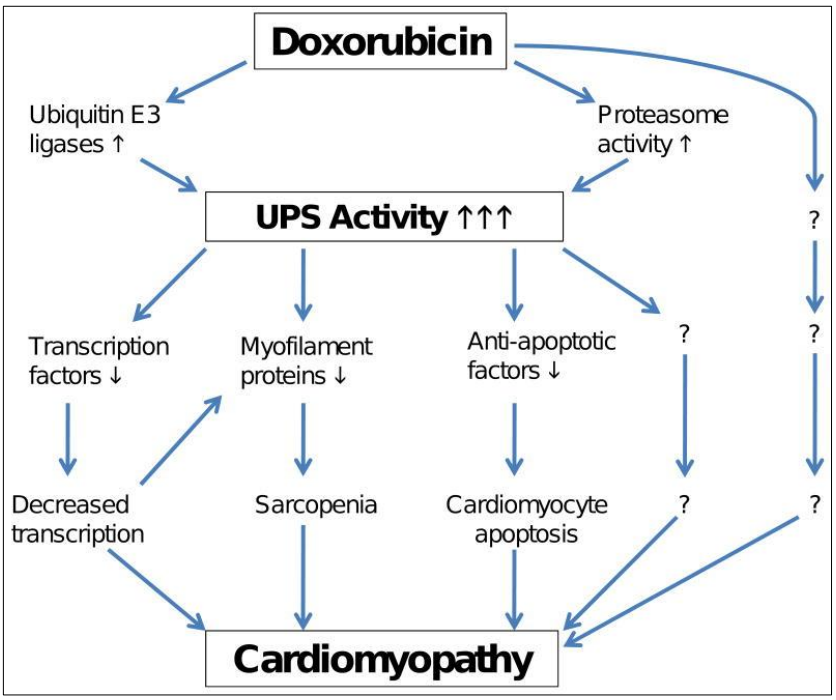

Curr Hypertens Rep. 2009 Dec; 11(6): 389–395.

Figure 2.22 Potential pathways by which DOX induced upregulation of UPS pathway leads to cardiomyopathy

The CHIP protein is a U box containing E3 ligase and a co-chaperone of Heat Shock Protein (HSP) 70. DOX treatment led to an increase in CHIP, which was accompanied by HSP70 depletion with HSP70 being a major substrate for CHIP E3 ligase. Although DOX mediated

increase in CHIP could improve the cell's capability to remove dysfunctional proteins, the decrease in HSP70 reduces the cell's ability to adapt to oxidative stress and thereby contributes to DOX cardiotoxicity[22].

2.5.5 DOX mediated stimulation of forkhead–box O (FoxO) target genes

The Forkhead family of transcription factors functions as a major regulator of muscle mass through the regulation of its select target E3 ubiquitin ligases such as MuRF-1, Atrogin-1/MaFbx and BNIP3. Further activation of cardiac proteolytic system has been attributed to the activation of FoxO mediated upregulation of E3 ubiquitin ligases.

Studies by Kavazis et al. have demonstrated that DOX administration displayed an increase in the mRNA transcripts of FoxO1 and FoxO3, found abundantly in heart, which subsequently caused an elevation in its select target genes including MaFbx, MuRF-1 and BCL2/adenovirus E1B 19KDa protein-interacting protein 3 (BNIP3). However, there have been several contradicting studies which have an opposing result[22]. One study demonstrated that constitutively active FoxO3a in cardiomyocytes displayed negative regulated hypertrophic growth[155]. This was supported by another study which displayed that reduction in cardiomyocyte size following transfection of FoxO3a which caused an increase in E3 ligases. Therefore there are controversial and contradicting observations on the role of ubiquitin E3 ligases and its role in cardiac hypertrophy.

In coherence with these findings our ongoing research indicates that treatment with DOX may induce post translational ubiquitination and degradation of FXN. The findings from this study are very preliminary and will be formulated into a manuscript.

2.6 The role of PPAR in mitochondrial energy metabolism

Peroxisome proliferator-activated receptors are a group of nuclear hormone receptors that function as ligand activated transcription factors that regulate the expression of several genes. PPARs play a major role in several physiological and pathological processes involved in energy homeostasis. They form heterodimers with retinoid X receptor and bind to PPAR responsive element (PPRE) in the regulatory region of specific target gene that play major role in several diverse processes such as adipogenesis, lipid metabolism, insulin sensitivity, cell growth and differentiation. PPARs also play a major role in several metabolic syndromes including insulin resistance, glucose intolerance, obesity, atherosclerosis and hypertension[156].
PPARs contain 3 isoforms, PPARα, PPARβ/δ and PPARγ.

2.6.1 PPARα and heart

PPARα are abundantly found in the liver, brown adipose tissue, heart and kidney. The class of PPARα ligands is called thiazolidinediones (TZD), rosiglitazone and pioglitazone have been shown to improve glycemic control and have been used in patients with type 2 diabetes. Synthetic PPARα agonists such as fenofibrate and clinofibrate are clinically approved lipid lowering drugs. PPARα is abundantly found in the heart where it plays a major role in cardiac metabolic homeostasis by regulating several key enzymes involved in fatty acid oxidation. This was confirmed when PPARα null mice demonstrated decrease fatty acid oxidation genes and reduced fatty acid oxidation rate[156].

2.6.2 PPARγ and heart

PPARγ a master regulator of adipogenesis and regulates many genes involved in metabolic homeostasis and tissue function. Hepatic PPARγ expression has been found to increase in obese and diabetic models. However in the heart increase in PPARγ lead to metabolic disturbances which contributed to cardiomyopathy. Human and mouse ventricular samples of cardiac hypertrophy displayed increased levels of HIFα and PPARγ. Further these studies demonstrated that under hypertrophy, HIF1α lead to increase in PPARγ expressions which in turn lead to ectopic lipid accumulation, apoptosis and cardiovascular diseases. Further another studies that overexpressed PPARγ demonstrated dilated cardiomyopathy[157].

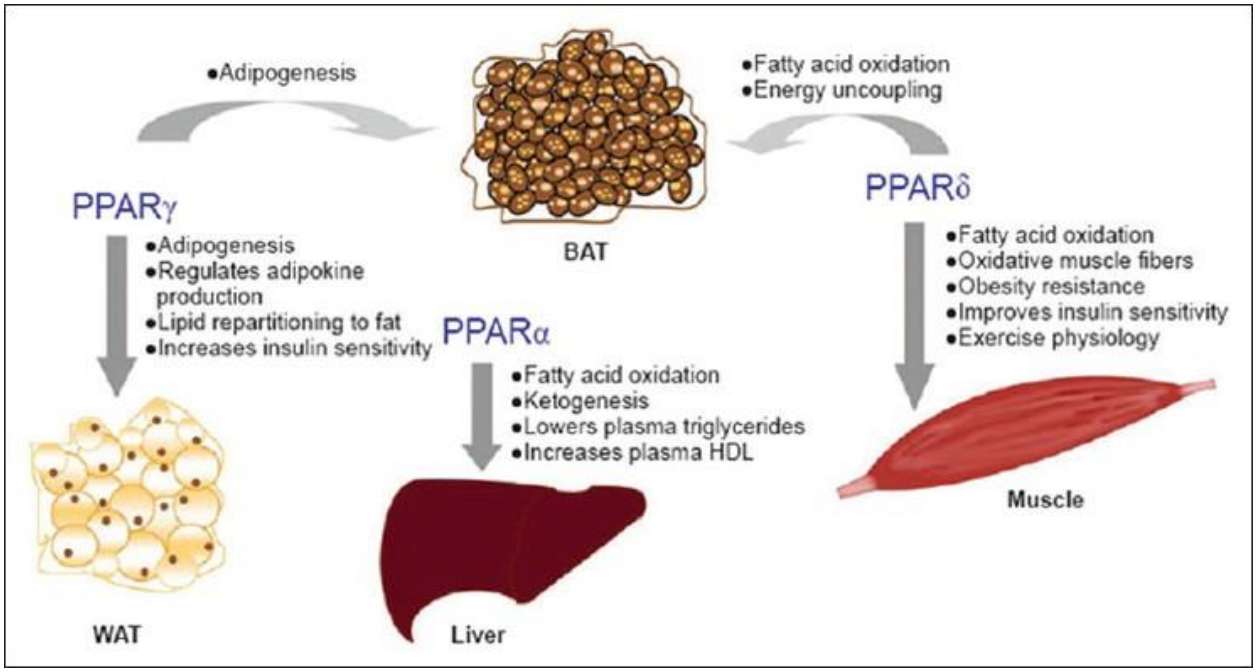

Cell Research (2010) 20:124–137. doi: 10.1038/cr.2010.13

Figure. 2.23 Role of PPARs in energy metabolism

2.6.3 PPARδ and heart

In contrast to the adipose enriched PPARγ, PPARδ is abundantly and ubiquitously expressed with highest expression in cardiomyocytes. While PPARγ and α have been studied in

several disease models and have been subject of investigation, very little is known of PPARδ. Recent studies demonstrated that mice with cardiac specific deletion of PPARδ developed cardiac lipid accumulation and cardiomyopathy, suggesting an important role of PPARδ in lipid homeostasis. PPARδ has been shown to transcriptionally induce fatty acid oxidative genes. This was confirmed when studies demonstrated that specific depletion of PPARδ displayed reduction in oxidative genes which in turn led to impaired fatty acid oxidation and subsequent increase in glucose oxidation. Upon further investigation, Planavila et al. demonstrated that PPARδ blocks the NF-κB mediated suppression of fatty acid oxidative genes[158]. Further PPARδ depleted hearts displayed decreased contraction and relaxation, increased ventricular diastolic pressure and overall reduced cardiac output which led to heart failure. Another study demonstrated that PPARδ null hearts demonstrated cardiac hypertrophy and cardiomyopathy and reduced longevity. Studies have also emphasized that PPARδ activation improved mitochondrial function and cardiac function under pressure overload hypertrophy. Together, these reports demonstrate the importance of PPARδ in preserving the cardiac energy reserves and in maintenance of cardiac function[158].

2.6.4 Structure of PPAR

PPARs contain a NH_2 terminal consisting of ligand inactivation domain (AF-1) and a C-terminal ligand binding domain (LBD) which is highly homologous with Y shaped ligand binding pocket (LBP), larger than many nuclear receptors, as observed by X-ray crystallographic studies and are composed of arms I, II, III. Arm I is polar and well conserved and arms II and III are hydrophobic and less conserved. All 3 isoforms of PPAR bind several natural and synthetic ligands. Most of PPAR agonists undertake a pharmacophoric model where ligands comprise a

hydrophilic head that binds arm I and a hydrophobic tail that binds arm II and III. PPARs bind to PPRE on the DNA containing the regulatory sequence AGGTCANAGGTCA (i.e., a direct repeat with a spacer)[159].

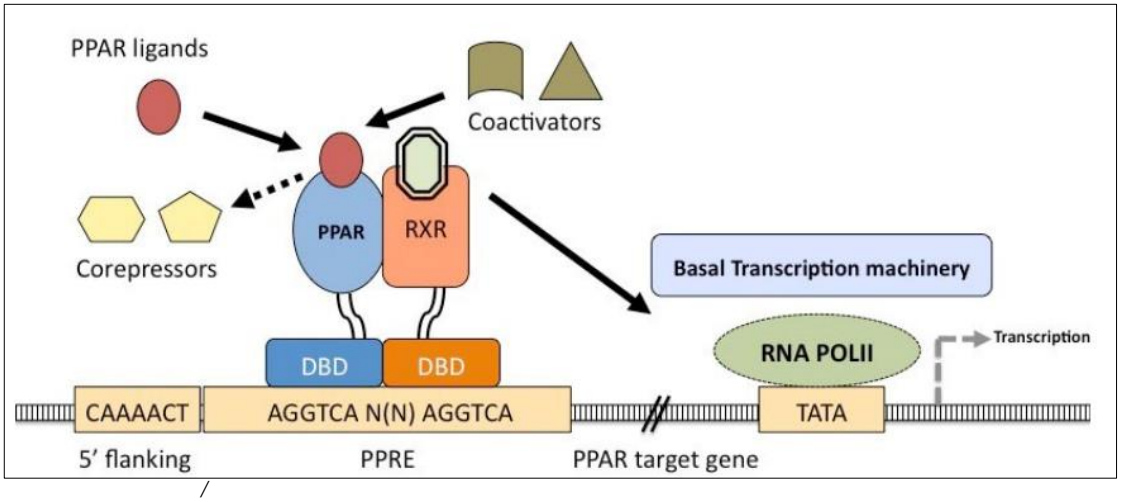

ijib.classicrus.com/trns/3471453186734.pdf

Figure. 2.24: PPAR activation. PPAR/RXR binds the PPRE present in the promoter to activate transcription[160]

2.6.4.1 PPARδ synthetic agonist - GW0742

GW0742 conforms to the pharmacophoric model of PPAR ligands, demonstrating about *300-1000 fold selectivity for PPARδ* isoform than others and is a *full a PPARδ agonist.* The carboxy group occupies arm I of the ligand binding pocket and the arms II contains the hydrophobic tail[161].

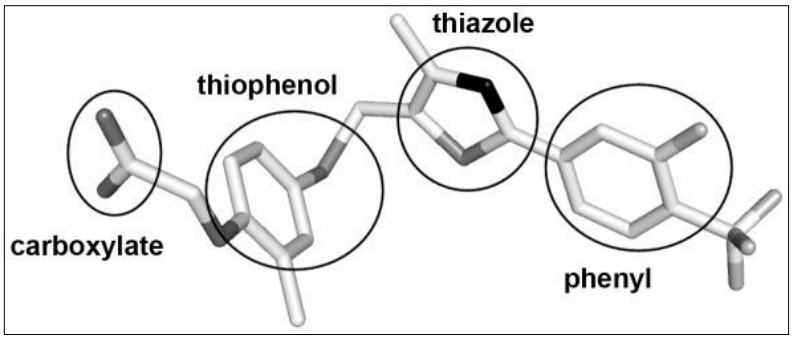

Batista FAH, et al. (2012) Structural Insights into Human Peroxisome Proliferator Activated Receptor Delta (PPAR-Delta) Selective Ligand Binding. PLoS ONE 7(5): e33643. doi:10.1371/journal.pone.0033643

Figure. 2.25 Three-dimensional structure of PPARδ agonist GW0742

GW0742 has been demonstrated to restore the expression of key fatty acid oxidative genes in cardiomyocytes isolated from PPARα -/- and PPARδ-/- mice. Further GW0742 has also demonstrated protection against right ventricular hypertrophy and fibrosis[162].

Besides being cardioprotective, GW0742 demonstrated protection against atherosclerosis at 60mg/kg for 16 weeks in LDL receptor -/- mice and resulted in reduced expression of ICAM-1, TNF-α in the aorta. In vivo, GW0742 has demonstrated protection against atherosclerosis, colon cancer, I/R injury and septic shock[163].

2.6.4.2 The role of PPARγ coactivator -1α (PGC1α)

PGC1α is an important transcription regulator of oxidative metabolism and mitochondrial biogenesis. They promote biogenesis, oxidative capacity by improving fatty acid oxidation and various mitochondrial transcription factors such as nuclear respiration factor 1 and 2 (NRF), PPAR and ERRα (estrogen–related receptor). Previous studies observed reduced oxidative capacity and mitochondrial biogenesis in PPARδ knock out mice and in addition observed

impaired PGC1α and transcription factor A. These findings led us to believe that PGC1α was a coactivator of PPARδ. Currently it has been observed that PGC1α was required for PPARδ mediated activation of carnitine palmitoyltransferase 1b (CPT1b) which plays a critical role in FAO and pyruvate dehydrogenase kinase 4 (PDK4) which plays a major role in switching the energy source from glucose to fatty acids, and uncoupling protein 3 (UCP3) which induces fatty acid oxidation[164, 165]. Further in the absence of PGC1α PPARδ minimally increased the expression of genes associated with fatty acid oxidation thus emphasizing the importance of PGC1α in PPARδ mediated activation of mitochondrial biogenesis[165].

2.6.4.3 Downstream targets of PPARδ

PPARδ is known to transcriptionally regulate SIRT1, which was further elevated by PPARδ agonist, SOD1 and SOD2, key cytosolic and mitochondrial antioxidants, mouse carnitine – acylcarnitine translocase (CACT) as observed by increase in response to GW0742, Pyruvate dehydrogenase kinase 2, 3 and 4 (PDK2, 3 and 4), Adipose differentiation-related protein (ADRP), a lipid droplet coating protein, Uncoupling protein 3 (UCP3), that helps in uncoupling ETC from ATP synthesis, insulin induced gene-1 in hepatocytes (Insig-1), acyl-coA oxidase -1 (ACOX1), carnitine palmitoyl transferase -1 in muscle, long chain acyl-coA dehydrogenase[166, 167].

2.6.4.4 Role of PPARs in FXN deficiency

Cellular and tissue analysis of FRDA models and FXN deficiency displayed dysfunction in the PPARγ/PGC1 pathway allowing us to understand the importance of this pathway in the

FXN deficiency. Similarly studies by Marmolino et al. demonstrated the effects of PPARγ agonist azeloyl-PAF (A-PAF) augmented FXN mRNA levels in FRDA fibroblasts and in neuroblastoma cells[168]. However the mechanisms which lead to this effect were not clear.

Pioglitazone a PPARγ agonist was found to induce mitochondrial biogenesis and activate SOD and was in phase 3 clinical trial for treatment for neuroprotection in FRDA. However Friedreich's ataxia research alliance (FARA) has eliminated pioglitazone from its pipeline after initial testing.

Currently we have identified PPRE within FXN promoter region and other supporting data that suggests that FXN may be a potential downstream target of PPARδ and that PPARδ transcriptionally regulates FXN expression.

Hypothesis and Objectives

My dissertation research has sought to determine the molecular mechanisms involved DOX mediated cardiotoxicity and in this manner determine the role of FXN in DOX mediated hypertrophy.

Chapter. 1 I have investigated how FXN impairment upon DOX treatment alters mitochondrial bioenergetics and leads to excessive ROS which in turn contributes to pathological hypertrophy.

Chapter. 2 I have explored how FXN is attenuated and subjected to degradation in response to DOX exposure by the ubiquitination proteasome pathway (UPP).

Chapter. 3 In this study we observed that PPARδ agonist GW0742 improve FXN mRNA and protein levels and was protective against DOX cardiotoxicity. We hypothesized that PPARδ agonist plays a major role in the treatment of DOX cardiotoxicity and in Friedreich's Ataxia models.

Chapter 3. Role of Frataxin in Doxorubicin Mediated Cardiac Hypertrophy

The current work was published in AJP heart. (Mouli et al. Am J Physiol Heart Circ Physiol. 2015 Sep; doi: 10.1152/ajpheart.00182.2015. Epub 2015 Jul 24).

3.1 Abstract

Doxorubicin (DOX) is a highly effective anti-neoplastic agent; however its cumulative dosing schedules are clinically limited by the development of cardiotoxicity. Previous studies have attributed the cause of DOX mediated cardiotoxicity to mitochondrial iron accumulation and the ensuing reactive oxygen species (ROS) formation. The present study investigates the role of frataxin (FXN), a mitochondrial iron-sulfur biogenesis protein, and its role in development of DOX mediated mitochondrial dysfunction. Athymic mice treated with DOX (5mg/kg, 1 dose per week with treatments, followed by 2 weeks recovery) displayed left ventricular hypertrophy as observed by impaired cardiac hemodynamic performance parameters. Further, we also observed significant reduction in FXN expression in DOX treated animals and H9C2 cardiomyoblast cell lines resulting in increased mitochondrial iron accumulation and the ensuing ROS formation. This observation was paralleled in DOX treated H9C2 cells by a significant reduction in the mitochondrial bioenergetics as observed by the reduction of myocardial energy regulation. Surprisingly, similar results were observed in our FXN knock down (FXN-KD) stable cell lines constructed by lentiviral technology using shRNA. To

better understand the cardioprotective role of FXN against DOX, we constructed frataxin over expressing cardiomyoblasts (FXN-OE) which displayed cardioprotection against mitochondrial iron accumulation, ROS formation and reduction of mitochondrial bioenergetics. Lastly our FXN-OE cardiomyoblasts were protected from DOX mediated cardiac hypertrophy. Together our findings reveal novel insights into the development of DOX mediated cardiomyopathy.

3.2 Introduction

The pathophysiological mechanisms involved in DOX mediated cardiotoxicity are complex and ambiguous. The current chapter examines the critical role of mitochondrial ISC biogenesis protein FXN in the pathogenesis of DOX mediated cardiac hypertrophy. Further overexpression of FXN may counteract the adverse effects of DOX by activating the mitochondrial energy homeostasis and metabolism thereby protecting the cardiomyocytes against DOX mediated cardiotoxicity.

Doxorubicin (DOX) is one of the most widely used anti-neoplastic agents used for the treatment of wide range of solid tumors and leukemia in children and adults[169, 170]. Despite its therapeutic usage, the clinical use of DOX is severely limited due to its cumulative dose dependent cardiotoxicity which develops over time into congestive heart failure[171]. During this process, mitochondrial dysfunction has been observed to be fundamentally involved in the development of heart failure due to the dysregulation of mitochondrial bioenergetics and the generation of intracellular reactive oxygen species (ROS). The mechanism of DOX induced cardiotoxicity at the cellular and subcellular levels is highly debatable. However much attention has been attributed to the DOX mediated formation of mitochondrial ROS[172]. Although the role of iron has not been emphasized in the failing myocardial model, the role of iron in the

formation of ROS has gained significance at the clinical setting with the usage of Dexrazoxane (DXZ)[9]. DXZ an iron chelator is known to induce degradation of topo2β and prevent the DOX mediated initiation of the DNA damage signal, H2AX-γ in H9C2 cardiomyoblasts[11]. However, the use of DXZ has been limited due to its interference with antitumor activity of DOX as observed by the decrease in tumor response and due to induction of myelodysplastic syndrome[11]. Therefore these disturbing findings have limited the clinical applicability of DXZ in cancer patients. These findings highlight the critical need to identify key molecular targets involved in mitochondrial bioenergetics and mitochondrial iron regulation that are altered by DOX. Identification of these targets will help foster development of potential adjuvant therapy to mitigate cardiac damage.

Frataxin (FXN), a nuclear encoded mitochondrial protein has been involved in maintaining mitochondrial iron homeostasis[128]. Although, the precise function of FXN remains elusive, studies have classified FXN as an important modulator of mitochondrial energy regulation. In this manner FXN is known to regulate iron-sulfur cluster (ISC) biogenesis resulting in modulating complexes I, and III, as well as aconitase and succinate dehydrogenase[13]. Further it has also been involved in increasing the tricarboxylic acid cycle function [16] and therefore highlights the significance of FXN for maintaining the mitochondrial energy flux.

Deficiency in FXN expression results in Friedreich's Ataxia (FRDA), an autosomal inherited neurodegenerative disease caused by unstable GAA trinucleotide repeat expansion (>120 repeats) in the first intron of the FXN gene. The deficit in transcription of FXN in FRDA patients is often characterized by mitochondrial damage and the ensuing energy dysregulation[173]. The central pathological outcomes of FRDA on the heart include

hypertrophic cardiomyopathy, myocardial fibrosis and myocardial infarction which often progress the heart to congestive heart failure[174-176].

Our findings suggest that chronic exposure to DOX with a cumulative dose of 25 mg/kg induced left ventricular hypertrophy. Further during the development of DOX mediated cardiac hypertrophy, we observed a significant reduction in mitochondrial FXN levels. In addition, we also observed in cells with DOX mediated reduced FXN levels: increased iron accumulation, mitochondrial energy dysregulation and ROS production which were also concurrently observed in our frataxin knock down (FXN-KD) cell lines. Further our FXN overexpressed (FXN-OE) cell lines displayed no alteration in mitochondrial energy regulation in response to DOX.

3.3 Materials and Methods

3.3.1 Animals.

Male athymic, NCr nude (nu/nu) mice (body weight, aprox .25 g), 6 weeks of age were obtained from Taconic Farms, Inc., (Germantown NY) maintained according to standard approved Institutional Animal Care Use Committee (IACUC) protocols at Auburn University. Mice were housed in Auburn University's Biological Research Facility in a controlled environment (23ºC; 12 hour light/ dark cycle) with free access to water and standard chow diet. The animals were maintained in pathogen free cages and light as well as temperature controlled rooms provided with rodent chows and sterile water. Juvenile athymic nu/nu mouse models, 6-weeks of age, were divided into two groups of saline treated control (vehicle) and DOX treated mice that received a cumulative dose of 25 mg/kg of DOX by tail vein injections, once/week

with 5 treatments, beginning at 6 weeks of age. Control mice were treated with saline and the body weights were measured every 3 days. Mice were monitored every day for survival.

3.3.2 MRI measurements of cardiac parameters.

Magnetic Resonance Imaging (MRI) scanning was done at the AU MRI research center. Mice were anaesthetized and maintained under sedation with 3% isoflurane during the MRI procedure. Cardiac functional parameters for left ventricular (LV) end-diastolic (ED) volume, end-systolic (ES) ejection fraction (EF), and LV mass were calculated off-line with an in-house program on Matlab (Mathworks, Natick, MA). Endo- and epicardial contours were traced on short-axis (SA) images acquired at the ED and ES phases. From the areas defined by these contours, the associated per-slice ED volume (EDV), ES volume (ESV), LV ejection fraction (LVEF), LV mass were determined where LV mass = LV volume * 1.055 g/cm3[177]. The sum of the individual SA slice parameters provided whole - LV volumetric values. Wall thickness was calculated as the radial distance between the endo- and epicardial contours and wall thickening as relative change from the ED wall thickness to ES wall thickness.

3.3.3 Construction of FXN-over expressed (FXN-OE) H9C2 cardiomyoblasts.

FXN-OE cell lines were developed using a GATEWAY-based lentiviral system. The lentiviral empty backbone pLX302 plasmid was purchased from ADDGENE and the plasmid, #25896 was a kind gift from David Root's lab (Broad Institute, MIT and Harvard). The plasmid is tagged with a V5 epitope at the C terminal backbone. The cDNA fragment of the FXN was cloned into the donor vector provided from the gateway system. Further, FXN was cloned into the pLX 302 (ampicillin and chloramphenicol resistant) lentiviral destination vector

(http://www.addgene.org/25896/) using LR Clonase (Life Sciences, Cat. #. 11789100). A puromycin selectable antibiotic marker exists in the pLX 302 vector. The cells were then subjected to transformation in a bacterial cell DH5alpha strain (Invitrogen, Cat. # -012) and the competent plasmid was isolated using PureYieldTM Midiprep system (Promega A2495). The expression vector was then purified and was transfected with a second generation lentiviral packaging vector (psPAX2, ADDGENE cat # 12260, a kind gift of the Didier Trono Lab (The Swiss Federal Institute of Technology Lausanne (EPFL) and the envelope vector (pMD2.G, ADDGENE Cat# 12259, a kind gift from the Didier Trono Lab) in a HEK 293T cell line. Further, the virus was extracted from the media and purified using a 0.45 μm syringe filter. Subsequently, purified virus was exposed to H9C2 cells for 24 hours and the next day, the cells were treated with 1 μg/ml of puromycin for selection of cells expressing FXN.

3.3.4 Construction of FXN-knock down (FXN-KD) H9C2 cardiomyoblasts.

FXN-KD cells were constructed using lentiviral system containing shRNA for FXN. The shRNA lentiviral backbone PLKO.1 plasmid was purchased from ADDGENE. (http://www.addgene.org/10878/) and the plasmid, #10878 was a kind gift from David Root's lab (Broad Institute, MIT and Harvard). ShRNA oligos were constructed according to the protocol described in the addgene website (http://www.addgene.org/tools/protocols/plko/). FXN-KD cells were stably transfected using second generation packaging for shRNA using lentiviral system. The shRNA oligos for FXN-KD3 forward, 5'-AATTCTTTGAAGACCTTGCAGCTC-3' and reverse 3'-TTAAGAAACTTCTGGAACGTCGAG-5' and FXN KD2 forward 5'-AAGAACTGGGTGTACTCCATCTC-3' and reverse 3'-TTCTTGACCCACATGAGGTAGAG-5' were digested using restriction enzymes Age1 (NEB #

R0552S) and EcoR1 (NEB #R0101S) and ligated using quick T4 DNA ligase from quick DNA ligase kit (NEB # M0202M). The ligated vector was then subjected to transformation into competent bacteria and the plasmid was isolated using PureYieldTM Midiprep system (Promega, A2495). The purified vector was then transfected using packaging plasmid (psPAX2) and envelope plasmid (pMD2.G) into HEK 293T cells. Stable cells lines were developed using purified virus and puromycin as described above.

3.3.5 Cell culture.

3.3.5.1 Neonatal cardiomyocyte isolation:

The isolation and culturing of neonatal mouse ventricular cardiomyocytes were performed from 3 day old C57BL/6J mice pups according to a modified protocol[178]. Briefly excised mouse ventricles were washed in Ca2+ and Mg2+ free Hank's balanced salt solution (HBSS), pH 7.4, (in g/l) 0.4 KCl, 0.06 KH_2PO4, 8.0 NaCl and 0.05 Na_2HPO4, and minced into small pieces on ice. Cardiac tissue was dissociated by the incubation with Trypsin - HBSS solution overnight at 4° C. The aggregates were then removed and digested with collagenase, type II (Calbiochem, #234155) at 37° C with gentle agitation in a shaker set at 65 rpm. The cardiomyocytes were centrifuged for 10 min, 200 g and then resuspended in DMEM containing 20% FBS and 1% Pen.-Strep. (100 U/ml penicillin and 100 μg/ml streptomycin). The cells were then pre-plated to remove fibroblasts and endothelial cells. The addition of proliferation inhibitor Bromodeoxyuridine (BrdU) (100 μM; Sigma Chemicals; St. Louis, MO) led to elimination of non-cardiomyocytes. Collected cardiomyocytes were then plated at a density of 1.5x105 cells per cm^2 at 37° C at 5% CO_2 and were observed for adherence the next day.

3.3.6 Cell lines.

H9C2 cells are a rat heart derived embryonic ventricular cardiomyoblast cell line and were purchased from ATCC and cultured according to guidelines from ATCC. Briefly cells were grown in DMEM (Lonza, #12-604F) supplemented with 10% (v/v) fetal bovine serum (FBS) (Hyclone, SH30088.03) and 1% (v/v) Pen.-Strep. The fibroblasts from Friedreich's Ataxia patients (GM03665) and healthy human patients (GM08402) were purchased from Coriell Cell Repository (Camden, NJ). Fibroblasts were grown at 37° C at 5% CO_2 and 15% (v/v) FBS and 1% (v/v) Pen.–Strep as suggested by the Coriell Repository.

3.3.7 Western Immunoblot.

Proteins were extracted from H9C2 cardiomyoblasts using the cell lysis buffer (Cell Signaling, # 9803) and supplemented with protease cocktail inhibitor (Thermo Scientific, # 87786). FXN detection in vivo and in vitro by western analysis was carried out as previously described using FXN (1:1000, SantaCruz, #25830) antibody[179]. In vitro detection of transferrin (TfR1) and ABCB8 proteins were performed using TfR1 (1:2000, Bethyl, #A304-381A-T) and ABCB8 (1:250, Rockland, #30981) antibodies respectively. Briefly, protein lysates were denatured at 95°C for 5 minutes, with loading buffer and then resolved in a 12% resolving gel and blotted on a nitrocellulose membrane. The blots were incubated overnight with FXN (1:1000, Santa Cruz, #25830) and α-tubulin (1:2000, DSHBY, #12G10) primary antibodies with 5% milk in TBS-T. The blots were then washed with TBS-T and incubated with HRP conjugated secondary antibody (1:2000, Rockland) for 1 hour. Blots were visualized with chemi-illuminescence reagent (Millipore), and imaged using a Bio-Rad gel dock system. Protein bands were analyzed using ImageJ software and standardized to α-tubulin. Data were averaged and

statistical analyses were based on an analysis of 4 independent experiments and were analyzed using graphpad prism software (version 5.0) using standard error mean (S.E.M).

3.3.8 Quantitative Real-time PCR.

Changes in gene expression of markers associated with hypertrophy were measured by 2 step qPCR analysis. Total cellular RNA was extracted from animal tissues and cultured H9C2 and FXN-OE cardiomyoblasts with or without DOX, using RNeasy mini kit (Qiagen, # 74014) and was subjected to reverse transcription using Thermo Scientific Verso cDNA synthesis kit, # AB-1453/A. Quantification of changes in gene expression was accomplished using real time PCR analysis techniques with a SYBER green mix (Thermo Scientific, # K0221) and was standardized to β-actin (IDT technologies). Sequences of probes for β-MHC are as follows: Forward 5'-AAG GAG GAG TTT GGG CGA GTC AAA-3' and reverse 5'-TGC ATC CGC CAA GTT GTC TTGTTC-3'. Sequences of probes for ANP are as follows: Forward 5'-AGA CAG CAA ACA TCA GAT CGT GCC-3' and reverse 5'-ATC TGT GTT GGA CAC CGC ACT GTA-3'. Sequences of probes for β-Actin are as follows: Forward 5'-TTG CTG ACA GGA TGC AGA AGG AGA-3' and reverse 5'-ACT CCT GCT TGC TGA TCC ACA TCT-3'. Sequence for probes for TfR1 are as follows: Forward 5'-GGC TGA CAG GGA TCA ATA TG -3' and reverse 5'- TGC TGA CTC ACA CTC TAT CT-3'. Sequence for probes for ABCB8 is as follows: Forward 5'- AGC CTC TCT GTC CTG TTT-3' and reverse 5'- CCT GGC TGA TGA AAC CTA TG -3'. Data analysis was conducted using ΔΔCt method [180]. Data were based on fold change from control H9C2 cells and analyzed by ANOVA with Tukey's post-hoc analysis for significances between and within groups.

3.3.9 Mitochondrial isolation/ fractionation.

The mitochondrial fractionate was isolated as described previously [181]. Briefly, cells were harvested in (sucrose homogenization buffer containing (mM): sucrose 250, EDTA 1, HEPES 10, pH 7.4 and freshly added Protease Inhibitor Cocktail Complete (Roche). Cells were then disrupted and lysate was cleared by centrifugation at 600 g for 5 minutes to eliminate the nuclear fraction and immiscible particulate material. Supernatants were then spun at 7000 g for 10 minutes, where by the pellets were resuspended in homogenization buffer and centrifuged at 7000 g for 10 minutes to obtain the final mitochondria-enriched pellet (heavy membrane fraction). Finally the pellets were resuspended in homogenization buffer supplemented with 1% Triton X- Samples were stored at −80° C until use.

3.3.10 Mitochondrial iron detection assays:

3.3.10.1 Mitochondrial iron detection: Ferrozine colorimetric assay

Iron detection assay was performed using ferrozine colorimetric assay which detects and quantifies iron by forming a complex.[182]. Cultured H9C2 cardiomyoblasts were treated with or without DOX for 24 hours. Mitochondrial and cytosolic fractions were isolated as previously discussed and then lysed with NaOH lysis buffer for 45 minutes. Iron levels from mitochondrial and cytosolic fractions were obtained from lysates treated with acidic $KMnO_4$ / HCl and iron detection was enhanced by incubating the cellular fractions with $HCl/KMnO_4$ for 2 hours at 60° C. Iron detection was measured by a multispectral plate reader (BioTek) with the absorbance read at 550 nm. Data were averaged from 4 independent experiments and were normalized to control H9C2 cells and were analyzed by ANOVA with Tukey's post-hoc analysis for significances between groups and within groups.

3.3.10.2 Mitochondrial iron detection by Fluorescence Resonance Energy Transfer (FRET) assay.

Mitochondrial iron was further detected by RNP1, a ratiometric fluorescent iron sensor, containing an alkyl triphenylphosphine, which helps it to permeate the mitochondrial membrane and a naphthalene chromophore. In the presence of iron, a deep red fluorescence was obtained. The dye exhibits pseudo-large stokes shift based on a FRET mechanism and the naphthalene chromophore[183]. Cultured H9C2 and FXN-OE cardiomyoblasts were treated with or without DOX (10μM) for 24 hours and incubated with RNP1 and co-localized with MitoTracker Green FM (1μM) for 30 minutes. Mitochondrial iron was detected by far red fluorescence imaging using a Nikon Eclipse Ti inverted fluorescence microscope. Fluorescence images of the RNP1 iron (red) and mitotracker (green) channels within the same fields were obtained and overlaid using the Nikon NIS-Elements software rendering areas of co-localization yellow in color.

3.3.11 Mitochondrial respiration.

Cellular respiration was measured as previously described[184]. In summary, the cells were washed in PBS, trypsinized and centrifuged at 800 g for 3 minutes. The pellets were then washed and resuspended in 4 00μl PBS containing 10mM glucose, 10mM Hepes, 0.2% BSA and maintained at 37° C. Thereafter, 300μl of glucose supplemented PBS was added to the oxymeter chamber (Hansatech Instruments, Pentney, UK) and equilibrated for approximately 1 minute after which, 350 μl of the cell suspension solution was added. Following this, the basal respiration rate was recorded for approximately 4.5 minutes. Subsequently, 6 μM FCCP, mitochondrial complex uncoupler, was added and monitored for approximately 1.5 minutes. The basal (coupled) and maximal (uncoupled) respiration rates were normalized to total protein

concentration on aliquots of cells in supplemented PBS. Data was analyzed using ANOVA with Tukey's-post hoc analysis and based upon mean ± S.E.M from 4 independent experiments.

3.3.12 NADH dehydrogenase activity assay.

H9C2 and FXN-OE cardiomyoblasts were cultured and treated with or without the addition of DOX and complex I inhibitor, rotenone (100 nM). Mitochondrial fractions from H9C2 cardiomyoblast cells were isolated as described previously[181]. NADH oxidation was measured according to protocol described by Ramsay et al.[185]. Oxidation of NADH by the NADH dehydrogenase enzyme present in the mitochondrial rich suspension was measured spectrophotometrically at 340 nm. 20 µl of mitochondrial suspension was added to the reaction mixture (10 µl of 8.4 mM NADH, 5 µl of co enzyme mM Q10 and 200 µl of 0.01 M PBS). Oxidation of NADH was measured by monitoring the absorbance at 340 nm. A standard curve for NADH oxidation was obtained by using known quantities of NADH dehydrogenase. The change in absorbance indicates the amount of NADH oxidized. The mitochondrial complex-I activity is expressed as the amount of NADH oxidized per microgram of protein. Data was analyzed using ANOVA with Tukey's-post hoc analysis and based upon mean ± S.E.M from 4 independent experiments.

3.3.13 Aconitase activity.

Aconitase activity was measured using Aconitase Assay Kit (Cayman chemicals, # 705502). The aconitase catalyzes the isomerization of citrate to isocitrate, which is then converted to α-ketoglutarate by isocitrate dehydrogenase. Cells were grown in plates and treated with or without DOX. Mitochondria were extracted from these samples and protein

concentration was determined by BCA assay kit (Thermo Scientific, # 23227). The assay was performed at room temperature and the activity of aconitase was monitored by measuring the increase in absorbance at 340 nm absorbance wavelength that is associated with the formation of NADH. Data was analyzed using ANOVA with Tukey's-post hoc analysis and based upon mean ± S.E.M from 4 independent experiments.

3.3.14 Mitochondrial membrane potential assay.

The mitochondrial membrane potential was measured utilizing tetramethylrhodamine ethyl ester, TMRE (Biotium, #70016) (2 μM) accumulation in the active mitochondrial membrane. Mitochondrial membrane potential was determined in a-well plate. Depolarized or inactive mitochondria have reduced membrane potential and therefore fail to display TMRE based fluorescence. N=3 independent experiments and are represented as mean ± S.E.M and analysis was accomplished by ANOVA with Tukey's post-hoc analysis for significance between and within groups based on averages from the assays.

3.3.15 ATP quantification.

The ATP levels were quantified using ATPlite luminescence ATP detection assay system (PerkinElmer, # 6016941). The luciferase catalyzes the reaction between D- luciferin and ATP to produce bioluminescence. The emitted bioluminescence is proportional to the ATP concentration. The cells were plated in 96-well plates and the assay was conducted according to the manufacturers' protocol. The luminescence was measured using Glomax luminometer (Promega). Data was analyzed using ANOVA with Tukey's-post hoc analysis and based upon mean ± S.E.M from 4 independent experiments.

3.3.15 Glutathione measurement assay.

Glutathione Reductase (GR) assay was performed in tissue homogenates from DOX treated athymic mice and H9C2 cardiomyoblasts using Glutathione Reductase Assay Kit, (Cayman Chemicals, #703202). The rate of NADPH oxidation is evaluated by measuring the decrease in GR activity. Absorbance was read at 340 nm with plate reader once every minute for 10 minutes to obtain 10 time points. Values were based upon a standard curve and calibrated to the total levels of protein concentrations. Data was analyzed using ANOVA with Tukey's-post hoc analysis and based upon mean ± S.E.M from 4 independent experiments.

3.3.16 ROS measurement.

Mitochondrial ROS was measured using mitochondrial specific dihydro rhodamine, DHR (Biotium, #10055). DHR is an uncharged non-fluorescent ROS indicator that accumulates in the mitochondria and becomes oxidized to form the cationic rhodamine123, thereby exhibiting a green fluorescence. The cells were seeded in a 24-well plate and stained according to the manufacture's protocol. Briefly, cells were treated with or without DOX for 24 hours, followed by incubation of DHR (10 μM) for 30 minutes. Fluorescence intensity was detected using a Nikon Eclipse Ti inverted fluorescence microscope and analysis was accomplished using ImageJ software from random images per treatment from 3 independent sets of experiments. The total densitometric values were obtained by comparisons of densitometric values to total area. N=3 independent experiments and are represented as mean ± S.E.M and analysis was accomplished by ANOVA with Tukey's post-hoc analysis for significance between and within groups based on averages from the assays.

3.3.17 Measurement of cardiac hypertrophy.

Cells were fixed with 4% formaldehyde and stained with phalloidin conjugated with rhodamine and randomly photographed by a naïve observer using a NIKON Eclipse Ti inverted fluorescence microscope. Cellular morphometric size analysis was accomplished using ImageJ software and 10 random images were captured per treatment from 3 independent sets of experiments. The total densitometric values were obtained by comparisons of densitometric values to total area. Data is represented as fold change from control and is standardized to β-actin. Indicated are mean ± S.E.M of replicates from 4 individual experiments.

3.3.18 Statistical analysis.

The mRNA and immunoblot protein densitometric analysis are presented as means ± S.E.M. Statistical analysis of data was accomplished using Prism software, version 5.0 and validated compared by a student two tailed T- test or where required two way ANOVA and a Tukey post hoc analysis with significance accepted at p value <0.05.

3.4 Results

DOX treated mice display cardiac hypertrophy and reduced frataxin levels.

Administration of DOX is known to induce cardiac hypertrophy[186, 187]. To better understand the mechanisms involved in DOX mediated cardiac hypertrophy; we subjected our athymic mice to DOX treatment with a cumulative dose of 25 mg/kg (5 mg/kg, one dose/week for 5 treatments and 2 weeks recovery). Computational analyses of the cardiac architecture as demonstrated by Bull's eye maping revealed enlargement in the antero-lateral segment of the left ventricle (Fig.3.1A). To further evaluate DOX mediated changes in cardiac architecture and

performance, mice were imaged using magnetic resonance imaging (MRI) techniques, two weeks after the last dose of DOX treatment. Our MRI imaging and analysis revealed an increase in left ventricular mass index (Fig.3.1B & C). Together, these data demonstrate an increase in size of the left ventricle with DOX treatment when compared to control mice. We observed that DOX alters cardiac performance by MRI analysis, including reduced end diastolic and end systolic volumes (data not shown), as well as reduced heart rate, muscle mass and overall cardiac output (Fig 3.1D & E). Further our in vitro findings for changes in cardiac morphology suggested an increase in the mRNA levels of markers of fetal gene program including atrial natriuretic peptide (ANP) (~4 fold) and beta myosin heavy chain (β-MHC) (~3.5 fold) in response to DOX treatment when compared to our control mice (Fig.3.1F). These data together suggest that our current chronic regimen of DOX induces ventricular dysfunction and hypertrophy.

Previous studies have demonstrated that at the cellular level, mitochondrial energy components were the primary targets for DOX mediated cardiomyopathy [188]. However, understanding the key cellular intermediaries involved in DOX mediated damage to the myocardium remains poorly understood. We observed a significant reduction in FXN protein expression (~4.5 fold) in DOX treated athymic mice ventricles when compared to our control athymic mice (Fig. 3.2A) and in isolated neonatal cardiomyoblasts treated with DOX (Fig 3.2B) while no changes were observed in the mRNA levels of FXN with DOX treatment. Further we also observed a significant reduction in the mature (18 KDa) and total (18 KDa+25KDa) forms of FXN in our DOX (1&10 μM) treated H9C2 cardiomyoblasts (Fig. 3.2C & D). To better understand the DOX mediated effects upon FXN cellular distribution, we observed changes in

FXN levels in mitochondrial and cytosolic fractions as demonstrated by our western analysis (Fig. 3.2E & F).

DOX mediated reduction in frataxin alters mitochondrial iron homeostasis.

Deficiency of FXN in yeast mutants (ΔYFH1) and FRDA fibroblasts have been found to be associated with elevated mitochondrial iron accumulation[12, 128]. Therefore, we hypothesize that DOX mediated reduction in mitochondrial FXN expression could alter sub-cellular iron distribution and thereby results in an increase in mitochondrial iron accumulation. Our chronic DOX treated mice displayed elevated mitochondrial iron levels (~2.5 fold increase) and reduced cytosolic iron levels when compared to our control mice, as demonstrated by our Ferrozine colorimetric iron assay (Fig. 3.4A). These results were verified in our mitochondrial fractions of H9C2 cardiomyoblasts treated with increasing doses of DOX (0, 1, 10 and 20 μM) for 24 hours. Our DOX treated H9C2 cardiomyoblasts displayed approximately a 4-fold increase in mitochondrial iron accumulation which was similar to basal iron levels observed in KD3 cells (Fig. 3.4C). However we observed only a 2-fold increase in iron accumulation in KD2 cells thus suggesting considerably reduced levels of FXN are required to significantly alter mitochondrial iron homeostasis. These findings were further supported in FXN-OE cells that demonstrated in response to increasing DOX concentrations, cardioprotection against mitochondrial iron accumulation (Fig. 3.4B). The role of FXN against DOX mediated cardiac damage was further supported in human FRDA fibroblasts, where elevated mitochondrial iron levels were observed under basal conditions (Fig. 3.4C). These results emphasize the role of FXN in DOX mediated cellular iron dyshomeostasis. To further justify these findings we developed a novel fluorescence iron sensor which measures mitochondrial iron[183]. An enhanced far red fluorescence was

observed using our RNP1 dye on the basis of fluorescence resonance energy transfer (FRET) mechanism in H9C2 cells treated with DOX (10 μM) for 24 hours. However, the same dose and duration of the treatment with DOX did not produce a fluorescent signal in our FXN-OE cells in the presence of RNP1 (Fig. 3.4D). These findings support that damage to FXN by DOX results in increased mitochondrial iron levels. In order to identify a possible mechanism for the increased iron accumulation in FXN depleted cells, we evaluated the expression levels of the mitochondrial iron transporters, transferrin (TfR1) and ATP-binding cassette, subfamily b, member8 (ABCB8). We observed an increase in the mRNA and protein levels of iron importer TfR1 in response to DOX (10 μM, 24 hours) (Fig. 3.5A and B). Furthermore, we also observed a significant reduction in mRNA and protein levels of mitochondrial iron exporter ABCB8 in response to DOX treatment in H9C2 cardiomyoblasts (Fig. 3.5C and D). Surprisingly, we also observed a similar pattern of expression of TfR1 and ABCB8 in our KD3 cardiomyoblasts under basal conditions. Although we observed an increase in TfR1 expression levels in KD2 cells, we did not find a substantial increase in mitochondrial iron accumulation in these cells and therefore changes in TfR1 and ABCB8 protein levels in KD2 cells were not explored. Lastly we observed no significant changes in TfR1 or ABCB8 expression in response to DOX in FXN-OE. Together, these data signify the importance of FXN upon mitochondrial iron homeostasis.

FXN overexpression prevents DOX mediated reduction in mitochondrial bioenergetics.

To explore the effects of DOX on mitochondrial bioenergetics and understand the role of FXN in this process, we evaluated the effects of DOX on iron-sulfur cluster (ISC) containing enzymes aconitase and NADH dehydrogenase with and without the addition of rotenone (100 nM). Rotenone is a complex I inhibitor that binds to the ubiquinone binding site on the enzyme

complex, thereby preventing the oxidation of NADH. Significant attenuation in the activities of ISC containing enzymes aconitase and NADH dehydrogenase was observed using spectrophotometric assays in our control cardiomyoblasts. However, FXN-OE cells were protected from the damaging effects of DOX on mitochondrial bioenergetics as demonstrated by observing higher activities of aconitase and NADH dehydrogenase (Fig. 3.6A & B). We have also observed reduced basal mitochondrial respiration rates in our DOX treated cardiomyoblasts (10 μM for 24 hours) as well as in our KD3 and FRDA fibroblasts. However, our FXN-OE cells were protected against the detrimental effects of DOX upon mitochondrial respiration as observed by an elevated mitochondrial respiration rate when compared to DOX treated H9C2 and FXN-KD cells (Fig. 3.6C and D). We then proposed that FXN overexpression would offer protection against DOX mediated impaired respiration and mitochondrial energetics. In line with findings from our respiration studies, we observed a dose dependent reduction in the ATP levels from our H9C2 cardiomyoblasts after DOX treatment and further that our FXN-OE cells were protected from these deleterious effects of DOX (Fig. 3.6 E). FXN deficiency has been found to be associated with reduced glutathione levels[132, 189]. In this manner, we observed a protection against DOX mediated reduction in glutathione reductase activity when compared to our DOX treated H9C2 cells. Further we also observed a marked improvement in glutathione reductase activity in our FXNOE cells when compared to our DOX treated H9C2 control cells (Fig. 3.6F). These data together suggest that FXN is implicitly involved in mitochondrial respiration, energetics and anti-oxidative mechanisms which are significantly altered by DOX.

FXN-OE protects against DOX mediated ROS.

Previous studies have observed that DOX induces an increase in free mitochondrial iron accumulation resulting in the development of ROS[190, 191]. Our findings display elevated ROS levels in DOX treated H9C2 cardiomyoblasts as well as in KD3 cardiomyoblasts. However, our FXN-OE cells were protected against DOX mediated mitochondrial ROS formation by demonstrating reduced fluorescence intensity as measured with Dihydro rhodamine (DHR) (10 μM). We also observed a similar protective effect with the use of mitochondrial iron chelator, pyridoxal isonicotinoyl hydrazone (PIH, 40 μM). Further, inhibition of complex I was implicated in the DOX mediated mitochondrial ROS, by the utilization of rotenone (100 nM) (Fig. 3.7A). To further investigate the consequence of the mitochondrial ROS on mitochondrial function, we utilized TMRE (2 μM) and observed reduced mitochondrial membrane potential ($\Delta\psi m$) as measured by diminished membrane fluorescence intensity in DOX treated (10 μM for 24 hours) H9C2 cells. However we observed in FXN-OE cells, an inherent protection against DOX mediated reduction in mitochondrial membrane potential (Fig 3.7B). These data suggest that attenuation of FXN levels can significantly alter mitochondrial activity and offers a potential molecular signaling target for explaining how DOX damages the myocardium.

Overexpression of frataxin protects against DOX mediated cardiac hypertrophy

The critical role of mitochondrial ROS and oxidative stress towards development of cardiac hypertrophy is well known. To further verify that DOX induced cardiac hypertrophy was a consequence of reduced FXN, we administered DOX to our control H9C2 and FXN-OE cardiomyoblasts. DOX treated H9C2 cells displayed an increase in size and markers for hypertrophy ANP and β-MHC. However, DOX treated FXN-OE cells were protected from the DOX mediated hypertrophic stress (Fig.3.8). The significance of iron homeostasis is verified by

the iron chelator PIH when co administered with DOX, and demonstrated a lack of cardiomyoblast hypertrophy.

3.5 Discussion

DOX chemotherapy has been found to propagate the development pathological cardiomyopathy. During the development of cardiac hypertrophy changes in the myocardial architecture are evidenced by the development of ventricular irregularities including nonspecific ST and T wave abnormalities, decreased QRS voltage, prolonged QT interval, supra ventricular and ventricular arrhythmias[192, 193]. Chronic dosing is primarily cumulative and dose dependent and leads the heart to further pathological damage which progresses to failure. The onset of cardiomyopathy from chronic DOX dosing usually appears after cessation of DOX therapy[194]. However the mechanisms associated with the development DOX mediated cardiotoxicity is unclear and complex. In order to better understand the mechanisms that are involved in development of DOX mediated cardiotoxicity, we observed enlargement in the antero-lateral segment of the left ventricle, indicating ventricular hypertrophy and reduced functional hemodynamic parameters. Further our dosing regimen is analogous to other reports which investigate the effects of similar chronic dosing on the myocardial architecture[195, 196]. Previously it has been proven that mitochondrial damage exists as an underlying factor in the progression of cardiomyopathy to heart failure[191]. Treatment with DOX induces free oxygen radical production which is a contributing factor for the disruption of mitochondrial bioenergetics. Therefore, identifying cellular targets that are altered by DOX in the mitochondria will help identify potential molecular therapeutic targets for preventing cardiotoxic effects of

DOX in cancer patients. The present study focuses on elucidating the mechanism of hypertrophic cardiomyopathy induced by DOX exposure and understanding the role of FXN in this process.

The significance of our central finding that DOX reduces the expression of FXN in both in vivo and in vitro models can be correlated to FRDA human patients that lack functional FXN and develop life threatening pathological hypertrophic cardiomyopathy. The significance of DOX mediated FXN reduction towards the development of cardiotoxicity was observed by demonstrating an increase in mitochondrial iron overload. These findings add significant knowledge to understanding the mechanism of DOX mediated increase in free mitochondrial iron accumulation. Further they were supported by our FXN-KD3 cardiomyoblast cell lines which displayed a similar increase in mitochondrial iron as found in DOX treated cardiomyoblasts. However our KD2 cells displayed slight mitochondrial iron accumulation under basal condition. These findings suggest that dysregulation of iron homeostasis requires significant reduction in FXN expression levels.

Although FXN plays a major role in the homeostasis of iron, iron transporters play a major role in the uptake, transport and export of iron within the cells. Other than the mitochondrion, the mechanism of iron homeostasis has been well characterized in the whole cell. Transferrin and ABCB8 plays a major role in controlling the influx, efflux of iron thereby contributing to balance in iron levels. Since modulation in iron transporter expression is believed to be key to explaining alterations in cellular iron homeostasis, we analyzed expression levels of TfR1 (influx) and ABCB8 (efflux). It has been reported that reduction in ABCB8 is critical for the accumulation of mitochondrial iron. However, our findings indicate that DOX induces an increase in TfR1 and a decrease in ABCB8 levels, thus suggesting that imbalance between influx and efflux axis of iron transporters is critical for alteration of mitochondrial iron homeostasis. Previous reports help link

the significance of altered FXN expression upon iron transporter regulation, by demonstrating in FXN deficient mice, increased TfR1 levels, which was due to transcriptional regulation by iron regulatory protein 2 (IRP2), the key cellular iron regulator[197, 198]. To further explain the significance of altered FXN levels upon iron homeostasis, we report that reduced FXN leads to alterations in both TfR1 and ABCB8. However, significantly reduced FXN levels as observed in KD3 cells are required to alter TfR1 and ABCB8 axis. Therefore significant reduction in FXN is required for changes in mitochondrial iron regulatory mechanisms. FRDA models are known to display severe mitochondrial energy deficits[199].

These deficits are characterized by reduced oxidative capacity due to depleted FXN levels and hence display impairment in Fe-S cluster enzyme activities, diminished respiratory capacity and reduced ATP levels. Similar events were observed in our DOX treated cardiomyoblasts which displayed severe reduction in the activities of ISC containing enzymes; NADH and aconitase, as well as oxygen consumption levels and ATP production. Under stress, glutathione reductase maintains the physiological GSH/GSSG balance in a NADPH dependent fashion.

Previous studies have demonstrated that FXN deficient and FRDA cells can be affiliated with the deficiency of glutathione pool (GSH/GSSG), that serves as a free radical scavenger and co-factor for various mitochondrial antioxidants[189, 200]. In light of these findings, we observed a DOX mediated reduction of glutathione reductase enzyme activity (a requirement for glutathione replenishment). However, our FXN-OE cardiomyoblasts were protected from the deleterious effects of DOX in the mitochondria which may be due to elevated anti-oxidative defense.

Therefore these findings, taken together, suggest that FXN-OE was protective against DOX mediated adverse effects by significantly improving the mitochondrial oxidative energy flux and anti-oxidative capacity thereby preserving the mitochondrial bioenergetics capacity. The

molecular mechanisms of DOX induced cardiotoxicity in cancer patients is highly debatable due to a variety of proposed mechanisms including the involvement of Topo2β[201], intramyocellular calcium dysregulation[85], myofibrillar integrity damage[202] and dysregulation of the INa redox balance leading to elevated ROS production. In addition, there has also been a great deal of attention towards understanding the development of DOX mediated mitochondrial ROS formation. Upon closer investigation of the origin of the mitochondrial ROS, it has been suggested to be result of DOX-iron complex and redox cycling[65]. Our observations of elevated ROS in DOX treated H9C2 cardiomyoblasts was an outcome of mitochondrial iron accumulation as validated with our iron chelator, PIH results. In addition we believe that DOX inhibits respiratory complex I activity and further contributes to total mitochondrial ROS levels as demonstrated by the addition of rotenone. The impact of FXN-OE on mitochondrial activity was further reflected in the preservation of the mitochondrial membrane potential against DOX insult. The significance of this ROS as discussed above links the concept for the involvement in the development of DOX mediated cardiac hypertrophy. Our PIH studies confirm this notion that the mitochondrial iron-ROS was involved in the development of cardiac hypertrophy. Further that FXN-OE cardiomyoblasts demonstrated reduced hypertrophy in response to DOX treatment.

Figures and Figure legends

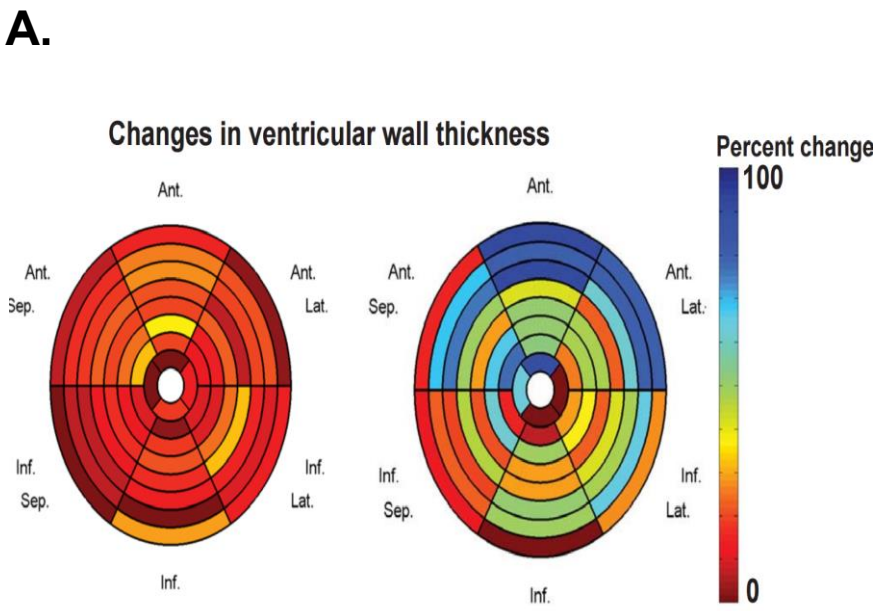

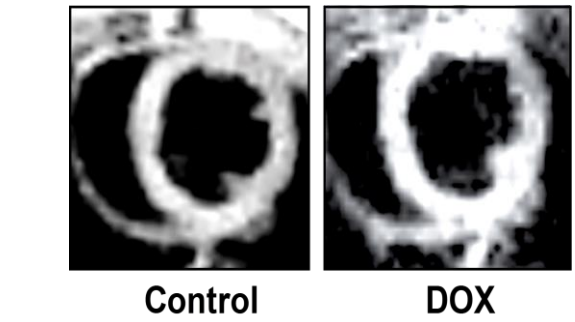

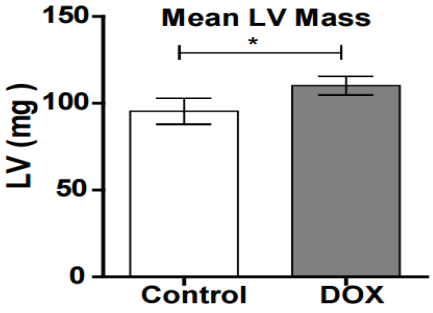

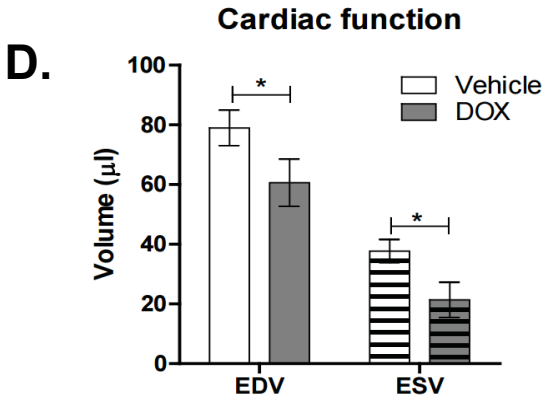

	Heart Rate (bpm)	Cardiac Output	LV mass (mg)
Baseline	425.03 ± 3.8	16.76 ± 2.33	94.19 ± 10.51
DOX	395.32 ± 27.15*	11.80 ± 2.84*	109.13 ± 18.08*

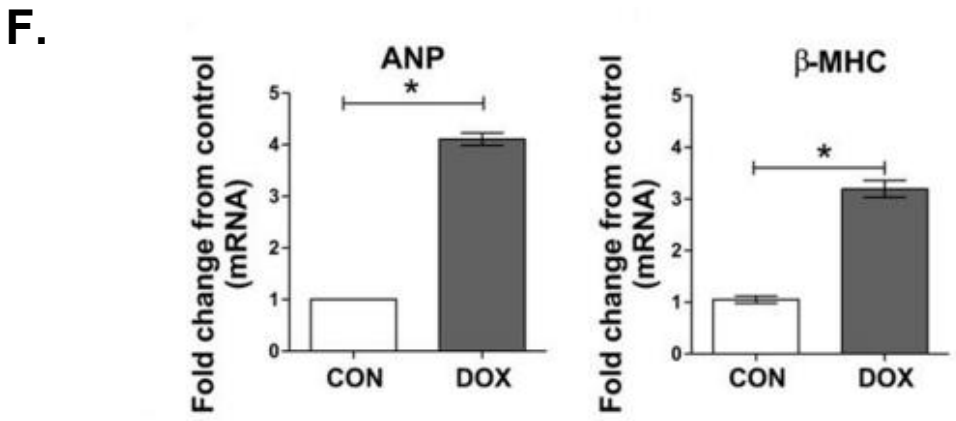

Figure. 3.1: Doxorubicin induces cardiac hypertrophy. (**A)** 16 segment model of LV portion of the Bull's eye plot from MRI scans show the antero-lateral geometry of the left ventricle (LV) in DOX treated mice (Ant, Anterior; sep, septum; Lat, Lateral; Inf, Inferior). **(B**) DOX mediated

changes in cardiac architecture and performance in athymic mice were imaged using MRI **(C)** MRI analysis revealed an increase in left ventricular mass index**. (D & E)** Effects of DOX on cardiac performance revealed a reduced heart rate, increased LV mass and overall reduced cardiac output. **(F)** Measurements of changes in markers for cardiac hypertrophy (ANP and β-MHC) as measured by qRT PCR analysis in athymic mice treated with doxorubicin (DOX) (5mg/kg, one dose per week for 5 treatments, 2 weeks recovery). Values were based on ΔΔct values which were standardized to β-actin expression. Values are represented as mean ± S.E.M. of N=4 independent experiments and analyzed by student t-test (two tailed) to evaluate significance between groups. Assessment of cardiac functional parameter values are represented as mean ± S.E.M. from 4 independent experiments normalized to the control mice and analyzed by ANOVA with Tukey's post-hoc analysis for significances between groups and within groups. *;P< 0.05, **;P<0.01, ***;P<0.001

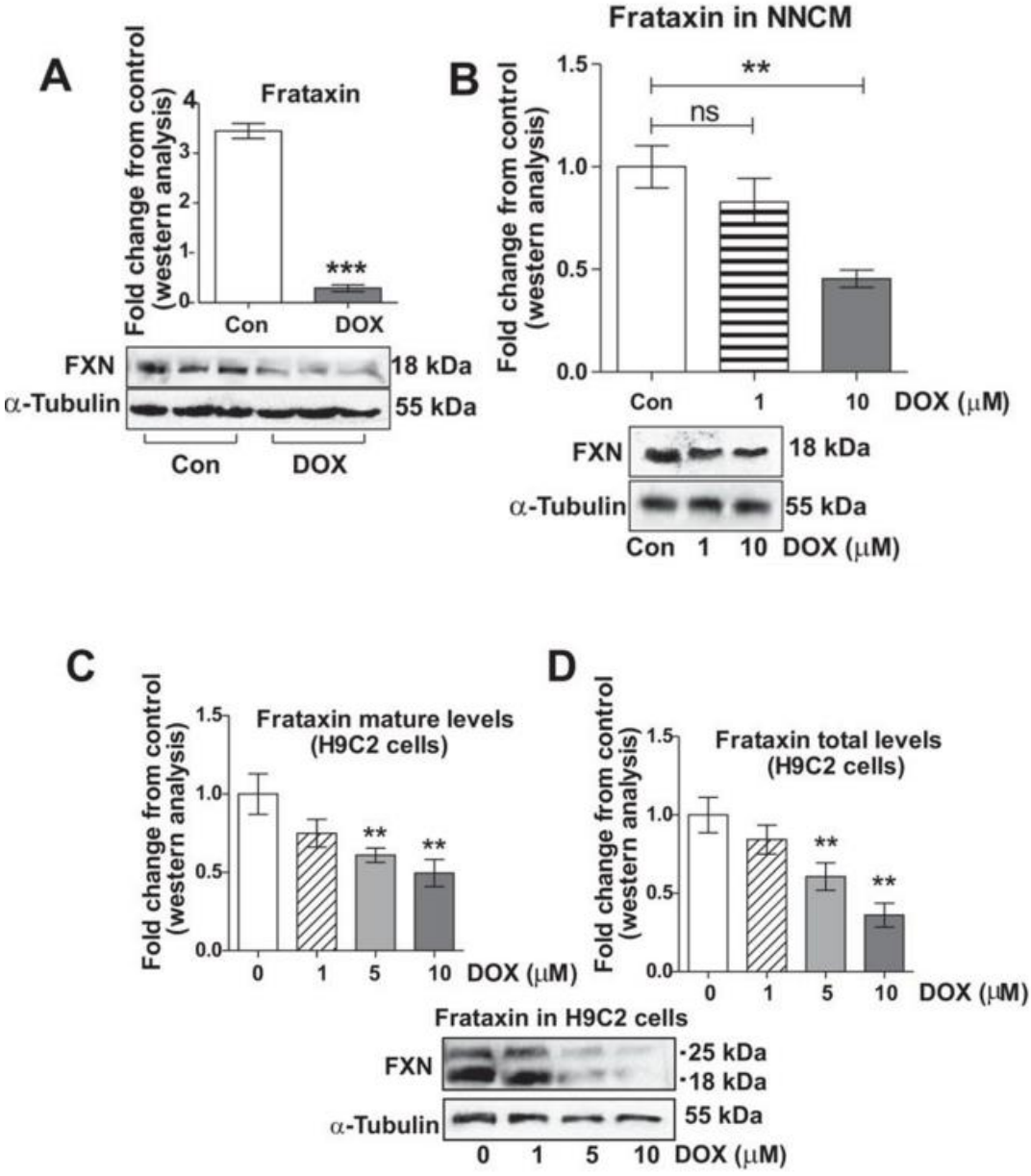
A
Frataxin
Fold change from control (western analysis)
***
Con
DOX
FXN
18 kDa
α-Tubulin
55 kDa
Con
DOX
B
Frataxin in NNCM
Fold change from control (western analysis)
**
ns
Con
1
10
DOX (μM)
FXN
18 kDa
α-Tubulin
55 kDa
Con 1 10 DOX (μM)
C
Frataxin mature levels (H9C2 cells)
Fold change from control (western analysis)
**
**
0 1 5 10 DOX (μM)
D
Frataxin total levels (H9C2 cells)
Fold change from control (western analysis)
**
**
0 1 5 10 DOX (μM)
Frataxin in H9C2 cells
FXN
25 kDa
18 kDa
α-Tubulin
55 kDa
0 1 5 10 DOX (μM)
E
Compartmentalization of frataxin
FXN
25 kDa
18 kDa
TOM70
70 kDa
α-Tubulin
55 kDa
0 1 5 10 MW 0 1 5 10 DOX (μM)
Mitochondrial
Cytosolic
F
Compartmentalization of frataxin
Fold change from control (western analysis)
Cytosolic
Mitochondrial
p=0.1302
τ
**
ττ
**
ττ
0 1 5 10
DOX (μM)

Figure. 3.2: Doxorubicin reduces frataxin expression levels. (**A**) Representative western blot image of FXN expression levels in mice treated with DOX (5 mg/kg; once/week for 5 treatments) and average densitometric values are represented as fold change from control in graphical form. (**B**) Western analysis of FXN expression levels in neonatal cardiomyocytes treated with 0, 1 μM and 10 μM DOX for 24 hours. Values are represented as fold change from control. (**C**) Evaluation of increasing DOX dosage (0, 1, 5 and10 μM) at 24 hours on FXN expression in H9C2 cardiomyoblasts by western analysis, representative densitometric measurements of mature (18 KDa) and (**D**) total (18 KDA+25 KDa) FXN levels with increasing concentrations of DOX. Experiment is represented as fold change from control. (**E and F**) Results from western analysis reflect the effects of DOX on mitochondrial and cytosolic FXN levels. Data are represented as fold change from control and standardized to TOM70 and α-tubulin. Values are represented as the mean ± S.E.M of 4 independent experiments and analyzed by student t-test (two tailed) to evaluate significance between groups **; $P<0.01$, ***; $P<0.001$, τ; $P<0.05$, ττ ; $P<0.01$.

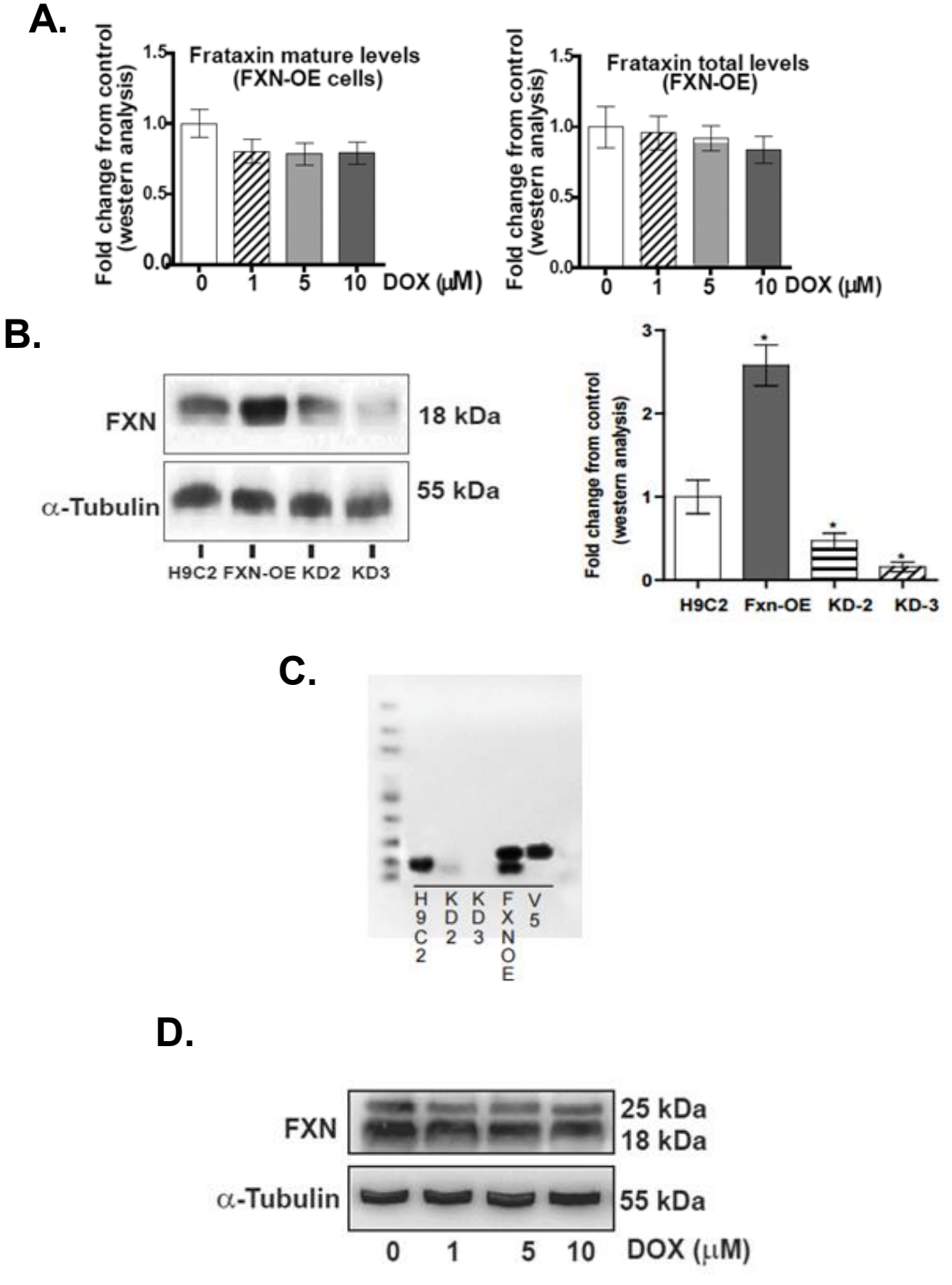
A.
Frataxin mature levels
(FXN-OE cells)
Fold change from control
(western analysis)
1.5
1.0
0.5
0.0
0
1
5
10
DOX (μM)
Frataxin total levels
(FXN-OE)
Fold change from control
(western analysis)
1.5
1.0
0.5
0.0
0
1
5
10
DOX (μM)
B.
FXN
18 kDa
α-Tubulin
55 kDa
H9C2
FXN-OE
KD2
KD3
Fold change from control
(western analysis)
3
2
1
0
*
*
*
H9C2
Fxn-OE
KD-2
KD-3
C.
H9C2
KD2
KD3
FXNOE
V5
D.
FXN
25 kDa
18 kDa
α-Tubulin
55 kDa
0
1
5
10
DOX (μM)

Figure. 3.3: Effects of doxorubicin on frataxin over expression. (**A**) FXN expression levels in non-FRDA and FRDA fibroblasts as determined by western analysis. **(B)** Evidence of frataxin expression levels in frataxin over expressing (FXN-OE) and frataxin knock down (KD2 and KD3) stable cell lines. (C) H9C2, KD2, KD3 and FXN OE and V5 tag displaying endogenous FXN levels. FXN OE consists of V5 tag (**D**) Graphical representation mature (18 KDa) levels and total levels of FXN by western immunoblot analysis, that demonstrates the effect of DOX (0, 1, 5 and 10 μM) on FXN-OE cardiomyoblasts. Values are represented as fold change from control and based upon mean ± S.E.M. of the replicates of 3 individual experiments. No statistical differences were observed between groups.

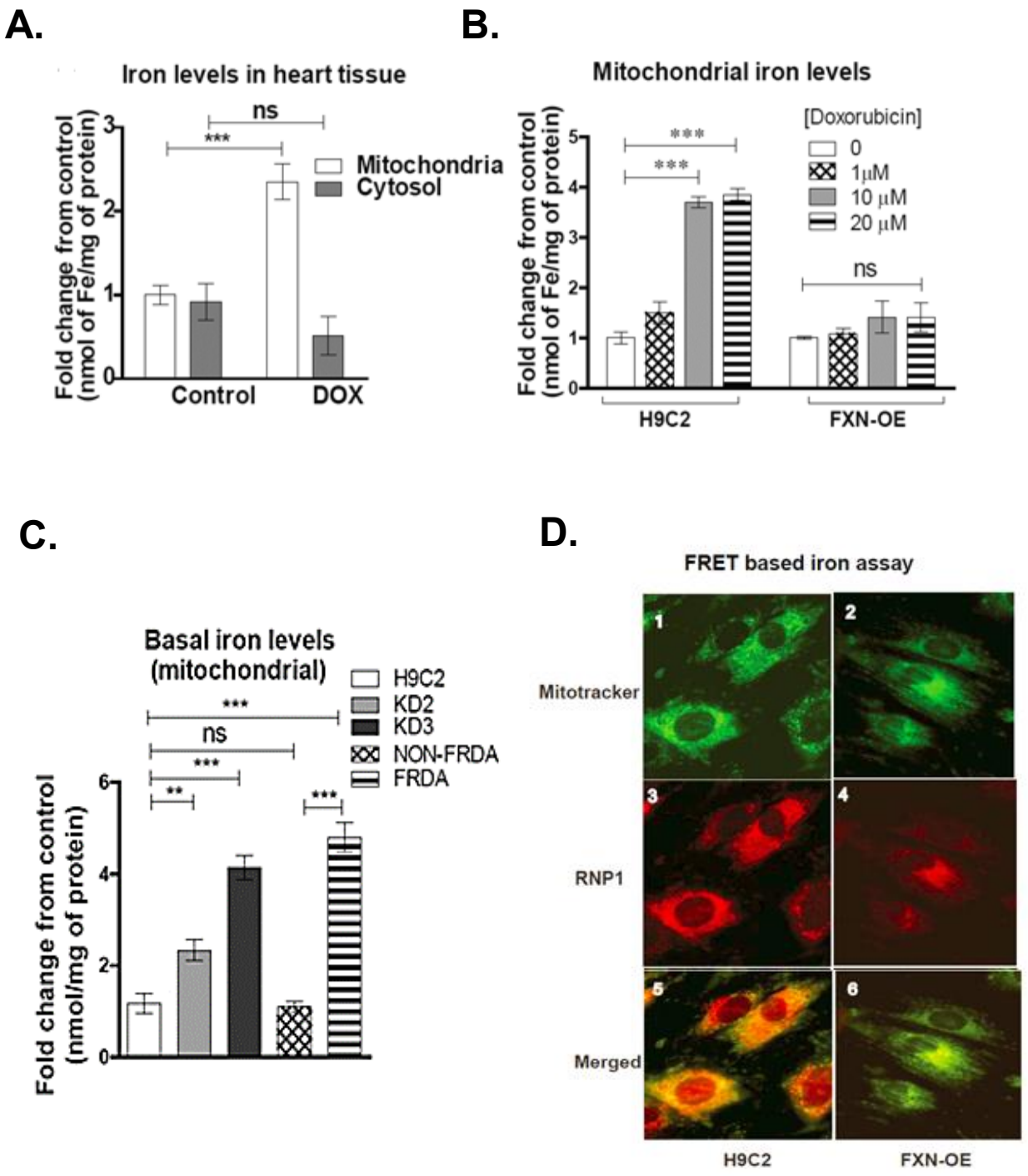

Figure. 3.4: Doxorubicin mediated reduction in frataxin leads to mitochondrial iron accumulation. (**A**) Ferrozine colorimetric iron assay in isolated mitochondria from control and DOX treated mice hearts, N=4. (**B)** Mitochondrial iron levels in H9C2 control and FXN-OE

cardiomyoblasts treated with DOX (0, 1, 10 and 20 μM), for 24 hours. **C**) Basal mitochondrial iron levels in cell lines expressing varying FXN levels. (**D**) Increased fluorescence intensity due to iron accumulation observed in DOX (10 μM, 24 hours) treated (1) control H9C2 cardiomyoblasts + MitoTracker (green), (2) FXN-OE cells + MitoTracker (green), (3) control H9C2 cardiomyoblasts + RNP1(Red), (4) FXN-OE cardiomyoblasts + RNP1, (5) merged image of control H9C2 cardiomyoblasts + MitoTracker + RNP1, (6) merged image of FXN-OE cells + MitoTracker + RNP1. Values are represented as mean ± S.E.M. from 4 independent experiments normalized to control H9C2 cells and analyzed by ANOVA with Tukey's post-hoc analysis for significances between groups and within groups.***;$P<0.001$, **, $P<0.01$, *

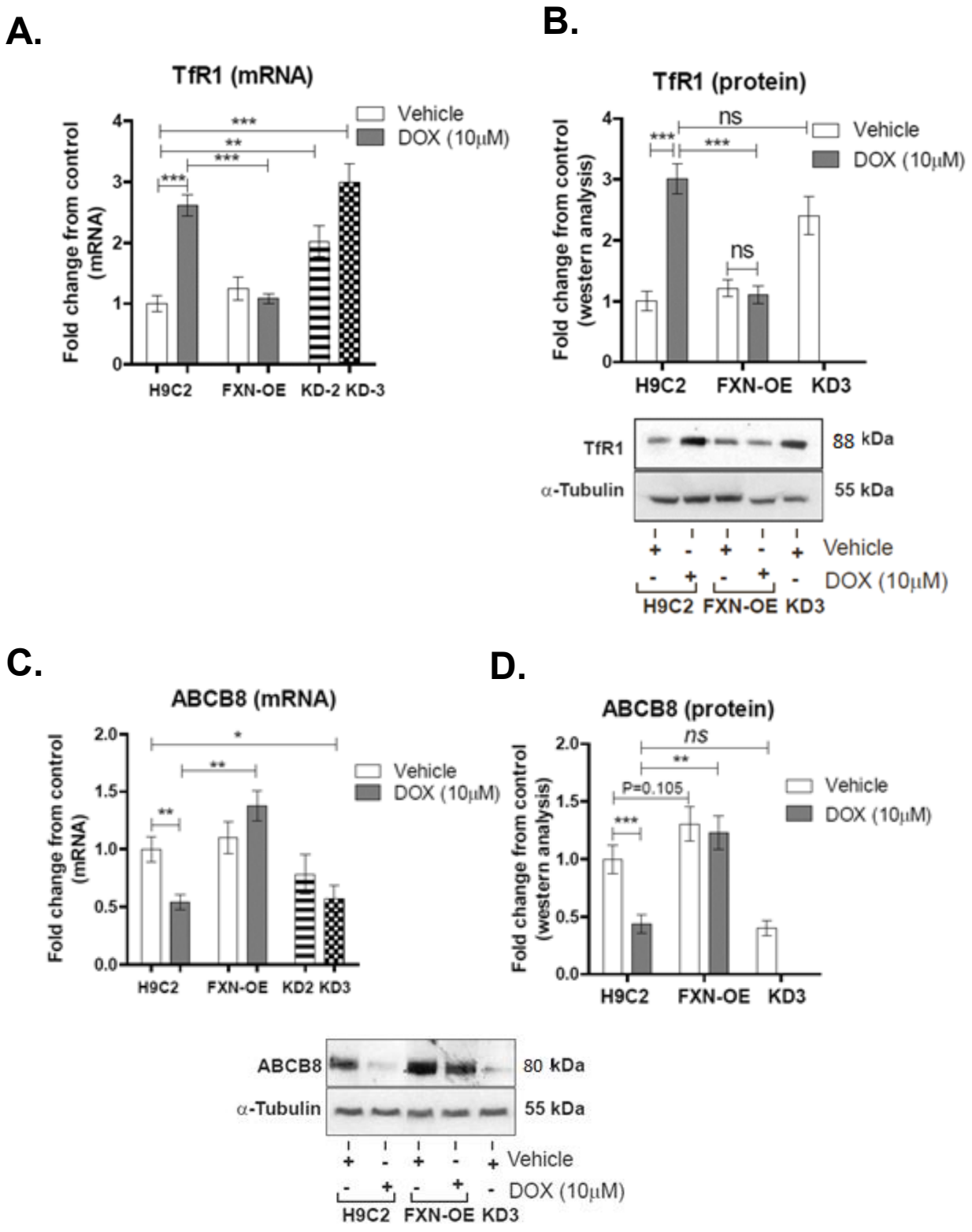
A.
TfR1 (mRNA)
Fold change from control (mRNA)
Vehicle
DOX (10μM)
H9C2
FXN-OE
KD-2
KD-3
B.
TfR1 (protein)
Fold change from control (western analysis)
ns
H9C2
FXN-OE
KD3
TfR1
88 kDa
α-Tubulin
55 kDa
Vehicle
DOX (10μM)
C.
ABCB8 (mRNA)
KD2
KD3
D.
ABCB8 (protein)
P=0.105
ABCB8
80 kDa

Figure. 3.5: Doxorubicin mediates alteration in iron transporter expressions. (**A**) qRT-PCR analysis of TfR1 mRNA levels in DOX treated (10 μM, 24 hours) control, FXN OE H9C2 cardiomyoblasts, KD2 and KD3 cardiomyoblasts. (**B**) Western analysis of TfR1 protein levels in control H9C2, H9C2+DOX, FXN-OE, FXN-OE +DOX and KD3 cardiomyoblasts. (**C**) QRT-PCR analysis of ABCB8 mRNA levels in DOX treated (10 μM, 24 hours) control and FXN-OE H9C2 cardiomyoblasts, KD2 and KD3 cardiomyoblasts. (**D**) Western analysis of ABCB8 protein levels in control H9C2, H9C2+DOX, FXN-OE, FXN-OE+ DOX and KD3 cardiomyoblasts. Densitometric values are standardized to α-Tubulin levels and are represented as fold change from control and are based upon mean ± S.E.M. from 4 independent experiments normalized to control H9C2 cells and analyzed by ANOVA with Tukey's post-hoc analysis for significances between groups *; $P<0.05$, **, $p<0.01$, ***; $P<0.001$.

A.

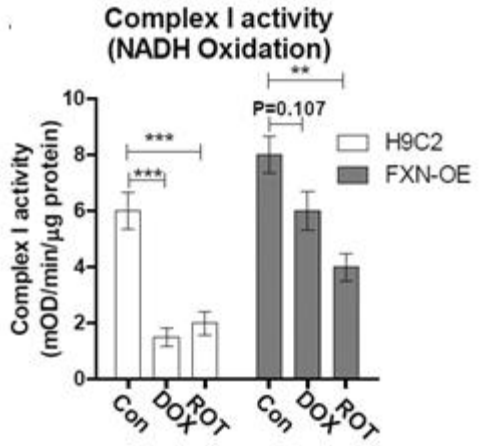
Complex I activity
(NADH Oxidation)
Complex I activity
(mOD/min/µg protein)
P=0.107
H9C2
FXN-OE
Con
DOX
ROT

B.

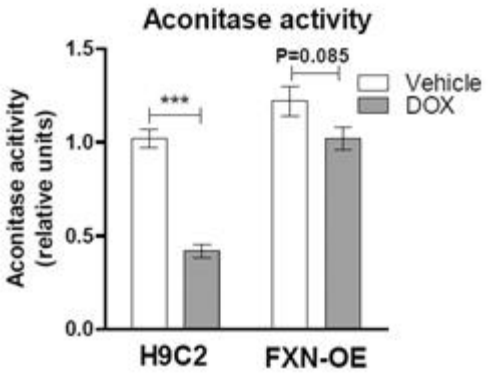
Aconitase activity
Aconitase acitivity
(relative units)
P=0.085
Vehicle
DOX
H9C2
FXN-OE

C.

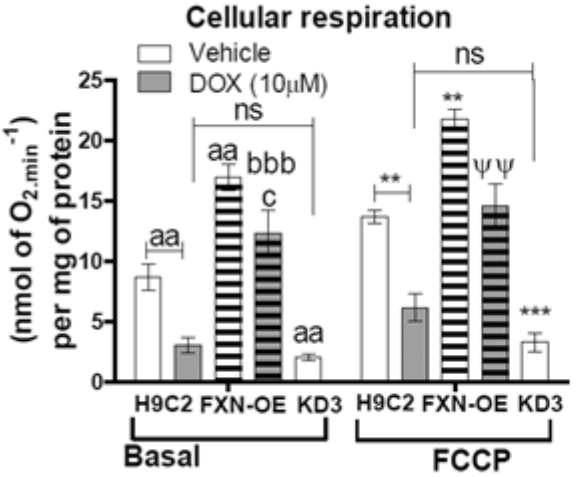
Cellular respiration
Vehicle
DOX (10µM)
(nmol of O2.min-1)
per mg of protein
H9C2 FXN-OE KD3 H9C2 FXN-OE KD3
Basal
FCCP

D.

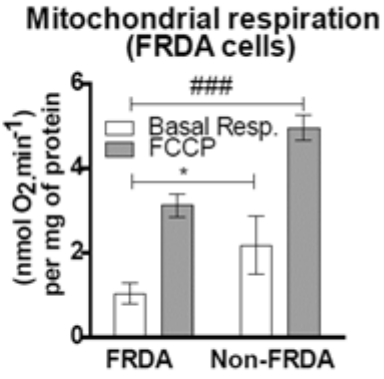
Mitochondrial respiration
(FRDA cells)
(nmol O2.min-1)
per mg of protein
Basal Resp.
FCCP
FRDA
Non-FRDA

E.

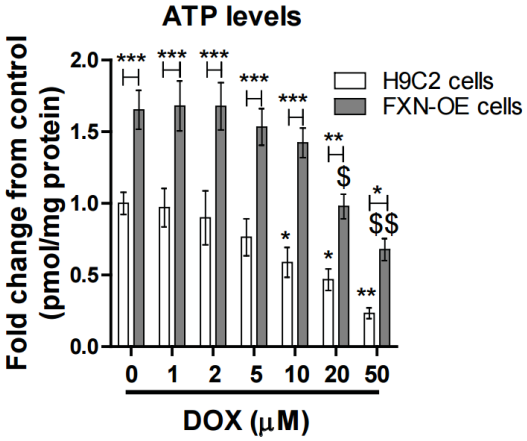
ATP levels
Fold change from control
(pmol/mg protein)
H9C2 cells
FXN-OE cells
DOX (µM)

F.

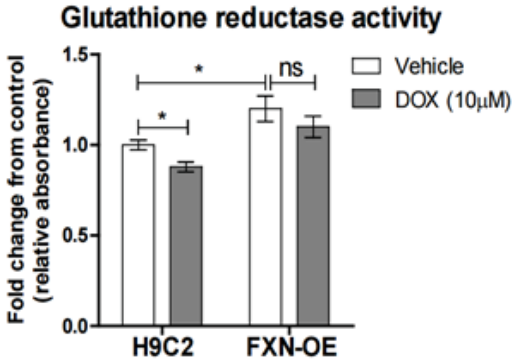
Glutathione reductase activity
Fold change from control
(relative absorbance)
Vehicle
DOX (10µM)
H9C2
FXN-OE

Figure. 3.6: Frataxin overexpression protects against doxorubicin mediated attenuation of mitochondrial energetics. (A and B) Measurement of NADH oxidation and aconitase activity levels in control H9C2 and FXN-OE cardiomyoblasts treated with DOX (10 μM) for 24 hours with and without rotenone (100 nM). Values were standardized to total protein concentrations. (**C**) Mitochondrial respiration from FXN-OE and KD3 cells with or without DOX were compared to control H9C2 cardiomyoblasts and normalized to total protein levels. (**D**) Mitochondrial respiration in FRDA fibroblasts were compared to non-FRDA fibroblasts and values were normalized to total protein levels. Mitochondrial complex activity was decoupled by adding Trifluorocarbonylcyanide (FCCP; 6 μM), where N=3 independent experiments. (**E**) ATP levels in H9C2 and FXN OE cardiomyoblasts treated with or without DOX (10 μM), for 24 hours. (N=4), where samples are mean ± S.E.M. with 4 replicates from 3 independent experiments. (**F**) Glutathione reductase levels in DOX (10 μM) treated and non-treated H9C2 and FXN OE cardiomyoblasts. All samples are average ± SD with 4 replicates from 3 independent experiments. Data with multiple comparisons were analyzed using ANOVA with Tukey's-*Post hoc* analysis and based upon mean ± S.E.M from 4 independent experiments, *; P<0.05, **; P<0.01, ***; P<0.001, ###; P<0.001, $; P<0.05, $$; P<0.01,aa; P<0.01, bbb; P<0.001, ψψ; P<0.01.

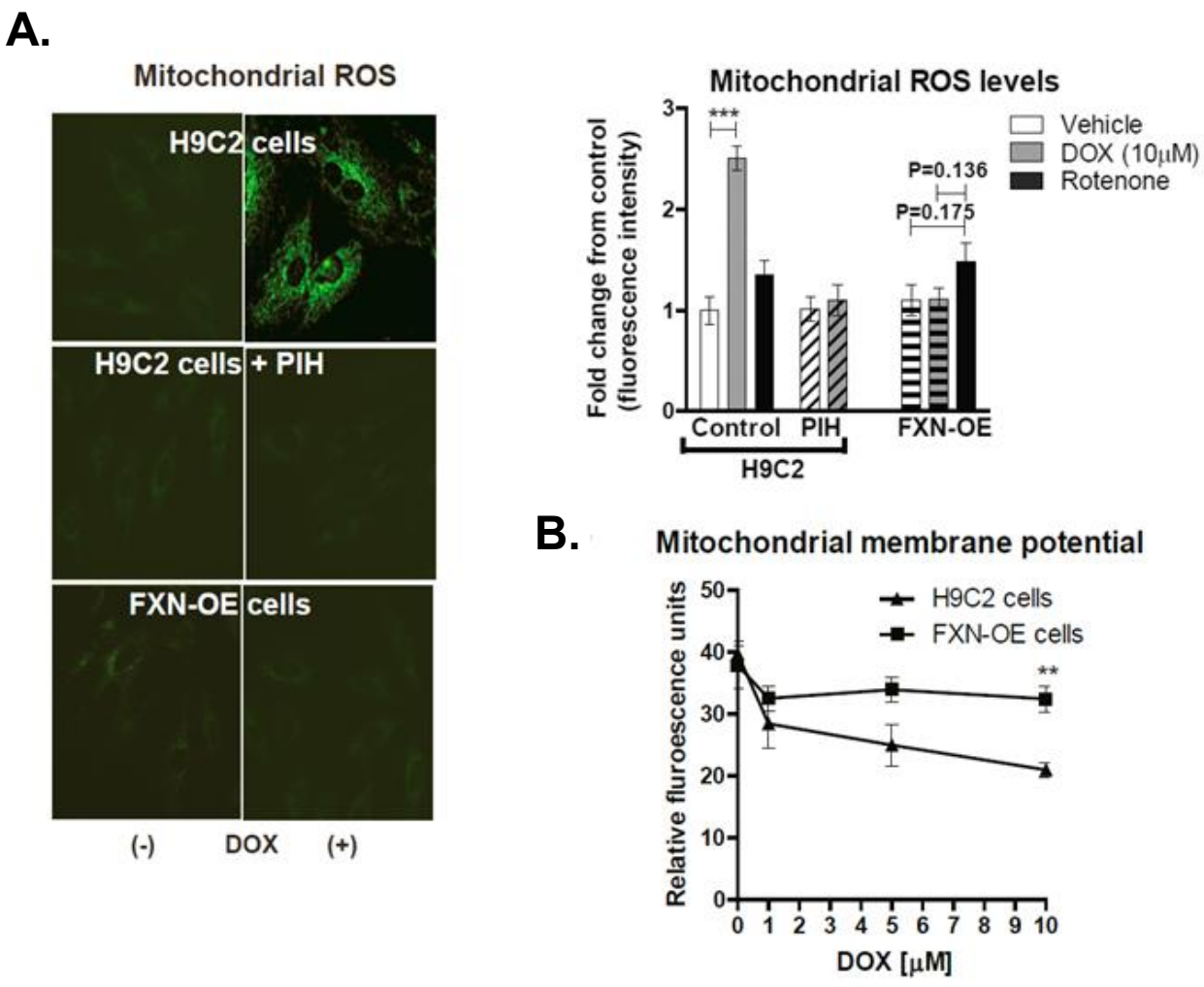

Figure. 3.7: Frataxin over expression mitigates doxorubicin mediated mitochondrial ROS formation and membrane depolarization. (**A and B**) Fluorescence images of mitochondrial DOX (10μM) mediated ROS formation (green) and graphical representation of ROS levels in FXN-OE and control H9C2 cardiomyoblasts with or without rotenone or PIH. (**C**) Mitochondrial membrane potential (Δψm) determined by TMRE (2 μM) immunofluorescence in DOX treated (1, 5, 10 μM) H9C2 and FXN OE cells for 24 hours where N= 3 independent experiments and are represented as mean ± S.E.M. and analysis was accomplished by ANOVA with Tukey's post-hoc analysis for significances between groups and within groups based upon averages from the assays **; P<0.01, ***; P<0.001.

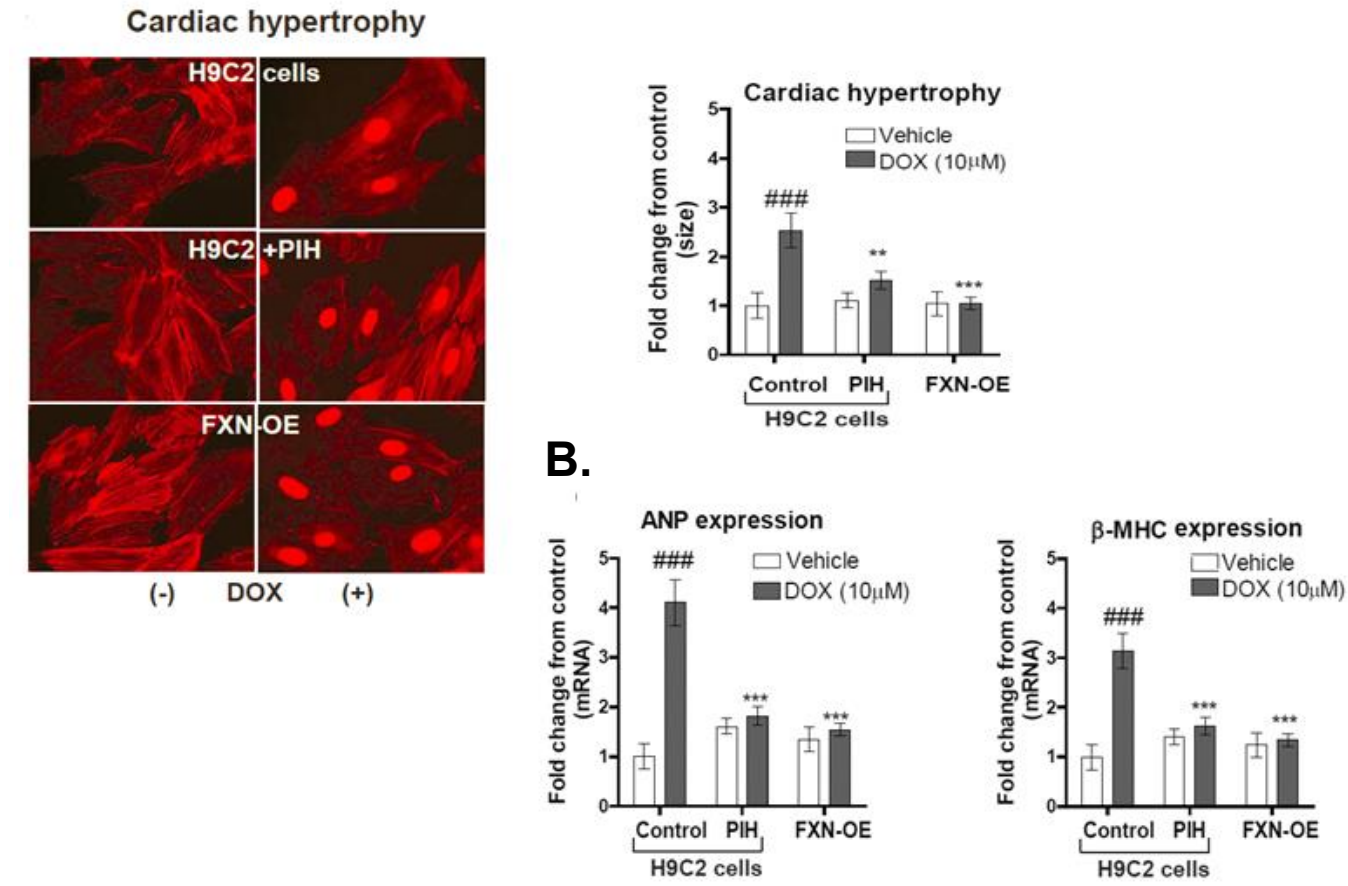

Figure. 3.8: FXN overexpression protects against DOX induced cardiac hypertrophy in H9C2 cardiomyoblasts. (A) Representative Phalloidin fluorescence imaging displays changes in H9C2 and FXN-OE cell size in response to DOX (10 μM) treatment. Mitochondrial iron chelator (PIH, 40 μM) was utilized. (**B**) ANP and β-MHC mRNA expression were evaluated by two step qPCR analysis from cells treated with DOX (10μM) for 24 hours, with or without PIH. Data are represented as fold change from control and in the case for qPCR analysis standardized to β-actin. Indicated above are the mean ± S.E.M. of the replicates of 4 individual experiments, **; P< 0.01, ***; P<0.001, ###; P<0.001.

3.6 Scope of the study and future directions

These findings for the first time provide evidence that DOX mediated damage to cardiomyocytes may be due to the disruption of FXN. Many of our findings were observed in H9C2 cardiomyoblasts and thus reflect a neonatal form of cardiomyocyte rather than adult. Second we utilized a nu/nu mouse model to reflect the direct effects of DOX in the heart. Our future work will address these issues with the development of a FXN over expressing mouse model to better understand and justify the role of FXN in the DOX mediated damage to the mitochondria and development of cardiac hypertrophy. **In the future, we plan to examine the mechanism of FXN degradation by DOX and investigate whether FXN protein maybe subject to ubiquitination mediated degradation by DOX.**

Chapter.4 Doxorubicin mediated reduction of frataxin may involve Ubiquitination Proteasome System (UPS)

(Preliminary studies)

4.1 Abstract

DOX is a widely used chemotherapeutic agent whose usage is limited by its dose-limiting cardiotoxic profile. DOX has been observed to activate the UPP and thereby promote cardiotoxicity. Our previous studies demonstrated that mitochondrial FXN was attenuated in response to DOX (Chapter 3). Our current findings further explore the mechanism by which FXN is attenuated. To better understand how DOX altered FXN expression, we utilized the proteasome inhibitor MG132 which reduces the degradation of ubiquitin-conjugated proteins and observed a significant increase in FXN expression in cardiomyoblasts treated with DOX. These observations provide an important link to understanding the mechanism of FXN attenuation by DOX. Since there exists a functional crosstalk between ubiquitination and acetylation, we examined whether FXN was acetylated prior to ubiquitination upon DOX exposure. We observed an increase in acetylation which was attributed to reduced SIRT3 levels by DOX. Our results collectively suggest a possible post translational alteration including elevated ubiquitination and hyperacetylation of FXN with DOX. The preliminary findings pave way to further determine potential lysine residues within the N terminal residue of FXN which may subject to alteration with DOX and probable E3 ligases which maybe elevated upon DOX exposure.

4.2 Introduction

DOX is a widely used cancer chemotherapeutic agent used in the treatment of wide range of cancers. However its utility is limited by its dose dependent development towards cardiomyopathy before leading to heart failure[78]. Although compensatory mechanisms may reverse the cardiotoxic side effects of DOX, limiting the dosing regimen to curb cardiotoxicity, interferes with the antitumor activity which is observed at a much higher dose. Therefore there is an increasing need to prevent morbidity and mortality associated with DOX cardiotoxicity. Extensive research has been carried out to understand the mechanism by which DOX impairs the heart. Several studies have attributed DOX mediated cardiotoxicity to increased ROS in cardiomyocytes. Ongoing research has implicated ubiquitination mediated proteasome degradation system (UPS) as a potential mechanism that contributes to cardiotoxicity[22].

Proteolysis by UPS involves (i) the attachment of Ub molecules that target the protein molecule and (ii) degradation of the targeted protein by proteasome. The UPS play a major role in controlling the protein quality and control and regulate several processes such as transcription, cell cycle and apoptosis[20, 21]. Therefore any alteration in the normal post translational modifications will have a significant impact on the cellular processes. Dysfunctional UPS has been implicated in I/R injury, hypertrophy and heart failure[203]. Ubiquitination mechanism involves a cascade of enzymes including Ub activating E1, Ub conjugating E2 and Ub ligase E3. The specificity of ubiquitination is dependent on E3 ligases, which has been implicated in several pathological conditions including cardiac hypertrophy and remodeling[151].

The UPS can not only activate direct degradation mechanisms but can be enhanced or attenuated by post translational modifications prior to the target protein such as acetylation. The ε group of lysine residue is a major target of protein ubiquitination. It is known that

hyperacetylation is highly profound in mitochondrial protein involved in energy metabolism[204]. For instance FRDA models of FXN deficiency displayed progressive hyperacetylation of mitochondrial protein associated with respiratory chain complex [205]. Therefore it can be reiterated that any alteration in the prior lysine acetylation will affect the ensuing protein ubiquitination.

Previously we have observed that mitochondrial ISC protein FXN was reduced in response to DOX treatment[206]. The reduction in FXN further led to decreased mitochondrial bioenergetics as observed by reduction in ISC containing mitochondrial aconitase, NADH dehydrogenase, respiration and ATP. DOX mediated reduction in FXN further led to elevated labile iron within the mitochondria and impaired the antioxidant-ROS balance within the cell.

Based on our observations we propose that FXN may be an early target of UPS mediated degradation which maybe a consequence of hyperacetylation by DOX treatment.

4.3 Materials and Methods

4.3.1 Construction of FXN-over expressed (FXN-OE) H9C2 cardiomyoblasts.

FXN-OE cell lines were developed using a GATEWAY-based lentiviral system. The lentiviral empty backbone pLX302 plasmid was purchased from ADDGENE and the plasmid, #25896 was a kind gift from David Root's lab (Broad Institute, MIT and Harvard). The plasmid is tagged with a V5 epitope at the C terminal backbone. The cDNA fragment of the FXN was cloned into the donor vector provided from the gateway system. Further, FXN was cloned into the pLX 302 (ampicillin and chloramphenicol resistant) lentiviral destination vector (http://www.addgene.org/25896/) using LR Clonase (Life Sciences, Cat. #. 11789100). A puromycin selectable antibiotic marker exists in the pLX 302 vector. The cells were then

subjected to transformation in a bacterial cell DH5alpha strain (Invitrogen, Cat. # -012) and the competent plasmid was isolated using PureYieldTM Midiprep system (Promega A2495). The expression vector was then purified and was transfected with a second generation lentiviral packaging vector (psPAX2, ADDGENE cat # 12260, a kind gift of the Didier Trono Lab, (The Swiss Federal Institute of Technology Lausanne (EPFL)) and the envelope vector (pMD2.G, ADDGENE Cat# 12259, a kind gift from the Didier Trono Lab) in a HEK 293T cell line. Further, the virus was extracted from the media and purified using a 0.45 μm syringe filter. Subsequently, purified virus was exposed to H9C2 cells for 24 hours and the next day, the cells were treated with 1μg/ml of puromycin for selection of cells expressing FXN.

4.3.2 Cell Culture

The myocytes were mixed with complete DMEM media containing 10% (v/v) FBS and 1% (v/v) penstrep, rocked back forth and were incubated at 37º C and 5% CO_2. After about 3-4 hours the cells were checked for attachment. The cells were treated the same day.

4.3.3 Western Immunoblot and immunoprecipitation.

Proteins were extracted from H9C2 cardiomyoblasts using the cell lysis buffer (Cell Signaling, # 9803) and supplemented with protease cocktail inhibitor (Thermo Scientific, # 87786). Detection of ubiquitination required the addition of 50 μM PR-619, a cell permeable reversible deubiquitylases that prevents deubiquitination of protein during cell lysis.

FXN detection in vivo and in vitro by western analysis was carried out as previously described using FXN (1:1000, SantaCruz, #25830) antibody[206]. For in vitro detection of ubiquitination, MG132 (Selleckchem, #S2619) a proteasome inhibitor, dissolved in DMSO was

incubated with and without DOX (5 μM) for 18 hours and DUB inhibitor (50 μM) (Life sensor, #S19649). Briefly, protein lysates were denatured at 95° C for 5 minutes, with loading buffer and then resolved in a 12% resolving gel and blotted on a nitrocellulose membrane. The blots were incubated overnight with FXN (1:1000, Santa Cruz, #25830) and α-tubulin (1:2000, DSHBY, #12G10) or VU-1 (1:1000, life sensors, #VU101) primary antibodies with 5% milk in TBS-T. The blots were then washed with TBS-T and incubated with HRP conjugated secondary antibody (1:2000, Rockland) for 1 hour. Blots were visualized with chemi-illuminescence reagent (Millipore), and imaged using a Bio-Rad gel dock system. Protein bands were analyzed using ImageJ software and standardized to α-tubulin.

For immunoprecipitation of ubiquitinated FXN, 200 μl of 100-200 μg of H9C2 lysates were incubated overnight with primary antibody by gently rocking at 4º C. Protein G agarose beads were added to the lysate and incubated with gentle rocking for 1-3 hours at 4º C. The bead was microcentrifuged for 30 seconds and washed with 300 μl cell lysis buffer. The pellet was washed with 3X SDS sample buffer boiled at 95º C for 2-5 minutes and was loaded on to SDS PAGE gel for immunoblot analysis.

4.3.4 Construction of mCherry-frataxin vector

The FXN-mCherry-N1vector was constructed using gateway LR cloning. Briefly, the FXN donor vector from above was cloned into pDest-mCherry-N1 (ADDGENE Cat. # 31907, a kind gift from the Robin Shaw lab, (Cedars Sinai, Heart Institute)) destination vector using LR clonase and the expression vector was then transformed into competent bacteria, DH5 alpha (Invitrogen, Cat. #18258-012). The competent plasmid was isolated and purified using PureYieldTM Midiprep system (Promega A2495).

4.3.4.1 mCherry FXN-Imaging

The mCherry-frataxin vector (500 ng) was transfected into H9C2 cardiomyoblasts using Polyplus jetPRIME transfection reagent (Cat. # 114-07). The next day cells were treated with or without DOX (10 μM) ± MG132 (Selleckchem, #S2619) a proteasome inhibitor (10 μM) for 24 hours. Cells were then incubated with MitoTracker Green FM (Molecular Probes, Cat. # M-7514) for mitochondrial visualization with mCherry FXN (red) using a Nikon Eclipse Ti inverted fluorescence microscope. Fluorescence images of the red (Rhodamine red) and green channels (FITC) within the same fields were obtained and overlaid using the Nikon NIS-Elements software rendering areas of co-localization yellow in color.

4.4 Results

DOX increases UPS activity

Proteasome degradation is preceded by enhanced ubiquitination. To determine the effect of DOX on UPS, cardiomyoblasts were treated with 5 μM at 0, 2, 6 and 12 h and observed a time dependent alteration in the pattern of ubiquitination. DOX treatment at 6 h displayed the highest ubiquitination of the substrate proteins following which we observed a reduction (Fig.4.1A). Cardiomyocytes were further treated with DOX (5 μM) with or without proteasome inhibitor MG132 (10 μM) and deubiquitylating enzyme inhibitor (DUBi).We observed elevated ubiquitination with the addition of MG132 and DUBi and DOX together in comparison to control non-treated cardiomyocytes (Fig.4.1B) leading us to believe that DOX induced ubiquitination in H9C2 cardiomyoblasts.

DOX induces ubiquitination of FXN in H9C2 cardiomyoblasts.

Previous observations have suggested that DOX mediates protein ubiquitination and degradation by the Ubiquitin-Proteasome System (UPS)[22]. In order to understand the mechanism of FXN attenuation by DOX, our H9C2 cardiomyoblasts were treated with MG132 with or without the addition of DOX. The addition of MG132 (10 μM) blocked the degradation of FXN, thus suggesting the possibility that DOX regulates FXN expression by an ubiquitination and degradative process (Fig.4.2A). The significance of our results was further supported by microscopic localization studies, which revealed reduced mitochondrial and cytosolic levels of FXN in DOX treated H9C2 cells. Further that co-treatment with MG132 and DOX resulted in comparable cytosolic and mitochondrial patterns found in control cells (yellow-merged image) (Fig. 4.2B).

.

Figures and Figure legends

A.

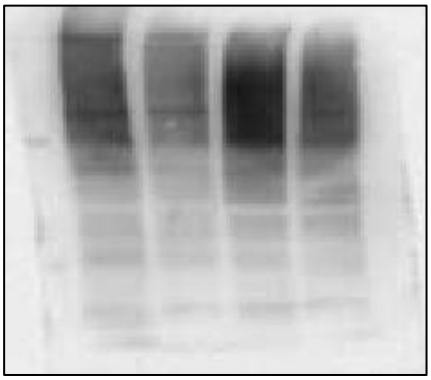

CON 2H 6H 12H

DOX (5μM)

B.

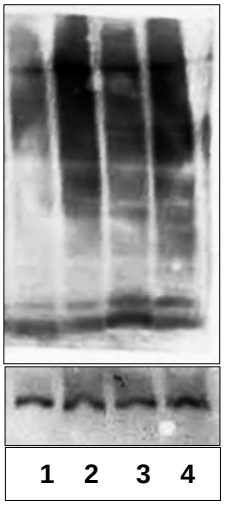

1. Control
2. DOX (5μM)
3. DUBi+MG132
4. DUBi+DOX+MG132

Figure. 4.1: DOX induces ubiquitination at 6h. (A) western blot analysis of total protein lysate from H9C2 cardiomyoblasts treated with DOX (5 µM) displayed increased ubiquitination of proteins at 6 h. (B) Immunoprecipitation of total protein extracted from H9C2 cardiomyoblasts treated with DOX (5 µM) concomitantly with or without the addition of DUBi and MG132 displayed highest ubiquitination at 6 h.

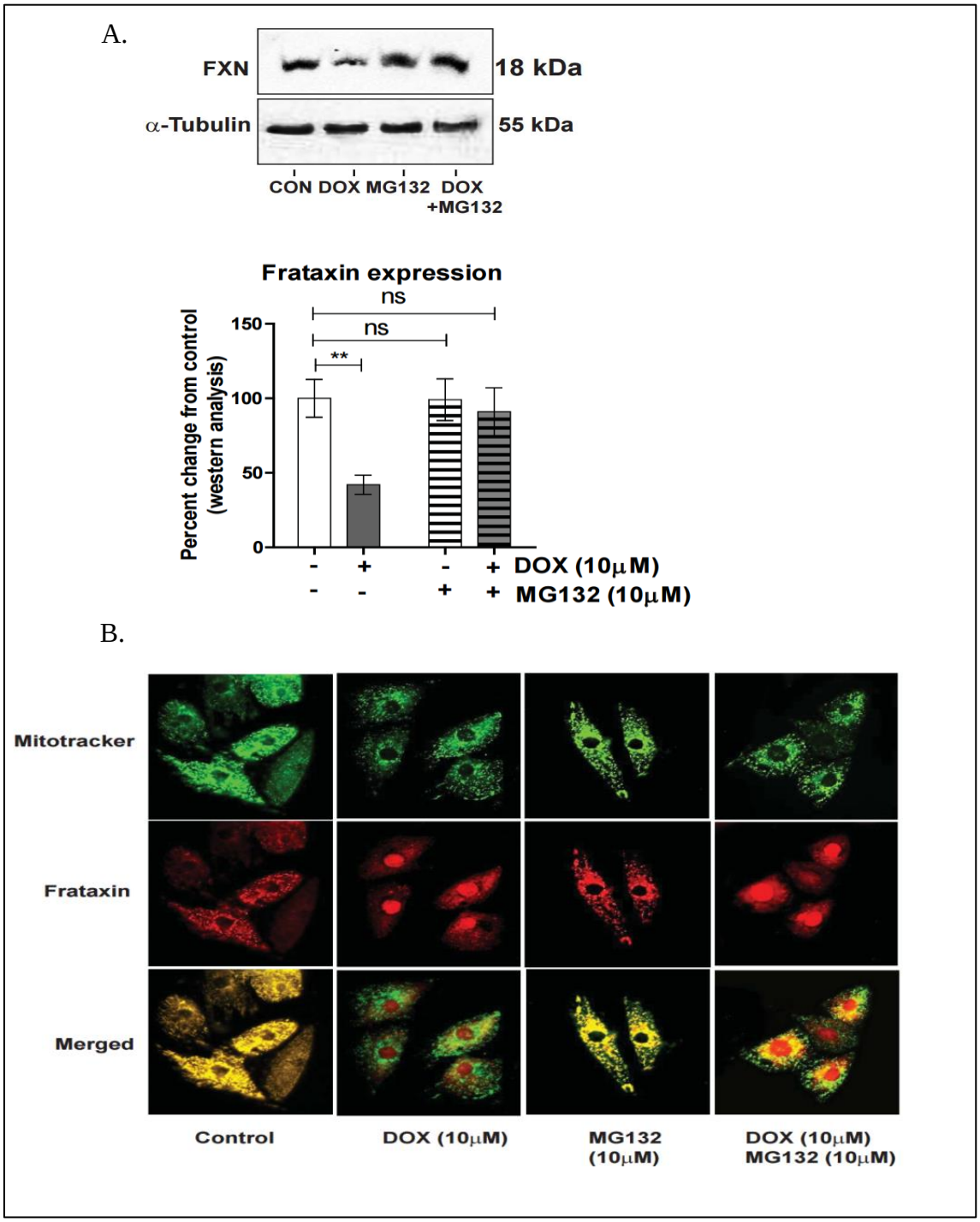

Figure. 4.2: DOX may induce ubiquitination of FXN. (A) western analysis of FXN expression from total H9C2 cardiomyoblasts extracts treated with DOX concomitantly with or without the

addition of MG132 (10 µM,18 h). Values are mean percent change ± SE from control and standardized to α-tubulin based on 4 independent experiments. **P<0.005 (B) immunofluorescence detection of H9C2 cardiomyoblasts transfected with mcherry tagged FXN (red) treated with MG132 (10 µM, 18 h) with and without DOX, co-localized with mitochondria (green) observed with MitoTracker FM (green). Merged image reveal co-localization of FXN (red) with mitochondria (green) which appear yellow. (C) Immunoprecipitation of FXN from H9C2 cardiomyoblasts treated with or without DOX displays increase in ubiquitination at 6 h. Values are represented as fold change from control and based on mean ± S.E.M of the 3 independent replicates.

4.5 Discussion

Alterations in post translational modifications are one of the major reasons for derangements in mitochondrial energy flux. Previous studies by Rufini et. al., have demonstrated that FXN maybe ubiquitinated before degradation[24]. In light of these findings we proposed that DOX treatment may induce an increase in ubiquitination and degradation of FXN. Our preliminary findings demonstrated that FXN may be ubiquitinated upon DOX treatment. The addition of MG132, a proteasome inhibitor that reduces the degradation of ubiquitin conjugated protein, to DOX demonstrated an increase in mitochondrial localization of FXN as observed by yellow fluorescence. Further our future work will focus on demonstrating increased ubiquitination of FXN using a deubiquitinase inhibitor and MG132 upon DOX treatment.

4.6 Scope of this study and Future directions

Increased ubiquitination and hyperacetylation of mitochondrial proteins involved in mitochondrial energy homeostasis may contribute to decreased fatty acid oxidation, energy utilization and hypertrophy which ultimately leads to heart failure. The pathophysiological mechanisms involved in DOX mediated cardiotoxicity is complex and requires further research. Previously we investigated the critical role of FXN upon DOX exposure, and how overexpression of FXN was protective against the mitohormetic effects of DOX by activating mitochondrial energy regulation and suppressing ROS. We expand upon these findings and the current study further explores the molecular mechanism of FXN degradation by DOX. Our future work will investigate whether FXN is ubiquitinated by DOX and whether this increase in ubiquitination will lead to degradation.

Acetylation is a post translational modification of lysine residues. Previous studies have reported the possibility of hyperacetylation of several mitochondrial energy transduction proteins which contribute to hypertrophy. Since there exists a functional crosstalk between ubiquitination and acetylation[207], we will be examining in the future whether FXN was acetylated prior to ubiquitination upon DOX exposure.

Lysine acetylated site prediction (LAceP) predicted potential acetylated lysine sites in FXN, which may be targeted by DOX.

FXN acetylated Lysine site prediction

Step.1

Acetylated lysine site prediction can be performed using computational method that uses logistic regression algorithm called LAceP and generates acetylated sites of the given

protein[208]. Upon entering the protein sequence of FXN sequence in FASTA format, I observed probable acetylated lysine sites of FXN (Figure 4.3).

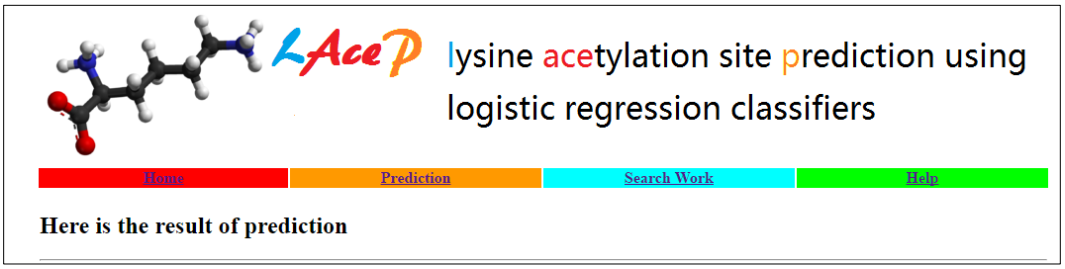

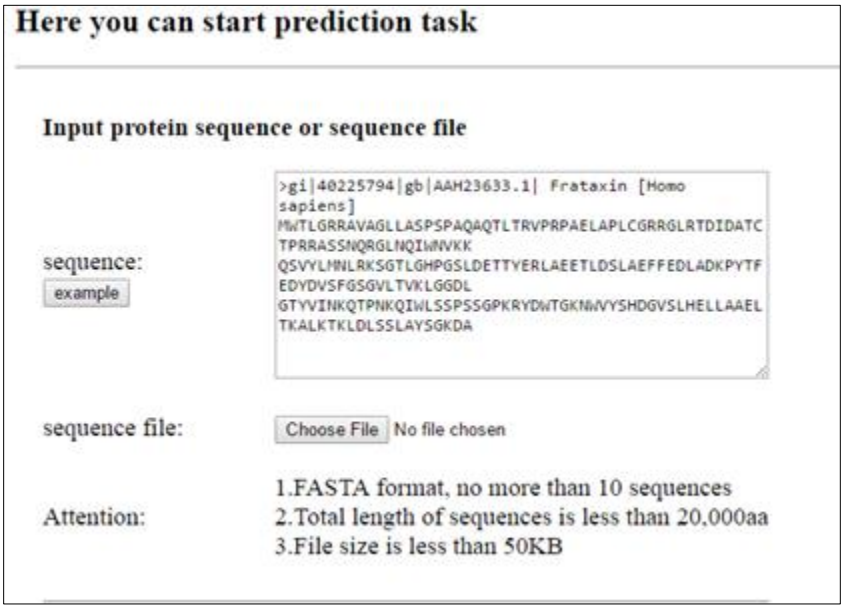

protein	position	sequence	score	acetylation
gi|40225794|gb|AAH23	69	QRGLNQIWNVKKQSVYLMNLR	0.21	NO
gi|40225794|gb|AAH23	70	RGLNQIWNVKKQSVYLMNLRK	0.03	NO
gi|40225794|gb|AAH23	80	KQSVYLMNLRKSGTLGHPGSL	0.041	NO
gi|40225794|gb|AAH23	116	LAEFFEDLADKPYTFEDYDVS	0.939	YES
gi|40225794|gb|AAH23	135	VSFGSGVLTVKLGGDLGTYVI	0.667	YES
gi|40225794|gb|AAH23	147	GGDLGTYVINKQTPNKQIWLS	0.202	NO
gi|40225794|gb|AAH23	152	TYVINKQTPNKQIWLSSPSSG	0.207	NO
gi|40225794|gb|AAH23	164	IWLSSPSSGPKRYDWTGKNWV	0.801	YES
gi|40225794|gb|AAH23	171	SGPKRYDWTGKNWVYSHDGVS	0.999	YES
gi|40225794|gb|AAH23	192	LHELLAAELTKALKTKLDLSS	0.957	YES
gi|40225794|gb|AAH23	195	LLAAELTKALKTKLDLSSLAY	0.0570000000000001	NO
gi|40225794|gb|AAH23	197	AAELTKALKTKLDLSSLAYSG	0.338	NO

www.scbit.org/iPTM/

Figure. 4.3: Potential acetylated lysine residues in FXN obtained computationally using LAceP

Step.2

Following this, we plan to observe if DOX treatment led to increase in acetyl-lysine residues in FXN. These results will demonstrate whether FXN is a target of hyperacetylation by DOX.

Recent studies have demonstrated reduced SIRT3 expression with DOX [25] and reduced SIRT3 expression consequently leads to hyperacetylation of mitochondrial proteins since mitochondrial acetylation of protein is regulated by SIRT3. Therefore increase in acetylation of FXN if observed, may be attributed to reduced mitochondrial lysine deacetylase SIRT3. Based on our preliminary findings and previous studies we propose two potential pathways by which FXN maybe ubiquitinated and degraded by DOX.

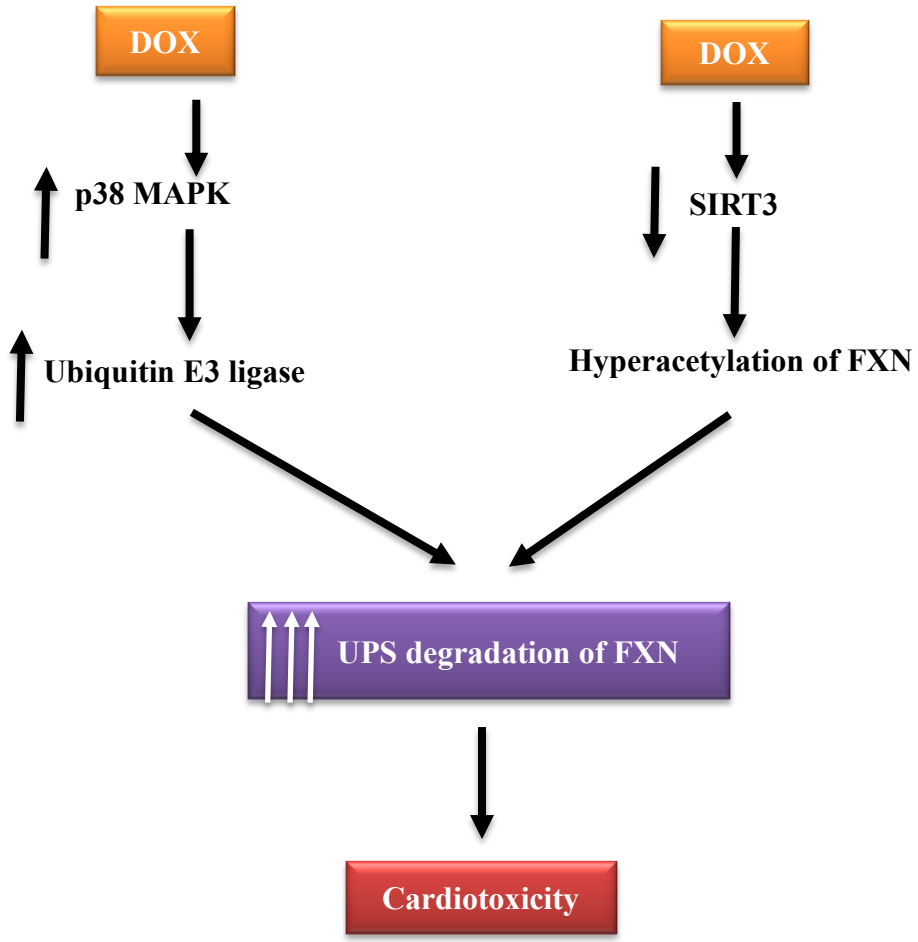

Figure. 4.4: Working model based on two different hypothesis that predicts the UPS mediated degradation of FXN by DOX.

The findings from the current study have been carried out in isolated rat ventricular cardiomyocytes and H9C2 cardiomyocytes. We are currently designing SIRT3 inhibitors to validate FXN hyperacetylation in FXN overexpressing mouse model and in TAC model. Protein degradation relies heavily on acetylation and the relationship between ubiquitination and acetylation depends on the nature of lysine modification. Therefore we are currently in the

process of identifying lysine residues which may be modified with DOX and the potential E3 ligases which catalyzes the transfer of Ub to FXN. We believe that findings from the current study will significantly add to the existing knowledgebase on the molecular mechanisms associated with DOX cardiotoxicity.

Chapter 5. PPARδ mediated cardioprotection against DOX mediated cardiotoxicity requires Frataxin

5.1 Abstract

DOX mediated cardiotoxicity centers around the cardio metabolic dysfunction associated with mitochondrial energy derangements and cardiac hypertrophy. Frataxin, a key regulator of mitochondrial energy regulation was observed to be severely attenuated and may possibly be degraded by the UPS system by DOX. PPARδ, a nuclear hormone receptor and a transcription factor, is abundantly expressed in heart. While PPARγ and α have been studied in several disease models and have been subject of investigation, very less is known of PPARδ. Emerging studies have demonstrated that ligand activation of this nuclear receptor was found to be improving mitochondrial oxidative capacity and biogenesis. In this study we test the hypothesis that PPARδ could ameliorate the cardiotoxic effects of DOX and is protective against DOX mediated cardiotoxicity. We observed a dose dependent increase in the transcript and protein levels of FXN with PPARδ agonist GW0742. We also observed PPRE in FXN promoter region thereby demonstrating a transcriptional activation by PPARδ. Further this transcriptional activation of FXN by PPARδ demonstrated protection against DOX mediated ROS production, increased p38 and p38 mediated hypertrophy, thus demonstrating a protective effect against DOX mediated cardiotoxicity.

5.2 Introduction

Previously we have demonstrated that overexpression of FXN was protective against DOX mediated mitohormetic effects of DOX by activating mitochondrial energy metabolism and alleviating the iron accumulation mediated by DOX. The current chapter demonstrates that stabilization of FXN by transcription factor PPARδ was cardioprotective against DOX mediated cardiac damage.

Doxorubicin (DOX) is a widely used anthracycline which has been used as a front line cancer chemotherapy regimen for decades. However the clinical application of DOX is limited due to its dose dependent cardiotoxic complications which eventually lead to heart failure. In recent years, research has attributed the cause of DOX cardiotoxicity to dysregulation in mitochondrial energy metabolism and the resulting damage due to overproduction of intracellular reactive oxygen species (ROS).The contribution of iron in the formation of ROS via the fenton reaction, has gained significant attention in recent times[82, 209]. The 'iron mediated ROS' hypothesis has led to the use of iron chelators such as Dexrazoxane (DXZ). However DXZ usage has been limited due to its detrimental clinical effects upon tumor response to anthracycline therapy and occurrence of myelodysplastic syndrome[11].

Peroxisome Proliferator-activated receptors (PPAR- α, γ δ), belongs to a nuclear hormone receptor family of ligand activated transcriptional factors and are considered "master" transcriptional modulators of genes that predominantly regulate myocardial energy homeostasis, inflammation and metabolic processes such as lipid homeostasis and glucose metabolism[4-6]. PPAR-α and PPAR-γ have been known to be highly expressed in liver and adipose tissue respectively and PPARδ has been found to be ubiquitously expressed in heart [210, 211]. While the roles of PPAR-α and PPAR-γ have been well established [211], the significance of PPARδ in the heart is not well understood.

Frataxin (FXN) is a nuclear encoded mitochondrial protein that is involved in the maintenance of iron homeostasis and in the biogenesis of ISC clusters thereby activating mitochondrial energy metabolism. Deficits in FXN expression is known to result in a Friedreich's Ataxia (FRDA), an autosomal recessive neurodegenerative disease that results due to an increased number of copies of GAA trinucleotide repeats[132]. FRDA patients are characterized by hypertrophic cardiomyopathy which is the primary cause of death due to subsequent arrhythmia and heart failure[17]. We have previously demonstrated that DOX led to a significant reduction in FXN expression in cardiomyocytes, resulting in accumulation of mitochondrial iron and ROS, thus suggesting a major role of FXN in the mechanism of DOX mediated cardiotoxicity (Chapter 3).

In the current study, we have for the first time demonstrated that pharmacological activation of PPARδ by GW0742 was cardioprotective against DOX mediated cardiotoxicity by significantly improving FXN expression levels. We have observed increased mRNA and protein transcripts of FXN with the addition of highly selective and potent PPARδ agonist GW0742 against DOX treatment. Further we have observed PPAR transcriptional response elements in the FXN promoter region, thus suggesting that PPARδ transcriptionally regulates FXN expression. In this manner, we observed improvement in mitochondrial energy parameters including iron homeostasis and ROS production and oxidative energy metabolism in response to DOX treatment in FXN deficient cardiomyoblasts that were preconditioned and treated with GW0742.

Lastly, we observed protection against ROS mediated induction in the principal MAP kinases which may be implicated in cardiomyocyte hypertrophy, including p38 kinases with PPARδ agonist GW0742 which in turn led to significant protection against DOX mediated

cardiac hypertrophy. Together, these results suggest that PPARδ mediated improvement in FXN was cardioprotective against DOX mediated cardiac damage.

5.3 Materials and Methods

5.3.1 Construction of FXN-over expressed (FXN-OE) H9C2 cardiomyoblasts.

FXN-OE cell lines were developed using a GATEWAY-based lentiviral system. The lentiviral empty backbone pLX302 plasmid was purchased from ADDGENE and the plasmid, #25896 was a kind gift from David Root's lab (Broad Institute, MIT and Harvard) [212]. The plasmid is tagged with a V5 epitope at the C terminal backbone. The cDNA fragment of the FXN was cloned into the donor vector provided from the gateway system. Further, FXN was cloned into the pLX 302 (ampicillin and chloramphenicol resistant) lentiviral destination vector (http://www.addgene.org/25896/) using LR Clonase (Life Sciences, Cat. #. 11789100). A puromycin selectable antibiotic marker exists in the pLX 302 vector. The cells were then subjected to transformation in a bacterial cell DH5alpha strain (Invitrogen, Cat. # -012) and the competent plasmid was isolated using PureYieldTM Midiprep system (Promega A2495). The expression vector was then purified and was transfected with a second generation lentiviral packaging vector (psPAX2, ADDGENE cat # 12260, a kind gift of the Didier Trono Lab, (The Swiss Federal Institute of Technology Lausanne (EPFL)) and the envelope vector (pMD2.G, ADDGENE Cat# 12259, a kind gift from the Didier Trono Lab) in a HEK 293T cell line. Further, the virus was extracted from the media and purified using a 0.45μm syringe filter. Subsequently, purified virus was exposed to H9C2 cells for 24 hours and the next day, the cells were treated with 1μg/ml of puromycin for selection of cells expressing FXN.

5.3.2 Construction of FXN-knock down (FXN-KD) H9C2 cardiomyoblasts.

FXN-KD cells were constructed using lentiviral system containing shRNA for FXN. The shRNA lentiviral backbone PLKO.1 plasmid was purchased from ADDGENE. (http://www.addgene.org/10878/) and the plasmid, #10878 was a kind gift from David Root's lab (Broad Institute, MIT and Harvard) [212]. ShRNA oligos were constructed according to the protocol described in the addgene website (http://www.addgene.org/tools/protocols/plko/). FXN-KD cells were stably transfected using second generation packaging for shRNA using lentiviral system. The shRNA oligos for FXN-KD3 forward, 5'-AATTCTTTGAAGACCTTGCAGCTC-3' and reverse 3'-TTAAGAAACTTCTGGAACGTCGAG-5' and FXN KD2 forward 5'-AAGAACTGGGTGTACTCCATCTC-3' and reverse 3'-TTCTTGACCCACATGAGGTAGAG-5' were digested using restriction enzymes Age1 (NEB # R0552S) and EcoR1 (NEB #R0101S) and ligated using quick T4 DNA ligase from quick DNA ligase kit (NEB # M0202M). The ligated vector was then subjected to transformation into competent bacteria and the plasmid was isolated using PureYieldTM Midiprep system (Promega, A2495). The purified vector was then transfected using packaging plasmid (psPAX2) and envelope plasmid (pMD2.G) into HEK 293T cells. Stable cells lines were developed using purified virus and puromycin as described above.

5.3.3 Western Immunoblot

Briefly, the protein lysates were extracted using cell lysis buffer (Cell signaling, #9803) with the addition of protease cocktail inhibitor (Thermo Scientific, #87786), denatured at 90°C for 5 min, with loading buffer. Proteins were resolved in a 12% gel bis-acrylamide gel on a nitrocellulose membrane using anti-rabbit anti frataxin antibody (1:1000, Santa Cruz, #25830)

overnight with 5% milk in TBS-T and a HRP conjugated secondary antibody (1:2000, Rockland). Phospho-p38 MAPK (cell signaling, #9215). Blots were visualized the next day using a chemilluminescence reagent (Millipore) and were imaged using a Bio-Rad gel dock system. The protein densitometric measurements were obtained and analyzed using ImageJ software.

5.3.4 Luciferase reporter assay

Binding of the PPARδ nuclear receptors were analyzed by luciferase assays in HEK-293 and standardized to beta galactosidase. The promoter activity is indicated by the light intensity in the cells. The assay was performed in 96-well plates and grown to a confluency of 70%. The reporter pGL3-basic-hFX-promoter 1, 1.3 and 2.5 Kb was a kind gift from Michael Ristow (Addgene plasmids, #14978, #14979, #14980 respectively). Human PPAR-delta pcDNA vector was a kind gift from Dr. Qinglin Yang. Cells were transfected with of PPAR-delta (1μg) vector with or without hFX promoter (1μg) reporter vector or a promoterless vector as a control, using jetPEI DNA transfection system (PolyPlus Transfection, Cat. #114-07)according to manufacturer's instructions. Cells were also transfected with β-galactosidase vector for standardizing relative transfection efficiency. Next day, the cells were treated with vehicle (DMSO), GW0742 (10μM) for 24 hours. Luciferase activities were determined and quantified using luciferase assay system (Promega) and luminescence was measured using Glomax luminometer (Promega). All values were standardized to beta galactosidase activity as determined by a colorimetric assay (Promega).

5.3.5 ROS generation and measurement studies

Mitochondria specific ROS was determined using mitochondria specific dihydrorhodamine DHR, (Biotium, #10055). Cells were incubated with 10µM DHR for 30 minutes and green fluorescence emitted as a result of oxidation of dihydrorhodamine to cationic rhodamine 123, was measured using multispectral-fluorescent plate reader (Bio-Tek) at λεx/λεm at 548/575nm. Fluorescence intensity was detected using a Nikon Eclipse Ti inserted fluorescence microscope and analyzed using imageJ software with 5-8 random images for each treatment following for which densitometric values were obtained.

5.3.6 Glutathione Assay

Glutathione assay was performed in a 24-well plate using a glutathione probe synthesized by Dr. Forrest Smith (Dept. of Drug, Discovery and Development, Auburn University). The probe binds the thiol group of the reduced form of glutathione (GSSG) thereby emitting red orange fluorescence observed using Cytation ^{TM} 5 Cell Imaging Multi-Mode Reader at emission 590 nm. The treated were placed in cytation 5 and were imaged using a FITC (green) and Texas Red (red) filters. Data was analyzed using prism software (GraphPad).

5.3.7 Hypertrophy measurements in cardiomyoblasts

Cardiomyoblasts were treated with DOX in the presence or absence GW0742 for 24 hours. Cells were fixed with 4% formaldehyde and stained with phalloidin conjugated with rhodamine and was imaged using inverted NIKON Ti inverted fluorescence microscope. 8-10 random images were captured and the morphometric analysis was performed using ImageJ software. The densitometric values were obtained by comparing it to total area.

5.3.8 Statistical analysis

The immunoblot protein densitometric analysis and luciferase are presented as means ± SE. Data is analyzed using statistical Analysis using Prism software and validated using one way ANOVA and Tukey's post hoc analysis for multiple comparisons. P value <0.05 is accepted to be statistically significant for all data.

5.4 Results

PPARδ improves FXN levels in DOX treated H9C2 cardiomyoblasts.

Earlier we have demonstrated significant reduction in FXN expression in DOX treated H9C2 cardiomyoblasts. Since PPARδ is known to regulate genes involved in myocardial fatty acid oxidation[163], we postulated that ligand activation of PPARδ directly regulates FXN expression. In order to verify this, our H9C2 cardiomyoblasts were preconditioned for 2 hours and treated with PPARδ agonist GW0742 with or without the addition of DOX. Treatment with GW0742 (10 μM) led to an improvement in the mRNA levels of FXN in our H9C2 cardiomyoblasts. In addition, our cardiomyoblasts also demonstrated a dose dependent increase in the active (18 KDa) levels of FXN in H9C2 cardiomyoblasts with GW0742 indicating that ligand activation of PPARδ improves FXN levels (Figure. 5.1 A).

Activation of PPARδ induces FXN promoter activity

In order to elucidate the mechanism of FXN regulation by PPARδ, we performed promoter activity assay using three putative regions of human FXN promoter (1.0, 1.3 and 2.5 Kb) that is localized upstream from the initiation site, spanning the PPAR response elements. The promoter constructs of the FXN encompassing the three putative PPREs was cloned into a

reporter PGL3 vector and cells were transfected with PPARδ vector and cells were treated with increasing concentrations of PPARδ agonist GW0742 to observe transcriptional activity by PPARδ. Co-transfection with PPARδ at 10 μM led to an increase in the basal promoter activity at 2.5 Kb FXN in comparison to untreated control cardiomyoblasts that did not display any increase in promoter activity (Figure.5.2B). Further we also observed an increase in FXN expression with increasing concentrations of GW0742 (Figure.5.2C). Together, these findings demonstrate that PPARδ transcriptionally increases FXN**.**

PPARδ mediated increase in FXN alters DOX mediated mitochondrial oxidative stress.

FXN has been shown to play a vital role in cellular iron balance and thereby modulate the production of ROS at cellular level. We have previously demonstrated that DOX mediated reduction in FXN led to a significant elevation in mitochondrial iron accumulation and subsequent ROS production in H9C2 cardiomyoblasts. We therefore hypothesized that ligand mediated activation of PPARδ induced an increase in FXN resulting in an improvement in iron homeostasis and ameliorates ROS production while sustaining antioxidant activity. In this manner, our DOX treated with GW0742 demonstrated a significant reduction in ROS in comparison to control untreated cardiomyoblasts (Figure. 5.4).

Oxidative stress due to imbalance in the cellular ROS and antioxidant status leads to cell death. Based on these observations, we investigated whether increase in FXN by GW0742 improved glutathione levels. Not surprisingly we observed a slight improvement in glutathione levels with GW0742 in DOX treated cardiomyocytes (Figure. 5.5).

This demonstrates that activation of FXN by PPARδ exerts a cardioprotective effect against DOX mediated oxidative damage.

PPARδ mediated activation of FXN protects against DOX mediated cardiac hypertrophy

Cardiomyocytes exposed to DOX have been shown to exhibit hypertrophy as a maladaptive response to oxidative stress by initiating major MAP kinase cascades including p38, JNK/SAPK and ERK pathways[213]. Therefore, we proposed that PPARδ protects against p38 mediated activation of hypertrophy (Figure. 5.6).

We hypothesized a central role of FXN in the cardioprotective pathway of PPARδ activation against DOX mediated cardiac damage. We speculated that stimulation of FXN by ligand activation of PPARδ protects against DOX mediated cardiac hypertrophy. Not surprisingly, we observed significant reduction in the size of DOX treated cardiomyocytes that were co-treated with GW0742 in comparison to untreated controls demonstrating a protecting effect (Figure. 5.7). This demonstrates that PPARδ mediated cardioprotection against DOX cardiotoxicity may significantly involve FXN.

Figures and figure legends

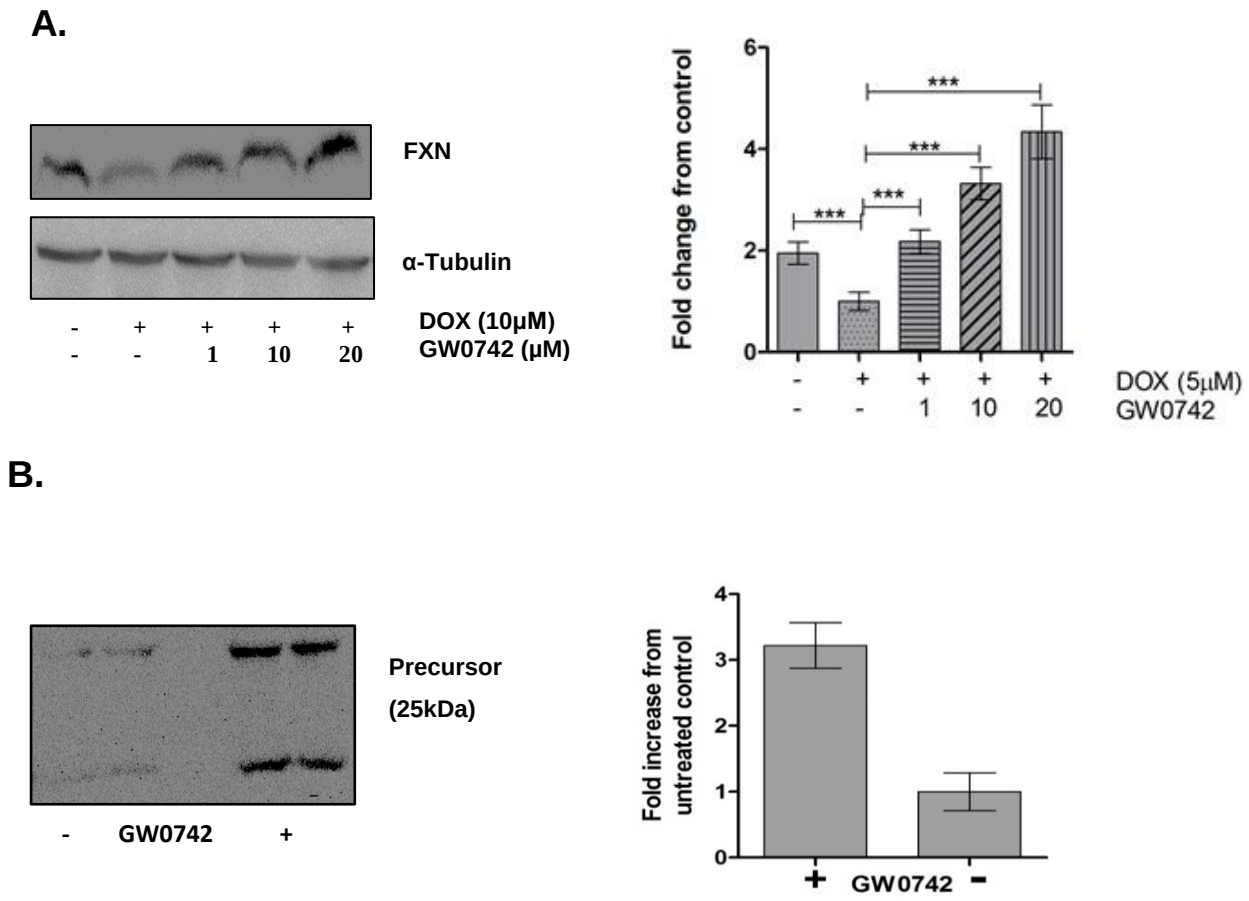

Figure. 5.1: PPARδ protects against DOX mediated attenuation of FXN. (A) Treatment of H9C2 cardiomyocytes with GW0742 (0, 1, 10, 20 μM), co-treated with DOX (10 μM) demonstrates stabilization of FXN and protects against DOX toxicity. (B) FRDA human fibroblasts displayed improved FXN levels with GW0742 treatment. Densitometric values are standardized to α-Tubulin levels and are represented as fold change from control and are based upon mean ± S.E.M. from 3 independent experiments normalized to control H9C2 cells and

analyzed by ANOVA with Tukey's post-hoc analysis for significances between groups ***; P<0.001.

A.

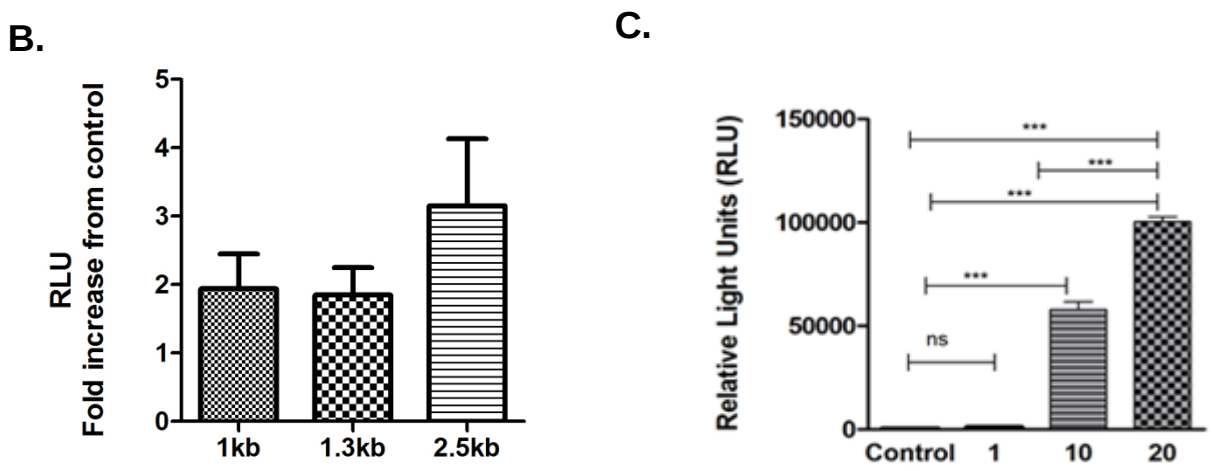

Figure. 5.2: PPARδ transcriptionally increases FXN. (A) Identification of putative PPRE in the FXN promoter regions 0 to 2.5 Kb with two PPRE predicted **(B)** PPARδ agonist GW0742 (10 μM) mediated activation of FXN promoter constructs 1, 1.3 and 2.5 Kb. H9C2 cardiomyocytes transfected with promoter fragments of FXN at 1, 1.3 and 2.5 Kb. 24 hours post transfection, cells were treated with or without 10 μM GW0742 for 24 hours. Control cells were treated with DMSO. Transcriptional activation was measured using luminescence and normalized using non transfected control and represented as fold increase from control. Data are represented as fold increase from control and are based on mean ± S.E.M. with N=3, (P=0.3789), non-significance observed between groups with P<0.05. **(C)** H9C2 cardiomyocytes treated with 0, 1, 10 and 20 μM of GW0742 demonstrated a dose dependent increase in FXN promoter region within 2.5 Kb region. Data was analyzed by one way ANOVA with post hoc Tukey's multiple comparison tests. CI =P<0.05, *** P<0.001 against control or between the indicated treatment groups.

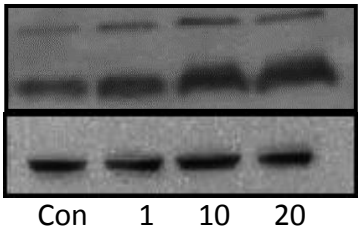

Figure. 5.3: PPARδ treatment stabilizes FXN levels. Cardiomyocytes treated with GW0742 (0, 1, 10, 20 μM) stabilizes FXN and protects against DOX toxicity. Densitometric values are standardized to α-tubulin levels and are represented as fold change from control and are based on mean ± S.E.M. from 3 independent experiments normalized to control H9C2 cells and analyzed by one way ANOVA and Tukey's post-hoc analysis for significances between groups, ns= non-significant, **;P<0.001, ***; P<0.001.

A.

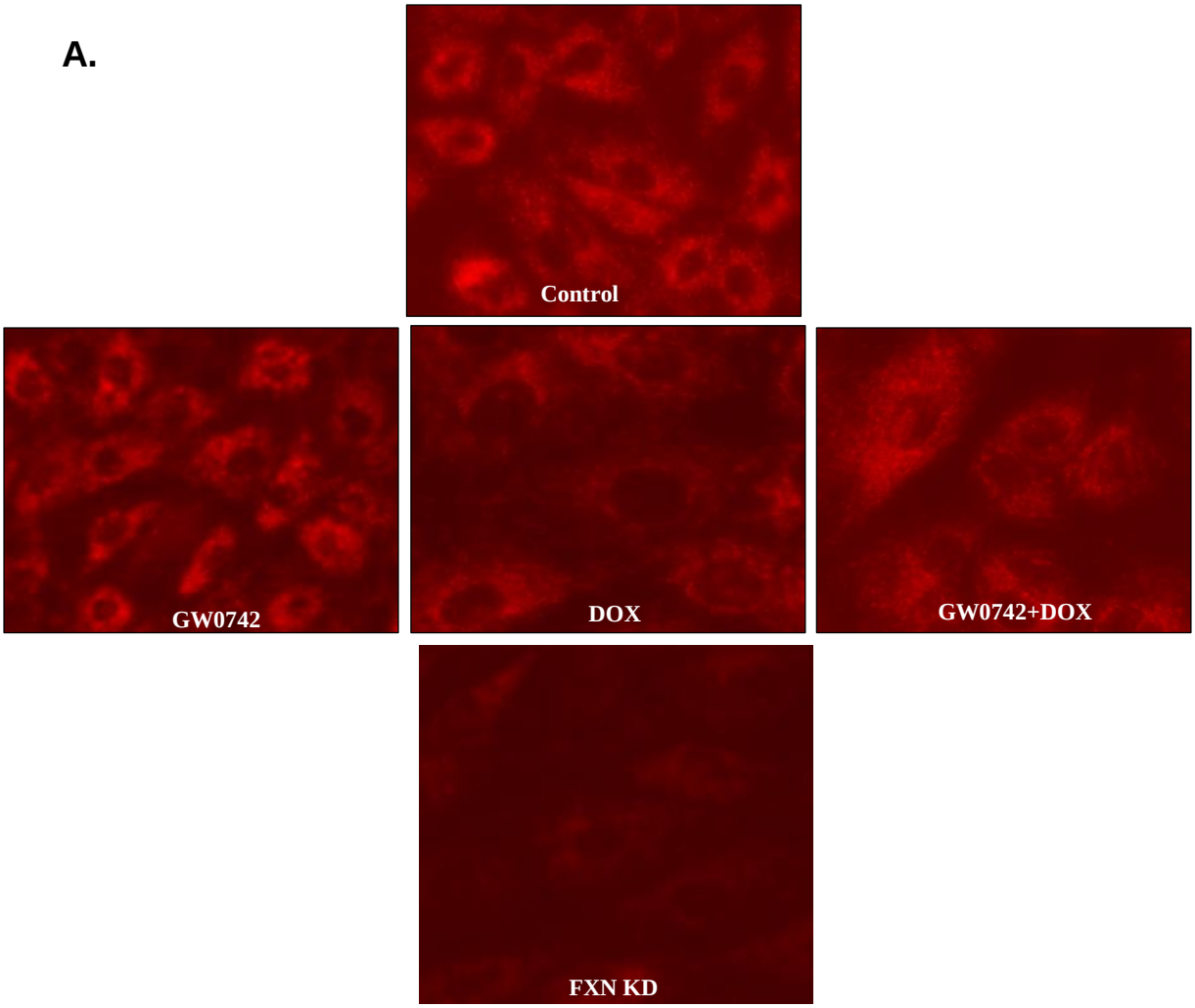
Control
GW0742
DOX
GW0742+DOX
FXN KD

B.

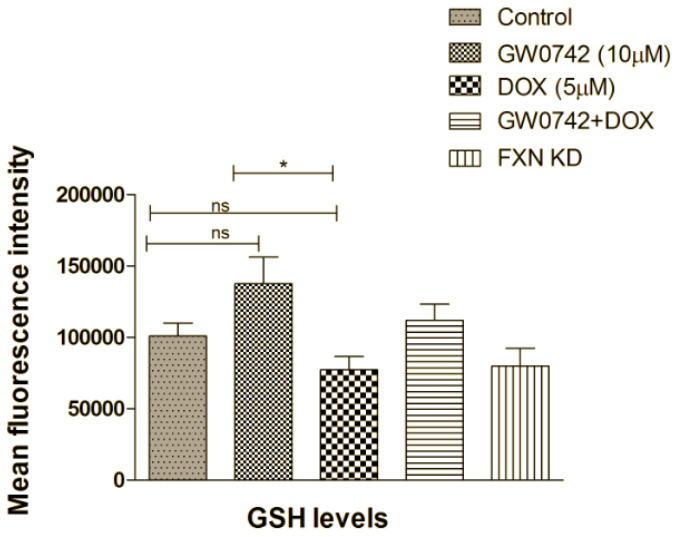
Control
GW0742 (10μM)
DOX (5μM)
GW0742+DOX
FXN KD
Mean fluorescence intensity
200000
150000
100000
50000
0
*
ns
ns
GSH levels

Figure. 5.4: PPARδ mediated FXN stabilization improves glutathione levels. Cardiomyocytes treated with GW0742 (10 μM) and DOX (10 μM) demonstrates improved GSH levels with the addition of GW0742. Fluorescence images of mitochondrial GSH formation (texas red) and graphical representation of GSH levels in Control, GW0742, DOX, GW0742+DOX, FXN KD cardiomyoblasts, based on mean ± S.E.M. from 5 different experiments and analyzed by one way ANOVA and Tukey's post-hoc analysis for significances between groups, ns= non-significant, *;P< 0.05

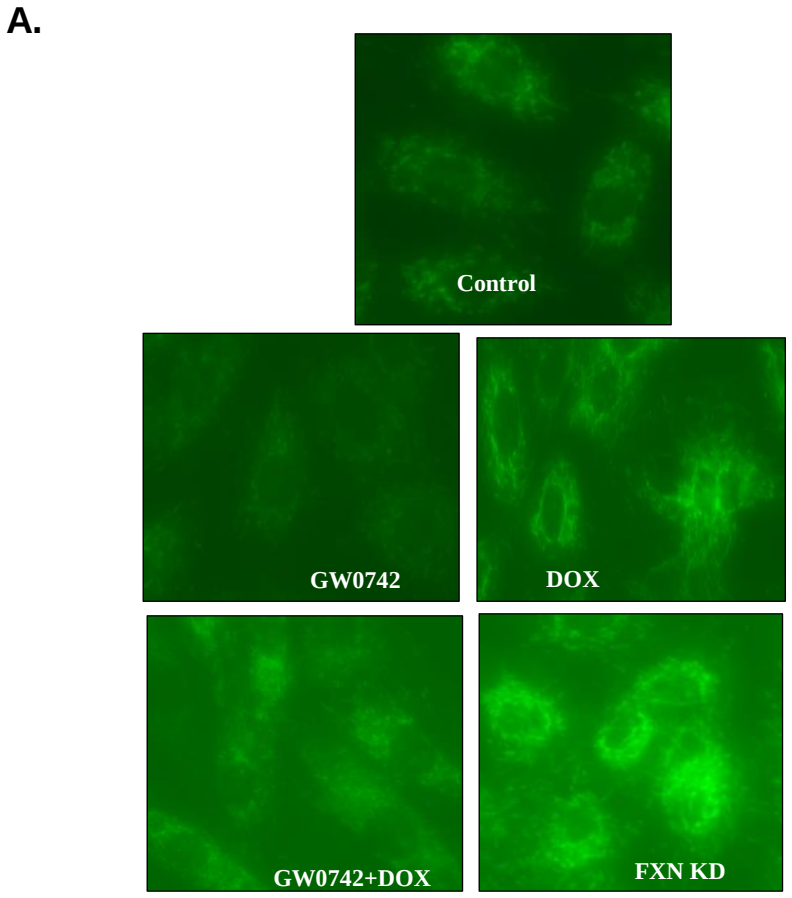

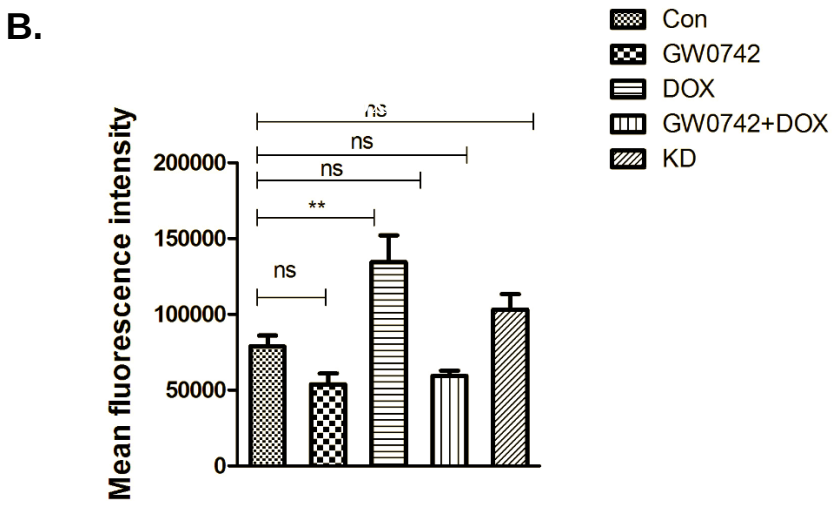

Figure. 5.5: PPARδ mediated FXN stabilization reduces DOX mediated ROS levels. Fluorescence images of mitochondrial DOX (10 μM) mediated ROS formation (green) and graphical representation of ROS levels in H9C2 and FXN KD cardiomyoblasts with or without GW0742, represented as mean ± S.E.M from 5 experiments and analysis was accomplished by ANOVA with Tukey's post-hoc analysis for significances between groups and within groups based upon averages from the assays, ns = non-significant **; P<0.01,

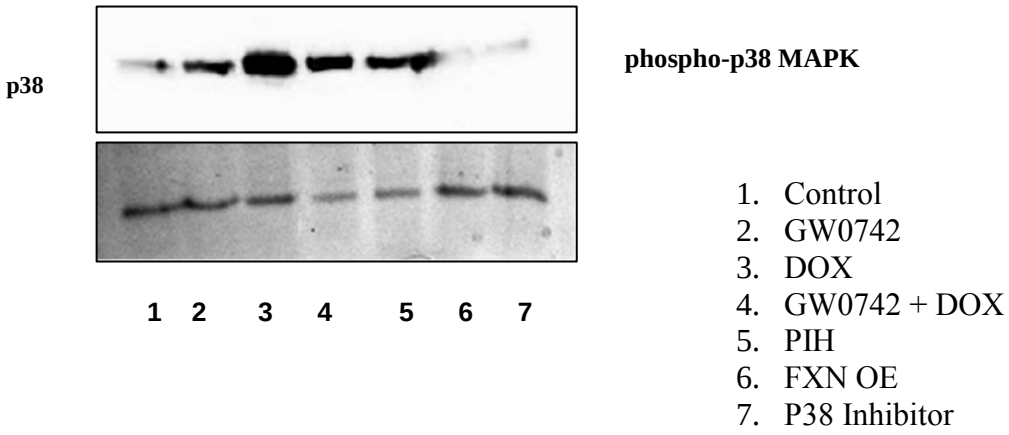

Figure. 5.6: PPARδ protects against DOX mediated activation of p38 MAPK. Western blot analysis of p38 MAPK compared to its ponceau stain. GW0742 treatment demonstrates reduction in p38 MAPK as observed with FXN OE (N=1).

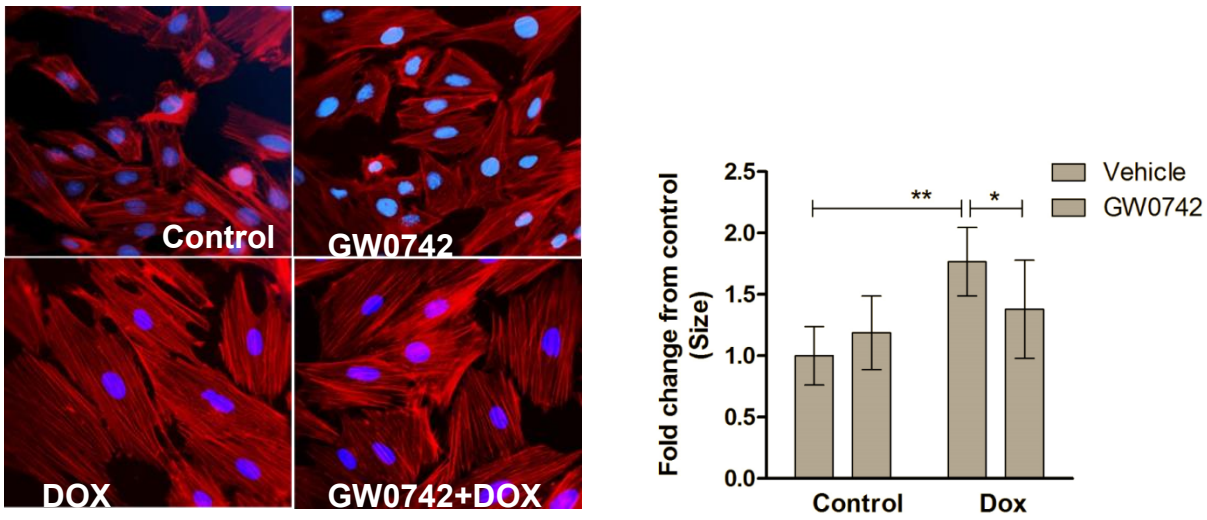

Figure. 5.7: PPARδ mediated activation of FXN protects against DOX mediated cardiac hypertrophy. (A) Representative Phalloidin fluorescence imaging displays changes in H9C2 and GW0742 treated cell size in response to DOX (10 μM) treatment. **(B)** Densitometric measurements of cardiomyocyte size. Data are represented as fold change from control. Indicated above are the mean ± S.E.M. of the replicates of 4 individual experiments ;*P<0.005 **; P< 0.01,

5.5 Discussion

PPARδ has been shown to primarily regulate the transcription of vital genes involved in fatty acid oxidation and activate lipid metabolism in the heart[163]. However its significance in the pathophysiology of cardiomyopathy and heart failure has not been well established. The present study has identified a cardioprotective role of PPARδ against DOX mediated myocardial energy dysregulation and subsequent cardiotoxicity. Previously we have demonstrated a significant reduction in mitochondrial iron-sulfur cluster biogenesis protein, frataxin in response to DOX treatment during the development of cardiac hypertrophy. The present study has demonstrated

that pharmacological activation of PPARδ by highly specific PPARδ ligand GW0742, significantly improved FXN levels against high doses of DOX thereby conferring cardioprotection in response to DOX mediated toxic effects. We have identified three putative PPREs located upstream of the promoter region of FXN and consequently observed an increase in the promoter activity at 2.5 Kb region by luciferase reporter gene assay. These data provide evidence for a mechanistic approach for PPARδ mediated transcriptional regulation of FXN which is essential for homeostasis of cellular iron.

DOX administration is known to induce ROS mediated hypertrophy and cardiomyopathy in the heart with the primary source of ROS being mitochondrial accumulation of iron[113]. Since FXN has been primarily associated with the distribution and homeostasis of cellular iron it was conceivable that improved regulation of FXN by PPARδ agonist will ameliorate the dyshomeostasis in iron regulation and subsequent ROS.

The significance of this finding was further demonstrated by observing reduced ROS and improved glutathione reductase levels in our DOX treated and FXN-KD cardiomyocytes in response to GW0742, thereby leading to a reduction in oxidative stress and a preservation of redox balance in cardiomyoblasts.

Based on these findings, we tried to better understand and establish the relationship between PPARδ and mitochondrial energy metabolism. Our preliminary findings demonstrate that PPARδ induces a protective response against DOX mediated mitochondrial energy dysregulation by improving FXN levels.

Activation of mitochondrial energy metabolism improves cardiac hemodynamic parameters[13]. The impact of improved FXN by PPARδ was further reflected in our cardiomyoblasts which was protected against DOX mediated hypertrophy. The addition of

GW0742 mitigated the DOX mediated hypertrophic response in our cardiomyocytes as observed in FXN-KD cardiomyoblasts. These observations supports our hypothesis, PPARδ mediated cardioprotection against DOX significantly involves FXN (**Fig. 5.8**).

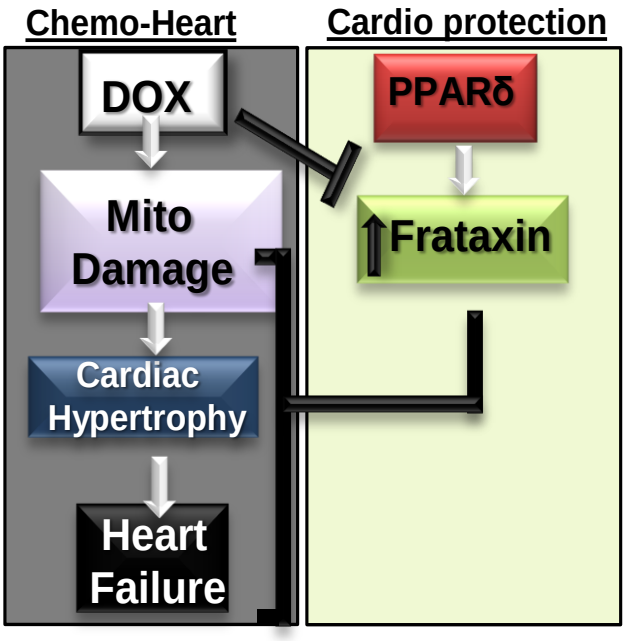

Figure. 5.8: Working model depicting activation of FXN by PPARδ is protective against DOX mediated mitochondrial dysfunction and subsequent hypertrophy

Our signaling mechanism has been validated in vitro in H9C2 cardiomyoblasts and has not been studied in mouse model which maybe one of the limitations. However we are currently developing breeding pairs of Yg8POOK mouse models that carry 75% FXN knock out, which will be subjected to GW0742 treatment to evaluate cardiac functional parameters. These results will further confirm this finding and add to the cardioprotective significance of PPARδ in the heart.

5.6 Scope of study and future directions

The present study has identified a novel role PPARδ against DOX mediated cardiac hypertrophy. Our study demonstrates that activation of PPARδ by GW0742 mediates an increase in FXN by transcriptional regulation, which in turn exerts a protective response by mitigating the detrimental effects of DOX in the mitochondria. The current findings add important new data to the existing body of knowledge. The observations from this study suggests a novel molecular signaling mechanism that may be a potential target for DOX mediated cardiotoxicity and subsequent heart failure and may also represent a therapeutic modality to improve frataxin levels in FRDA patients.

6 References

1. Organization WH: **19th WHO Model List of Essential Medicines (April 2015)**. Geneva.
2. Lefrak EA, Piťha J, Rosenheim S, Gottlieb JA: **A clinicopathologic analysis of adriamycin cardiotoxicity**. *Cancer* 1973, **32**(2):302-314.
3. Yeh ET, Tong AT, Lenihan DJ, Yusuf SW, Swafford J, Champion C, Durand J-B, Gibbs H, Zafarmand AA, Ewer MS: **Cardiovascular complications of cancer therapy diagnosis, pathogenesis, and management**. *Circulation* 2004, **109**(25):3122-3131.
4. Kremer L, Van Dalen E, Offringa M, Ottenkamp J, Voute P: **Anthracycline-induced clinical heart failure in a cohort of 607 children: long-term follow-up study**. *Journal of Clinical Oncology* 2001, **19**(1):191-196.
5. Šimůnek T, Štěrba M, Popelová O, Adamcová M, Hrdina R, Geršl V: **Anthracycline-induced cardiotoxicity: overview of studies examining the roles of oxidative stress and free cellular iron**. *Pharmacological Reports* 2009, **61**(1):154-171.
6. Sarvazyan N: **Visualization of doxorubicin-induced oxidative stress in isolated cardiac myocytes**. *American Journal of Physiology-Heart and Circulatory Physiology* 1996, **271**(5):H2079-H2085.
7. Carreño JE, Apablaza F, Ocaranza MP, Jalil JE: **Cardiac hypertrophy: molecular and cellular events**. *Revista Española de Cardiología (English Edition)* 2006, **59**(5):473-486.
8. Diwan A, Dorn GW: **Decompensation of cardiac hypertrophy: cellular mechanisms and novel therapeutic targets**. *Physiology* 2007, **22**(1):56-64.

9. Deng S, Yan T, Jendrny C, Nemecek A, Vincetic M, Gödtel-Armbrust U, Wojnowski L: **Dexrazoxane may prevent doxorubicin-induced DNA damage via depleting both topoisomerase II isoforms**. *BMC cancer* 2014, **14**(1):1.

10. Gordeuk V, Thuma P, Brittenham G, McLaren C, Parry D, Backenstose A, Biemba G, Msiska R, Holmes L, McKinley E: **Effect of iron chelation therapy on recovery from deep coma in children with cerebral malaria**. *New England Journal of Medicine* 1992, **327**(21):1473-1477.

11. Tebbi CK, London WB, Friedman D, Villaluna D, De Alarcon PA, Constine LS, Mendenhall NP, Sposto R, Chauvenet A, Schwartz CL: **Dexrazoxane-associated risk for acute myeloid leukemia/myelodysplastic syndrome and other secondary malignancies in pediatric Hodgkin's disease**. *Journal of Clinical Oncology* 2007, **25**(5):493-500.

12. Cavadini P, Gellera C, Patel PI, Isaya G: **Human frataxin maintains mitochondrial iron homeostasis in Saccharomyces cerevisiae**. *Human Molecular Genetics* 2000, **9**(17):2523-2530.

13. Schulz TJ, Westermann D, Isken F, Voigt A, Laube B, Thierbach R, Kuhlow D, Zarse K, Schomburg L, Pfeiffer A: **Activation of mitochondrial energy metabolism protects against cardiac failure**. *Aging (Albany NY)* 2010, **2**(11):843-853.

14. Yoon T, Cowan J: **Iron-sulfur cluster biosynthesis. Characterization of frataxin as an iron donor for assembly of [2Fe-2S] clusters in ISU-type proteins**. *Journal of the American Chemical Society* 2003, **125**(20):6078-6084.

15. Tong W-H, Rouault TA: **Metabolic regulation of citrate and iron by aconitases: role of iron–sulfur cluster biogenesis**. *Biometals* 2007, **20**(3-4):549-564.

16. Ristow M, Pfister MF, Yee AJ, Schubert M, Michael L, Zhang C-Y, Ueki K, Michael MD, Lowell BB, Kahn CR: **Frataxin activates mitochondrial energy conversion and oxidative phosphorylation**. *Proceedings of the National Academy of Sciences* 2000, **97**(22):12239-12243.

17. Dürr A, Cossee M, Agid Y, Campuzano V, Mignard C, Penet C, Mandel J-L, Brice A, Koenig M: **Clinical and genetic abnormalities in patients with Friedreich's ataxia**. *New England Journal of Medicine* 1996, **335**(16):1169-1175.

18. Koeppen AH: **Friedreich's ataxia: pathology, pathogenesis, and molecular genetics**. *Journal of the neurological sciences* 2011, **303**(1):1-12.

19. Tsou AY, Paulsen EK, Lagedrost SJ, Perlman SL, Mathews KD, Wilmot GR, Ravina B, Koeppen AH, Lynch DR: **Mortality in Friedreich ataxia**. *Journal of the neurological sciences* 2011, **307**(1):46-49.

20. Orlowski RZ: **The role of the ubiquitin-proteasome pathway in apoptosis**. *Cell Death & Differentiation* 1999, **6**(4).

21. Muratani M, Tansey WP: **How the ubiquitin–proteasome system controls transcription**. *Nature Reviews Molecular Cell Biology* 2003, **4**(3):192-201.

22. Ranek MJ, Wang X: **Activation of the ubiquitin-proteasome system in doxorubicin cardiomyopathy**. *Current hypertension reports* 2009, **11**(6):389-395.

23. Gilliam LA, Moylan JS, Patterson EW, Smith JD, Wilson AS, Rabbani Z, Reid MB: **Doxorubicin acts via mitochondrial ROS to stimulate catabolism in C2C12 myotubes**. *American Journal of Physiology-Cell Physiology* 2012, **302**(1):C195-C202.

24. Rufini A, Fortuni S, Arcuri G, Condò I, Serio D, Incani O, Malisan F, Ventura N, Testi R: **Preventing the ubiquitin–proteasome-dependent degradation of frataxin, the**

protein defective in Friedreich's ataxia. *Human Molecular Genetics* 2011, **20**(7):1253-1261.

25. Cheung KG, Cole LK, Xiang B, Chen K, Ma X, Myal Y, Hatch GM, Tong Q, Dolinsky VW: **Sirtuin-3 (SIRT3) protein attenuates doxorubicin-induced oxidative stress and improves mitochondrial respiration in H9c2 cardiomyocytes**. *Journal of Biological Chemistry* 2015, **290**(17):10981-10993.

26. Tyagi S, Gupta P, Saini AS, Kaushal C, Sharma S: **The peroxisome proliferator-activated receptor: a family of nuclear receptors role in various diseases**. *Journal of advanced pharmaceutical technology & research* 2011, **2**(4):236.

27. Liu J, Wang P, Luo J, Huang Y, He L, Yang H, Li Q, Wu S, Zhelyabovska O, Yang Q: **Peroxisome proliferator-activated receptor β/δ activation in adult hearts facilitates mitochondrial function and cardiac performance under pressure-overload condition**. *Hypertension* 2011, **57**(2):223-230.

28. Jucker BM, Doe CP, Schnackenberg CG, Olzinski AR, Maniscalco K, Williams C, Hu TC, Lenhard SC, Costell M, Bernard R: **PPARδ activation normalizes cardiac substrate metabolism and reduces right ventricular hypertrophy in congestive heart failure**. *Journal of cardiovascular pharmacology* 2007, **50**(1):25-34.

29. Association AH: *Heart facts*: The Association; 1988.

30. Maron BJ, Gardin JM, Flack JM, Gidding SS, Kurosaki TT, Bild DE: **Prevalence of hypertrophic cardiomyopathy in a general population of young adults Echocardiographic analysis of 4111 subjects in the CARDIA Study**. *Circulation* 1995, **92**(4):785-789.

31. Rowland T: **Sudden cardiac death in athletes: rethinking" hypertropic cardiomyopathy"**. *Pediatric exercise science* 2007, **19**(4):373.

32. MacIver DH, Dayer MJ: **An alternative approach to understanding the pathophysiological mechanisms of chronic heart failure**. *International journal of cardiology* 2012, **154**(2):102-110.

33. Eguchi K, Boden-Albala B, Jin Z, Rundek T, Sacco RL, Homma S, Di Tullio MR: **Association between diabetes mellitus and left ventricular hypertrophy in a multiethnic population**. *The American journal of cardiology* 2008, **101**(12):1787-1791.

34. Otterstad J: **Ischaemia and left ventricular hypertrophy**. *European heart journal* 1993, **14**(suppl F):2-6.

35. Dunn FG, Pfeffer MA: **Left ventricular hypertrophy in hypertension**. *New England Journal of Medicine* 1999, **340**(16):1279-1280.

36. Mihl C, Dassen W, Kuipers H: **Cardiac remodelling: concentric versus eccentric hypertrophy in strength and endurance athletes**. *Netherlands Heart Journal* 2008, **16**(4):129-133.

37. van Berlo JH, Maillet M, Molkentin JD: **Signaling effectors underlying pathologic growth and remodeling of the heart**. *The Journal of clinical investigation* 2013, **123**(1):37-45.

38. Shende P, Plaisance I, Morandi C, Pellieux C, Berthonneche C, Zorzato F, Krishnan J, Lerch R, Hall MN, Rüegg MA: **Cardiac raptor ablation impairs adaptive hypertrophy, alters metabolic gene expression, and causes heart failure in mice**. *Circulation* 2011, **123**(10):1073-1082.

39. Rosca MG, Tandler B, Hoppel CL: **Mitochondria in cardiac hypertrophy and heart failure**. *Journal of molecular and cellular cardiology* 2013, **55**:31-41.

40. Garnier A, Fortin D, Delomenie C, Momken I, Veksler V, Ventura-Clapier R: **Depressed mitochondrial transcription factors and oxidative capacity in rat failing cardiac and skeletal muscles**. *The Journal of physiology* 2003, **551**(2):491-501.

41. Dai D-F, Johnson SC, Villarin JJ, Chin MT, Nieves-Cintrón M, Chen T, Marcinek DJ, Dorn GW, Kang YJ, Prolla TA: **Mitochondrial oxidative stress mediates angiotensin II–induced cardiac hypertrophy and Gαq overexpression–induced heart failure**. *Circulation research* 2011, **108**(7):837-846.

42. Griffiths ER, Friehs I, Scherr E, Poutias D, McGowan FX, Pedro J: **Electron transport chain dysfunction in neonatal pressure-overload hypertrophy precedes cardiomyocyte apoptosis independent of oxidative stress**. *The Journal of thoracic and cardiovascular surgery* 2010, **139**(6):1609-1617.

43. Kahan T, Bergfeldt L: **Left ventricular hypertrophy in hypertension: its arrhythmogenic potential**. *Heart* 2005, **91**(2):250-256.

44. Feng B, Chen S, Chiu J, George B, Chakrabarti S: **Regulation of cardiomyocyte hypertrophy in diabetes at the transcriptional level**. *American Journal of Physiology-Endocrinology and Metabolism* 2008, **294**(6):E1119-E1126.

45. Rose BA, Force T, Wang Y: **Mitogen-activated protein kinase signaling in the heart: angels versus demons in a heart-breaking tale**. *Physiological reviews* 2010, **90**(4):1507-1546.

46. Machackova J, Barta J, Dhalla NS: **Myofibrillar remodelling in cardiac hypertrophy, heart failure and cardiomyopathies**. *Canadian Journal of Cardiology* 2006, **22**(11):953-968.

47. Rehsia NS, Dhalla NS: **Mechanisms of the beneficial effects of beta-adrenoceptor antagonists in congestive heart failure**. *Experimental & Clinical Cardiology* 2010, **15**(4):e86.

48. Takimoto E, Kass DA: **Role of oxidative stress in cardiac hypertrophy and remodeling**. *Hypertension* 2007, **49**(2):241-248.

49. Xu F-P, Chen M-S, Wang Y-Z, Yi Q, Lin S-B, Chen AF, Luo J-D: **Leptin induces hypertrophy via endothelin-1–reactive oxygen species pathway in cultured neonatal rat cardiomyocytes**. *Circulation* 2004, **110**(10):1269-1275.

50. Cosentino-Gomes D, Rocco-Machado N, Meyer-Fernandes JR: **Cell signaling through protein kinase C oxidation and activation**. *International journal of molecular sciences* 2012, **13**(9):10697-10721.

51. Adams JW, Brown JH: **G-proteins in growth and apoptosis: lessons from the heart**. *Oncogene* 2001, **20**(13).

52. Jastroch M, Divakaruni AS, Mookerjee S, Treberg JR, Brand MD: **Mitochondrial proton and electron leaks**. *Essays in biochemistry* 2010, **47**:53-67.

53. Matsushima S, Ide T, Yamato M, Matsusaka H, Hattori F, Ikeuchi M, Kubota T, Sunagawa K, Hasegawa Y, Kurihara T: **Overexpression of mitochondrial peroxiredoxin-3 prevents left ventricular remodeling and failure after myocardial infarction in mice**. *Circulation* 2006, **113**(14):1779-1786.

54. Venkatasubramanian S, Noh RM, Daga S, Langrish JP, Joshi NV, Mills NL, Hoffmann E, Jacobson EW, Vlasuk GP, Waterhouse BR: **Cardiovascular effects of a novel SIRT1 activator, SRT2104, in otherwise healthy cigarette smokers**. *Journal of the American Heart Association* 2013, **2**(3):e000042.

55. Heilbrunn SM, Shah P, Bristow MR, Valantine HA, Ginsburg R, Fowler MB: **Increased beta-receptor density and improved hemodynamic response to catecholamine stimulation during long-term metoprolol therapy in heart failure from dilated cardiomyopathy**. *Circulation* 1989, **79**(3):483-490.

56. Vahanian A, Baumgartner H, Bax J, Butchart E, Dion R, Filippatos G, Flachskampf F, Hall R, Iung B, Kasprzak J: **Guidelines on the management of valvular heart disease**. *European heart journal* 2007, **28**(2):230-268.

57. Lorell BH: **Use of calcium channel blockers in hypertrophic cardiomyopathy**. *The American journal of medicine* 1985, **78**(2):43-54.

58. Brown NJ, Vaughan DE: **Angiotensin-converting enzyme inhibitors**. *Circulation* 1998, **97**(14):1411-1420.

59. Strauss MH, Hall AS: **Angiotensin receptor blockers may increase risk of myocardial infarction unraveling the ARB-MI paradox**. *Circulation* 2006, **114**(8):838-854.

60. Minotti G, Menna P, Salvatorelli E, Cairo G, Gianni L: **Anthracyclines: molecular advances and pharmacologic developments in antitumor activity and cardiotoxicity**. *Pharmacological reviews* 2004, **56**(2):185-229.

61. Pegram MD, Konecny GE, O'Callaghan C, Beryt M, Pietras R, Slamon DJ: **Rational combinations of trastuzumab with chemotherapeutic drugs used in the treatment of breast cancer**. *Journal of the National Cancer Institute* 2004, **96**(10):739-749.

62. Cortés-Funes H, Coronado C: **Role of anthracyclines in the era of targeted therapy**. *Cardiovascular toxicology* 2007, **7**(2):56-60.

63. Torres VM, Simic VD: *Doxorubicin-Induced Oxidative Injury of Cardiomyocytes-Do We Have Right Strategies for Prevention?*: INTECH Open Access Publisher; 2012.

64. Tewey K, Rowe T, Yang L, Halligan B, Liu L: **Adriamycin-induced DNA damage mediated by mammalian DNA topoisomerase II**. *Science* 1984, **226**(4673):466-468.

65. Minotti G, Cairo G, Monti E: **Role of iron in anthracycline cardiotoxicity: new tunes for an old song?** *The FASEB Journal* 1999, **13**(2):199-212.

66. Cullinane C, Cutts SM, van Rosmalen A, Phillips DR: **Formation of adriamycin-DNA adducts in vitro**. *Nucleic acids research* 1994, **22**(12):2296-2303.

67. Pollakis G, Goormaghtigh E, Ruysschaert J-M: **Role of the quinone structure in the mitochondrial damage induced by antitumor anthracyclines**. *FEBS letters* 1983, **155**(2):267-272.

68. Xu X, Persson H, Richardson D: **Molecular pharmacology of the interaction of anthracyclines with iron**. *Molecular pharmacology* 2005, **68**(2):261-271.

69. El-Deiry WS, Harper JW, O'Connor PM, Velculescu VE, Canman CE, Jackman J, Pietenpol JA, Burrell M, Hill DE, Wang Y: **WAF1/CIP1 is induced in p53-mediated G1 arrest and apoptosis**. *Cancer research* 1994, **54**(5):1169-1174.

70. Poizat C, Sartorelli V, Chung G, Kloner RA, Kedes L: **Proteasome-mediated degradation of the coactivator p300 impairs cardiac transcription**. *Molecular and cellular biology* 2000, **20**(23):8643-8654.

71. Suter TM, Ewer MS: **Cancer drugs and the heart: importance and management**. *European heart journal* 2013, **34**(15):1102-1111.

72. Volkova M, Russell R: **Anthracycline cardiotoxicity: prevalence, pathogenesis and treatment**. *Current cardiology reviews* 2011, **7**(4):214-220.

73. Takemura G, Fujiwara H: **Doxorubicin-induced cardiomyopathy: from the cardiotoxic mechanisms to management**. *Progress in cardiovascular diseases* 2007, **49**(5):330-352.

74. Singal PK, Deally CM, Weinberg LE: **Subcellular effects of adriamycin in the heart: a concise review**. *Journal of molecular and cellular cardiology* 1987, **19**(8):817-828.

75. Broder H, Gottlieb RA, Lepor NE: **Chemotherapy and cardiotoxicity**. *Reviews in cardiovascular medicine* 2008, **9**(2):75.

76. Muppidi R, Spranklin L, Scialla W, Islam N, Freudenberger R, Malacoff R: **Cardiotoxicity of Anticancer Therapies**. *Reviews in cardiovascular medicine* 2015, **16**(4):225-234.

77. Von Hoff DD, Layard MW, Basa P, Davis HL, Von Hoff AL, Rozencweig M, Muggia FM: **Risk factors for doxorubicin-lnduced congestive heart failure**. *Annals of internal medicine* 1979, **91**(5):710-717.

78. Chatterjee K, Zhang J, Honbo N, Karliner JS: **Doxorubicin Cardiomyopathy**. *Cardiology* 2010, **115**(2):155-162.

79. Hescheler J, Meyer R, Plant S, Krautwurst D, Rosenthal W, Schultz G: **Morphological, biochemical, and electrophysiological characterization of a clonal cell (H9c2) line from rat heart**. *Circulation research* 1991, **69**(6):1476-1486.

80. Wang B, Shravah J, Luo H, Raedschelders K, Chen DD, Ansley DM: **Propofol protects against hydrogen peroxide-induced injury in cardiac H9c2 cells via Akt activation**

and Bcl-2 up-regulation. *Biochemical and biophysical research communications* 2009, **389**(1):105-111.

81. Sardão VA, Oliveira PJ, Holy J, Oliveira CR, Wallace KB: **Morphological alterations induced by doxorubicin on H9c2 myoblasts: nuclear, mitochondrial, and cytoskeletal targets**. *Cell biology and toxicology* 2009, **25**(3):227-243.

82. Ichikawa Y, Ghanefar M, Bayeva M, Wu R, Khechaduri A, Prasad SVN, Mutharasan RK, Naik TJ, Ardehali H: **Cardiotoxicity of doxorubicin is mediated through mitochondrial iron accumulation**. *The Journal of clinical investigation* 2014, **124**(2):617-630.

83. Paranka N, Dorr R: **Effect of doxorubicin on glutathione and glutathione-dependent enzymes in cultured rat heart cells**. *Anticancer research* 1993, **14**(5A):2047-2052.

84. Vásquez-Vivar J, Martasek P, Hogg N, Masters BSS, Pritchard KA, Kalyanaraman B: **Endothelial nitric oxide synthase-dependent superoxide generation from adriamycin**. *Biochemistry* 1997, **36**(38):11293-11297.

85. Arai M, Yoguchi A, Takizawa T, Yokoyama T, Kanda T, Kurabayashi M, Nagai R: **Mechanism of doxorubicin-induced inhibition of sarcoplasmic reticulum Ca2+-ATPase gene transcription**. *Circulation research* 2000, **86**(1):8-14.

86. Angsutararux P, Luanpitpong S, Issaragrisil S: **Chemotherapy-Induced Cardiotoxicity: Overview of the Roles of Oxidative Stress**. *Oxidative medicine and cellular longevity* 2015, **2015**.

87. Zhang Y, Chen Y, Zhang M, Tang Y, Xie Y, Huang X, Li Y: **Doxorubicin Induces Sarcoplasmic Reticulum Calcium Regulation Dysfunction via the Decrease of**

SERCA2 and Phospholamban Expressions in Rats. *Cell biochemistry and biophysics* 2014, **70**(3):1791-1798.

88. Tokarska-Schlattner M, Zaugg M, Da Silva R, Lucchinetti E, Schaub MC, Wallimann T, Schlattner U: **Acute toxicity of doxorubicin on isolated perfused heart: response of kinases regulating energy supply**. *American Journal of Physiology-Heart and Circulatory Physiology* 2005, **289**(1):H37-H47.

89. Wang S, Song P, Zou M-H: **Inhibition of AMP-activated Protein Kinase α (AMPKα) by Doxorubicin Accentuates Genotoxic Stress and Cell Death in Mouse Embryonic Fibroblasts and Cardiomyocytes ROLE OF p53 AND SIRT1**. *Journal of Biological Chemistry* 2012, **287**(11):8001-8012.

90. Lee K, Qian DZ, Rey S, Wei H, Liu JO, Semenza GL: **Anthracycline chemotherapy inhibits HIF-1 transcriptional activity and tumor-induced mobilization of circulating angiogenic cells**. *Proceedings of the National Academy of Sciences* 2009, **106**(7):2353-2358.

91. Valko M, Rhodes C, Moncol J, Izakovic M, Mazur M: **Free radicals, metals and antioxidants in oxidative stress-induced cancer**. *Chemico-biological interactions* 2006, **160**(1):1-40.

92. Cao Y, Eble JM, Moon E, Yuan H, Weitzel DH, Landon CD, Nien CY-C, Hanna G, Rich JN, Provenzale JM: **Tumor cells upregulate normoxic HIF-1α in response to doxorubicin**. *Cancer research* 2013, **73**(20):6230-6242.

93. Jang YM, Kendaiah S, Drew B, Phillips T, Selman C, Julian D, Leeuwenburgh C: **Doxorubicin treatment in vivo activates caspase-12 mediated cardiac apoptosis in both male and female rats**. *FEBS letters* 2004, **577**(3):483-490.

94. Park SS, Kim MA, Eom Y-W, Choi KS: **Bcl-xL blocks high dose doxorubicin-induced apoptosis but not low dose doxorubicin-induced cell death through mitotic catastrophe**. *Biochemical and biophysical research communications* 2007, **363**(4):1044-1049.

95. Tsang W, Chau SP, Kong S, Fung K, Kwok T: **Reactive oxygen species mediate doxorubicin induced p53-independent apoptosis**. *Life sciences* 2003, **73**(16):2047-2058.

96. Zhu W, Zou Y, Aikawa R, Harada K, Kudoh S, Uozumi H, Hayashi D, Gu Y, Yamazaki T, Nagai R: **MAPK superfamily plays an important role in daunomycin-induced apoptosis of cardiac myocytes**. *Circulation* 1999, **100**(20):2100-2107.

97. Solem LE, Henry TR, Wallace KB: **Disruption of mitochondrial calcium homeostasis following chronic doxorubicin administration**. *Toxicology and applied pharmacology* 1994, **129**(2):214-222.

98. Saeki K, Obi I, Ogiku N, Shigekawa M, Imagawa T, Matsumoto T: **Doxorubicin directly binds to the cardiac-type ryanodine receptor**. *Life sciences* 2002, **70**(20):2377-2389.

99. Schröder F, Handrock R, Beuckelmann DJ, Hirt S, Hullin R, Priebe L, Schwinger RH, Weil J, Herzig S: **Increased availability and open probability of single L-type calcium channels from failing compared with nonfailing human ventricle**. *Circulation* 1998, **98**(10):969-976.

100. Keung E, Toll L, Ellis M, Jensen R: **L-type cardiac calcium channels in doxorubicin cardiomyopathy in rats morphological, biochemical, and functional correlations**. *Journal of Clinical Investigation* 1991, **87**(6):2108.

101. Caroni P, Villani F, Carafoli E: **The cardiotoxic antibiotic doxorubicin inhibits the Na+/Ca 2+ exchange of dog heart sarcolemmal vesicles**. *FEBS letters* 1981, **130**(2):184-186.

102. Rosenstock T, Carvalho A, Jurkiewicz A, Frussa-Filho R, Smaili S: **Mitochondrial calcium, oxidative stress and apoptosis in a neurodegenerative disease model induced by 3-nitropropionic acid**. *Journal of neurochemistry* 2004, **88**(5):1220-1228.

103. Hrelia S, Fiorentini D, Maraldi T, Angeloni C, Bordoni A, Biagi PL, Hakim G: **Doxorubicin induces early lipid peroxidation associated with changes in glucose transport in cultured cardiomyocytes**. *Biochimica et Biophysica Acta (BBA)-Biomembranes* 2002, **1567**:150-156.

104. Momparler RL, Karon M, Siegel SE, Avila F: **Effect of adriamycin on DNA, RNA, and protein synthesis in cell-free systems and intact cells**. *Cancer research* 1976, **36**(8):2891-2895.

105. Calderone A, de Champlain J, Rouleau JL: **Adriamycin-induced changes to the myocardial beta-adrenergic system in the rabbit**. *Journal of molecular and cellular cardiology* 1991, **23**(3):333-342.

106. Jeyaseelan R, Poizat C, Wu H-Y, Kedes L: **Molecular mechanisms of doxorubicin-induced cardiomyopathy selective suppression of reiske iron-sulfur protein, adp/atp translocase, and phosphofructokinase genes is associated with atp depletion in rat cardiomyocytes**. *Journal of Biological Chemistry* 1997, **272**(9):5828-5832.

107. Nikitovic D, Juranek I, Wilks MF, Tzardi M, Tsatsakis A, Tzanakakis GN: **Anthracycline-dependent cardiotoxicity and extracellular matrix remodeling**. *CHEST Journal* 2014, **146**(4):1123-1130.

108. Goetzenich A, Hatam N, Zernecke A, Weber C, Czarnotta T, Autschbach R, Christiansen S: **Alteration of matrix metalloproteinases in selective left ventricular adriamycin-induced cardiomyopathy in the pig**. *The Journal of Heart and Lung Transplantation* 2009, **28**(10):1087-1093.

109. Johansen PB, Jensen SE, Rasmussen SN, Dalmark M: **Pharmacokinetics of doxorubicin and its metabolite doxorubicinol in rabbits with induced acid and alkaline urine**. *Cancer chemotherapy and pharmacology* 1984, **13**(1):5-8.

110. PANTOPOULOS K: **Iron metabolism and the IRE/IRP regulatory system: an update**. *Annals of the New York Academy of Sciences* 2004, **1012**(1):1-13.

111. Riddick DS, Lee C, Ramji S, Chinje EC, Cowen RL, Williams KJ, Patterson AV, Stratford IJ, Morrow CS, Townsend AJ: **Cancer chemotherapy and drug metabolism**. *Drug Metabolism and Disposition* 2005, **33**(8):1083-1096.

112. De Jong J, Schoofs P, Snabilié A, Bast A, Van der Vijgh W: **The role of biotransformation in anthracycline-induced cardiotoxicity in mice**. *Journal of Pharmacology and Experimental Therapeutics* 1993, **266**(3):1312-1320.

113. Gammella E, Maccarinelli F, Buratti P, Recalcati S, Cairo G: **The role of iron in anthracycline cardiotoxicity**. *Frontiers in Pharmacology* 2014, **5**.

114. Alvarado LJ: **Site-specific interaction of doxorubicin in the iron responsive element RNA: Implications in cellular iron homeostasis and non-iron deficiency anemia**. 2014.

115. Kotamraju S, Chitambar CR, Kalivendi SV, Joseph J, Kalyanaraman B: **Transferrin receptor-dependent iron uptake is responsible for doxorubicin-mediated apoptosis**

in endothelial cells role of oxidant-induced iron signaling in apoptosis. *Journal of Biological Chemistry* 2002, **277**(19):17179-17187.

116. Gozzelino R, Levi S: **Mitochondrial ferritin in the regulation of brain iron homeostasis and neurodegenerative diseases**. *The Importance Of Iron In Pathophysiologic Conditions* 2015:410.

117. Nie G, Sheftel AD, Kim SF, Ponka P: **Overexpression of mitochondrial ferritin causes cytosolic iron depletion and changes cellular iron homeostasis**. *Blood* 2005, **105**(5):2161-2167.

118. Xu W, Barrientos T, Mao L, Rockman HA, Sauve AA, Andrews NC: **Lethal cardiomyopathy in mice lacking transferrin receptor in the heart**. *Cell reports* 2015, **13**(3):533-545.

119. Ichikawa Y, Bayeva M, Ghanefar M, Potini V, Sun L, Mutharasan RK, Wu R, Khechaduri A, Naik TJ, Ardehali H: **Disruption of ATP-binding cassette B8 in mice leads to cardiomyopathy through a decrease in mitochondrial iron export**. *Proceedings of the National Academy of Sciences* 2012, **109**(11):4152-4157.

120. Bencze KZ, Kondapalli KC, Cook JD, McMahon S, Millán-Pacheco C, Pastor N, Stemmler TL: **The structure and function of frataxin**. *Critical reviews in biochemistry and molecular biology* 2006, **41**(5):269-291.

121. Koutnikova H, Campuzano V, Foury F, Dollé P, Cazzalini O, Koenig M: **Studies of human, mouse and yeast homologues indicate a mitochondrial function for frataxin**. *Nature genetics* 1997, **16**(4):345-351.

122. Anzovino A, Lane D, Huang MH, Richardson D: **Fixing frataxin:'ironing out'the metabolic defect in Friedreich's ataxia**. *British journal of pharmacology* 2014, **171**(8):2174-2190.

123. Guccini I, Serio D, Condo I, Rufini A, Tomassini B, Mangiola A, Maira G, Anile C, Fina D, Pallone F: **Frataxin participates to the hypoxia-induced response in tumors**. *Cell death & disease* 2011, **2**(2):e123.

124. Shan Y, Napoli E, Cortopassi G: **Mitochondrial frataxin interacts with ISD11 of the NFS1/ISCU complex and multiple mitochondrial chaperones**. *Human Molecular Genetics* 2007, **16**(8):929-941.

125. Zanella I, Derosas M, Corrado M, Cocco E, Cavadini P, Biasiotto G, Poli M, Verardi R, Arosio P: **The effects of frataxin silencing in HeLa cells are rescued by the expression of human mitochondrial ferritin**. *Biochimica et Biophysica Acta (BBA)-Molecular Basis of Disease* 2008, **1782**(2):90-98.

126. Puccio H, Kœnig M: **Recent advances in the molecular pathogenesis of Friedreich ataxia**. *Human Molecular Genetics* 2000, **9**(6):887-892.

127. Bulteau A-L, Ikeda-Saito M, Szweda LI: **Redox-dependent modulation of aconitase activity in intact mitochondria**. *Biochemistry* 2003, **42**(50):14846-14855.

128. Huang ML-H, Becker EM, Whitnall M, Rahmanto YS, Ponka P, Richardson DR: **Elucidation of the mechanism of mitochondrial iron loading in Friedreich's ataxia by analysis of a mouse mutant**. *Proceedings of the National Academy of Sciences* 2009, **106**(38):16381-16386.

129. Campuzano V, Montermini L, Moltò MD, Pianese L, Cossée M, Cavalcanti F, Monros E, Rodius F, Duclos F, Monticelli A: **Friedreich's ataxia: autosomal recessive disease**

caused by an intronic GAA triplet repeat expansion. *Science* 1996, **271**(5254):1423-1427.

130. Gomes CM, Santos R: **Neurodegeneration in friedreich's ataxia: From defective frataxin to oxidative stress**. *Oxidative medicine and cellular longevity* 2013, **2013**.

131. Bunse M, Bit-Avragim N, Riefflin A, Perrot A, Schmidt O, Kreuz FR, Dietz R, Jung WI, Osterziel KJ: **Cardiac energetics correlates to myocardial hypertrophy in Friedreich's ataxia**. *Annals of neurology* 2003, **53**(1):121-123.

132. Santos R, Lefevre S, Sliwa D, Seguin A, Camadro J-M, Lesuisse E: **Friedreich Ataxia: Molecular Mechanisms, Redox Considerations, and Therapeutic Opportunities**. *Antioxidants & redox signaling* 2010, **13**(5):651-690.

133. De Biase I, Chutake YK, Rindler PM, Bidichandani SI: **Epigenetic silencing in Friedreich ataxia is associated with depletion of CTCF (CCCTC-binding factor) and antisense transcription**. *PloS one* 2009, **4**(11):e7914.

134. Patel PI, Isaya G: **Friedreich Ataxia: From GAA Triplet–Repeat Expansion to Frataxin Deficiency**. *The American Journal of Human Genetics* 2001, **69**(1):15-24.

135. Scheinberg D: **Friedreich's Ataxia**.

136. Rai M, Soragni E, Jenssen K, Burnett R, Herman D, Coppola G, Geschwind DH, Gottesfeld JM, Pandolfo M: **HDAC inhibitors correct frataxin deficiency in a Friedreich ataxia mouse model**. *PloS one* 2008, **3**(4):e1958.

137. Sandi C, Sandi M, Virmouni SA, Al-Mahdawi S, Pook MA: **Epigenetic-based therapies for Friedreich ataxia**. 2014.

138. Vickers CJ, Olsen CA, Leman LJ, Ghadiri MR: **Discovery of HDAC inhibitors that lack an active site Zn2+-binding functional group**. *ACS medicinal chemistry letters* 2012, **3**(6):505-508.

139. Wagner FF, Weïwer M, Lewis MC, Holson EB: **Small molecule inhibitors of zinc-dependent histone deacetylases**. *Neurotherapeutics* 2013, **10**(4):589-604.

140. Chou CJ, Herman D, Gottesfeld JM: **Pimelic diphenylamide 106 is a slow, tight-binding inhibitor of class I histone deacetylases**. *Journal of Biological Chemistry* 2008, **283**(51):35402-35409.

141. Rai M, Soragni E, Chou CJ, Barnes G, Jones S, Rusche JR, Gottesfeld JM, Pandolfo M: **Two new pimelic diphenylamide HDAC inhibitors induce sustained frataxin upregulation in cells from Friedreich's ataxia patients and in a mouse model**. *PloS one* 2010, **5**(1):e8825.

142. Gryder BE, Sodji QH, Oyelere AK: **Targeted cancer therapy: giving histone deacetylase inhibitors all they need to succeed**. *Future medicinal chemistry* 2012, **4**(4):505-524.

143. Borutinskaite VV, Navakauskiene R, MAGNUSSON KE: **Retinoic Acid and Histone Deacetylase Inhibitor BML-210 Inhibit Proliferation of Human Cervical Cancer HeLa Cells**. *Annals of the New York Academy of Sciences* 2006, **1091**(1):346-355.

144. Cooper J, Korlipara L, Hart P, Bradley J, Schapira A: **Coenzyme Q10 and vitamin E deficiency in Friedreich's ataxia: predictor of efficacy of vitamin E and coenzyme Q10 therapy**. *European journal of neurology* 2008, **15**(12):1371-1379.

145. Kadar K: **[Successful idebenone therapy of hypertrophic cardiomyopathy in Friedreich ataxia]**. *Orvosi hetilap* 2003, **144**(25):1241-1244.

146. HIDER RC, Zhou T: **The design of orally active iron chelators**. *Annals of the New York Academy of Sciences* 2005, **1054**(1):141-154.

147. Gardner PR, Raineri I, Epstein LB, White CW: **Superoxide radical and iron modulate aconitase activity in mammalian cells**. *Journal of Biological Chemistry* 1995, **270**(22):13399-13405.

148. Renfroe JL, Forbes P, Braunstein J, Neufeld EJ: **Relationship of Transfusion and Iron-Related Complications to Cost of Care in Thalassemia**. *ashmtg* 2005, **106**(11):2240-2240.

149. Bence NF, Sampat RM, Kopito RR: **Impairment of the ubiquitin-proteasome system by protein aggregation**. *Science* 2001, **292**(5521):1552-1555.

150. Chen D, Dou QP: **The ubiquitin-proteasome system as a prospective molecular target for cancer treatment and prevention**. *Current protein & peptide science* 2010, **11**(6):459.

151. Willis MS, Schisler JC, Patterson C: **Appetite for destruction: E3 ubiquitin-ligase protection in cardiac disease**. 2008.

152. Berlett BS, Stadtman ER: **Protein oxidation in aging, disease, and oxidative stress**. *Journal of Biological Chemistry* 1997, **272**(33):20313-20316.

153. Liu J, Zheng H, Tang M, Ryu Y-C, Wang X: **A therapeutic dose of doxorubicin activates ubiquitin-proteasome system-mediated proteolysis by acting on both the ubiquitination apparatus and proteasome**. *American Journal of Physiology-Heart and Circulatory Physiology* 2008, **295**(6):H2541-H2550.

154. Yamamoto Y, Hoshino Y, Ito T, Nariai T, Mohri T, Obana M, Hayata N, Uozumi Y, Maeda M, Fujio Y: **Atrogin-1 ubiquitin ligase is upregulated by doxorubicin via p38-MAP kinase in cardiac myocytes**. *Cardiovascular research* 2008, **79**(1):89-96.

155. Tan W-Q, Wang K, Lv D-Y, Li P-F: **Foxo3a inhibits cardiomyocyte hypertrophy through transactivating catalase**. *Journal of Biological Chemistry* 2008, **283**(44):29730-29739.

156. Finck BN: **The PPAR regulatory system in cardiac physiology and disease**. *Cardiovascular research* 2007, **73**(2):269-277.

157. Wang Y-X: **PPARs: diverse regulators in energy metabolism and metabolic diseases**. *Cell research* 2010, **20**(2):124-137.

158. Planavila A, Rodríguez-Calvo R, Jové M, Michalik L, Wahli W, Laguna JC, Vázquez-Carrera M: **Peroxisome proliferator-activated receptor β/δ activation inhibits hypertrophy in neonatal rat cardiomyocytes**. *Cardiovascular research* 2005, **65**(4):832-841.

159. Weindl G, Schäfer-Korting M, Schaller M, Korting HC: **Peroxisome Proliferator-Activated Receptors and their Ligands**. *Drugs* 2005, **65**(14):1919-1934.

160. Venkatachalam G, Sakharkar MK, Kumar AP, Clement MV: **PPRESearch: peroxisome proliferator activator element search database**. *International Journal of Integrative Biology* 2009, **8**(1):37-42.

161. Batista FA, Trivella DB, Bernardes A, Gratieri J, Oliveira PS, Figueira ACM, Webb P, Polikarpov I: **Structural insights into human peroxisome proliferator activated receptor delta (PPAR-delta) selective ligand binding**. *PloS one* 2012, **7**(5):e33643.

162. Kojonazarov B, Luitel H, Sydykov A, Dahal BK, Paul-Clark MJ, Bonvini S, Reed A, Schermuly RT, Mitchell JA: **The peroxisome proliferator–activated receptor β/δ agonist GW0742 has direct protective effects on right heart hypertrophy**. *Pulmonary circulation* 2013, **3**(4):926-935.

163. Barish GD, Narkar VA, Evans RM: **PPARδ: a dagger in the heart of the metabolic syndrome**. *The Journal of clinical investigation* 2006, **116**(3):590-597.

164. Lehman JJ, Barger PM, Kovacs A, Saffitz JE, Medeiros DM, Kelly DP: **Peroxisome proliferator–activated receptor γ coactivator-1 promotes cardiac mitochondrial biogenesis**. *The Journal of clinical investigation* 2000, **106**(7):847-856.

165. Kleiner S, Nguyen-Tran V, Baré O, Huang X, Spiegelman B, Wu Z: **PPARδ agonism activates fatty acid oxidation via PGC-1α but does not increase mitochondrial gene expression and function**. *Journal of Biological Chemistry* 2009, **284**(28):18624-18633.

166. Ricote M, Glass CK: **Peroxisome Proliferator-Activated Receptors (PPARs)**. *Encyclopedia Of Molecular Medicine*.

167. Ahmed W, Ziouzenkova O, Brown J, Devchand P, Francis S, Kadakia M, Kanda T, Orasanu G, Sharlach M, Zandbergen F: **PPARs and their metabolic modulation: new mechanisms for transcriptional regulation?** *Journal of internal medicine* 2007, **262**(2):184-198.

168. Marmolino D, Acquaviva F, Pinelli M, Monticelli A, Castaldo I, Filla A, Cocozza S: **PPAR-γ agonist azelaoyl PAF increases frataxin protein and mRNA expression. New implications for the friedreich's ataxia therapy**. *The Cerebellum* 2009, **8**(2):98-103.

169. Christou L, Hatzimichael E, Chaidos A, Tsiara S, Bourantas KL: **Treatment of plasma cell leukemia with vincristine, liposomal doxorubicin and dexamethasone**. *European journal of haematology* 2001, **67**(1):51-53.

170. Pan XQ, Zheng X, Shi G, Wang H, Ratnam M, Lee RJ: **Strategy for the treatment of acute myelogenous leukemia based on folate receptor β–targeted liposomal doxorubicin combined with receptor induction using all-trans retinoic acid**. *Blood* 2002, **100**(2):594-602.

171. Mitani I, Jain D, Joska TM, Burtness B, Zaret BL: **Doxorubicin cardiotoxicity: prevention of congestive heart failure with serial cardiac function monitoring with equilibrium radionuclide angiocardiography in the current era**. *Journal of nuclear cardiology* 2003, **10**(2):132-139.

172. Berthiaume J, Wallace K: **Adriamycin-induced oxidative mitochondrial cardiotoxicity**. *Cell biology and toxicology* 2007, **23**(1):15-25.

173. Raman SV, Phatak K, Hoyle JC, Pennell ML, McCarthy B, Tran T, Prior TW, Olesik JW, Lutton A, Rankin C: **Impaired myocardial perfusion reserve and fibrosis in Friedreich ataxia: a mitochondrial cardiomyopathy with metabolic syndrome**. *European heart journal* 2011, **32**(5):561-567.

174. Payne RM, Pride PM, Babbey CM: **Cardiomyopathy of Friedreich's ataxia: use of mouse models to understand human disease and guide therapeutic development**. *Pediatric cardiology* 2011, **32**(3):366-378.

175. Payne RM, Wagner GR: **Cardiomyopathy in Friedreich ataxia clinical findings and research**. *Journal of child neurology* 2012, **27**(9):1179-1186.

176. Smith ER, Sangalang VE, Heffernan LP, Welch JP, Flemington CS: **Hypertrophic cardiomyopathy: the heart disease of Friedreich's ataxia**. *American heart journal* 1977, **94**(4):428-434.

177. Cain PA, Ahl R, Hedstrom E, Ugander M, Allansdotter-Johnsson A, Friberg P, Arheden H: **Age and gender specific normal values of left ventricular mass, volume and function for gradient echo magnetic resonance imaging: a cross sectional study**. *BMC medical imaging* 2009, **9**(1):1.

178. Louch WE, Sheehan KA, Wolska BM: **Methods in cardiomyocyte isolation, culture, and gene transfer**. *Journal of molecular and cellular cardiology* 2011, **51**(3):288-298.

179. Campuzano V, Montermini L, Lutz Y, Cova L, Hindelang C, Jiralerspong S, Trottier Y, Kish SJ, Faucheux B, Trouillas P: **Frataxin is reduced in Friedreich ataxia patients and is associated with mitochondrial membranes**. *Human Molecular Genetics* 1997, **6**(11):1771-1780.

180. Zhang JD, Ruschhaupt M, Biczok R: **ddCt method for qRT–PCR data analysis**. 2010; 2010.

181. Huang C, Andres AM, Ratliff EP, Hernandez G, Lee P, Gottlieb RA: **Preconditioning involves selective mitophagy mediated by Parkin and p62/SQSTM1**. *PloS one* 2011, **6**(6):e20975.

182. Riemer J, Hoepken HH, Czerwinska H, Robinson SR, Dringen R: **Colorimetric ferrozine-based assay for the quantitation of iron in cultured cells**. *Analytical biochemistry* 2004, **331**(2):370-375.

183. Chen W-d, Gong W-t, Ye Z-q, Lin Y, Ning G-l: **FRET-based ratiometric fluorescent probes for selective Fe 3+ sensing and their applications in mitochondria**. *Dalton Transactions* 2013, **42**(28):10093-10096.

184. Koves TR, Li P, An J, Akimoto T, Slentz D, Ilkayeva O, Dohm GL, Yan Z, Newgard CB, Muoio DM: **Peroxisome proliferator-activated receptor-γ co-activator 1α-mediated metabolic remodeling of skeletal myocytes mimics exercise training and reverses lipid-induced mitochondrial inefficiency**. *Journal of Biological Chemistry* 2005, **280**(39):33588-33598.

185. Ramsay RR, Krueger MJ, Youngster SK, Gluck MR, Casida JE, Singer TP: **Interaction of 1-methyl-4-phenylpyridinium ion (MPP+) and its analogs with the rotenone/piericidin binding site of NADH dehydrogenase**. *Journal of neurochemistry* 1991, **56**(4):1184-1190.

186. Karagiannis TC, Lin A, Ververis K, Chang L, Tang MM, Okabe J, El-Osta A: **Trichostatin A accentuates doxorubicin-induced hypertrophy in cardiac myocytes**. *Aging (Albany NY)* 2010, **2**(10):659-668.

187. Bartoli CR, Brittian KR, Giridharan GA, Koenig SC, Hamid T, Prabhu SD: **Bovine model of doxorubicin-induced cardiomyopathy**. *BioMed Research International* 2010, **2011**.

188. Gilliam LAA, Fisher-Wellman KH, Lin C-T, Maples JM, Cathey BL, Neufer PD: **The anticancer agent doxorubicin disrupts mitochondrial energy metabolism and redox balance in skeletal muscle**. *Free radical biology & medicine* 2013, **65**:10.1016/j.freeradbiomed.2013.1008.1191.

189. Jauslin ML, Wirth T, Meier T, Schoumacher F: **A cellular model for Friedreich Ataxia reveals small-molecule glutathione peroxidase mimetics as novel treatment strategy**. *Human Molecular Genetics* 2002, **11**(24):3055-3063.

190. Myers C: **The role of iron in doxorubicin-induced cardiomyopathy**. In *Seminars in oncology: 1998*; 1998:10-14.

191. Papadopoulou LC, Theophilidis G, Thomopoulos GN, Tsiftsoglou AS: **Structural and functional impairment of mitochondria in adriamycin-induced cardiomyopathy in mice: suppression of cytochrome c oxidase II gene expression**. *Biochemical pharmacology* 1999, **57**(5):481-489.

192. Rudzinski T, Ciesielczyk M, Religa W, Bednarkiewicz Z, Krzeminska-Pakula M: **Doxorubicin-induced ventricular arrhythmia treated by implantation of an automatic cardioverter-defibrillator**. *Europace* 2007, **9**(5):278-280.

193. Lushchak VI: **Glutathione homeostasis and functions: potential targets for medical interventions**. *Journal of amino acids* 2012, **2012**.

194. Wood AJ, Shapiro CL, Recht A: **Side effects of adjuvant treatment of breast cancer**. *New England Journal of Medicine* 2001, **344**(26):1997-2008.

195. Zhu W, Shou W, Payne RM, Caldwell R, Field LJ: **A mouse model for juvenile doxorubicin-induced cardiac dysfunction**. *Pediatric research* 2008, **64**(5):488-494.

196. Pacher P, Liaudet L, Bai P, Mabley JG, Kaminski PM, Virág L, Deb A, Szabó É, Ungvári Z, Wolin MS: **Potent metalloporphyrin peroxynitrite decomposition catalyst protects against the development of doxorubicin-induced cardiac dysfunction**. *Circulation* 2003, **107**(6):896-904.

197. Li K, Besse EK, Ha D, Kovtunovych G, Rouault TA: **Iron-dependent regulation of frataxin expression: implications for treatment of Friedreich ataxia**. *Human Molecular Genetics* 2008, **17**(15):2265-2273.

198. Martelli A, Schmucker S, Reutenauer L, Mathieu JR, Peyssonnaux C, Karim Z, Puy H, Galy B, Hentze MW, Puccio H: **Iron regulatory protein 1 sustains mitochondrial iron loading and function in frataxin deficiency**. *Cell metabolism* 2015, **21**(2):311-322.

199. González-Cabo P, Palau F: **Mitochondrial pathophysiology in Friedreich's ataxia**. *Journal of neurochemistry* 2013, **126**(s1):53-64.

200. Auchère F, Santos R, Planamente S, Lesuisse E, Camadro J-M: **Glutathione-dependent redox status of frataxin-deficient cells in a yeast model of Friedreich's ataxia**. *Human Molecular Genetics* 2008, **17**(18):2790-2802.

201. Zhang S, Liu X, Bawa-Khalfe T, Lu L-S, Lyu YL, Liu LF, Yeh ET: **Identification of the molecular basis of doxorubicin-induced cardiotoxicity**. *Nature medicine* 2012, **18**(11):1639-1642.

202. Sawyer DB, Zuppinger C, Miller TA, Eppenberger HM, Suter TM: **Modulation of anthracycline-induced myofibrillar disarray in rat ventricular myocytes by neuregulin-1β and anti-erbB2 potential mechanism for trastuzumab-induced cardiotoxicity**. *Circulation* 2002, **105**(13):1551-1554.

203. Pagan J, Seto T, Pagano M, Cittadini A: **Role of the ubiquitin proteasome system in the heart**. *Circulation research* 2013, **112**(7):1046-1058.

204. Horton JL, Martin OJ, Lai L, Riley NM, Richards AL, Vega RB, Leone TC, Pagliarini DJ, Muoio DM, Bedi Jr KC: **Mitochondrial protein hyperacetylation in the failing heart**. *JCI insight* 2016, **2**(1).

205. Wagner GR, Pride PM, Babbey CM, Payne RM: **Friedreich's ataxia reveals a mechanism for coordinate regulation of oxidative metabolism via feedback inhibition of the SIRT3 deacetylase**. *Human Molecular Genetics* 2012, **21**(12):2688-2697.

206. Mouli S, Nanayakkara G, AlAlasmari A, Eldoumani H, Fu X, Berlin A, Lohani M, Nie B, Arnold RD, Kavazis A: **The role of frataxin in doxorubicin-mediated cardiac hypertrophy**. *American Journal of Physiology-Heart and Circulatory Physiology* 2015, **309**(5):H844-H859.

207. Caron C, Boyault C, Khochbin S: **Regulatory cross-talk between lysine acetylation and ubiquitination: role in the control of protein stability**. *Bioessays* 2005, **27**(4):408-415.

208. Hou T, Zheng G, Zhang P, Jia J, Li J, Xie L, Wei C, Li Y: **LAceP: lysine acetylation site prediction using logistic regression classifiers**. *PloS one* 2014, **9**(2):e89575.

209. Green PS, Leeuwenburgh C: **Mitochondrial dysfunction is an early indicator of doxorubicin-induced apoptosis**. *Biochimica et Biophysica Acta (BBA)-Molecular Basis of Disease* 2002, **1588**(1):94-101.

210. Bishop-Bailey D: **Peroxisome proliferator-activated receptors in the cardiovascular system**. *British journal of pharmacology* 2000, **129**(5):823-834.

211. Robinson E, Grieve DJ: **Significance of peroxisome proliferator-activated receptors in the cardiovascular system in health and disease**. *Pharmacology & therapeutics* 2009, **122**(3):246-263.

212. Yang X, Boehm JS, Yang X, Salehi-Ashtiani K, Hao T, Shen Y, Lubonja R, Thomas SR, Alkan O, Bhimdi T: **A public genome-scale lentiviral expression library of human ORFs**. *Nature methods* 2011, **8**(8):659-661.

213. Wang Y, Huang S, Sah VP, Ross J, Brown JH, Han J, Chien KR: **Cardiac muscle cell hypertrophy and apoptosis induced by distinct members of the p38 mitogen-activated protein kinase family**. *Journal of Biological Chemistry* 1998, **273**(4):2161-2168.